DEVELOPMENT OF SiC-BASED COMPOSITE MATERIAL FOR FUSION APPLICATION

Aljaž Iveković

Doctoral Dissertation
Jožef Stefan International Postgraduate School
Ljubljana, Slovenia, March 2013

Evaluation Board:

Asst. Prof. Goran Dražić, Chairman, Jožef Stefan Institute, Jamova cesta 39, 1000 Ljubljana

Prof. Dr. Milan Čerček, Member, Faculty of Mathematics and Physics, University of Ljubljana, Jadranska ulica 19, 1000 Ljubljana

Asst. Prof. Darja Lisjak, Member, Jožef Stefan Institute, Jamova cesta 39, 1000 Ljubljana

MEDNARODNA PODIPLOMSKA ŠOLA JOŽEFA STEFANA
JOŽEF STEFAN INTERNATIONAL POSTGRADUATE SCHOOL

Aljaž Iveković

DEVELOPMENT OF SiC-BASED COMPOSITE MATERIAL FOR FUSION APPLICATION

Doctoral Dissertation

PRIPRAVA KOMPOZITNEGA MATERIALA NA OSNOVI SiC ZA UPORABO V FUZIJSKEM REAKTORJU

Doktorska disertacija

Supervisor: Asst. Prof. Saša Novak Krmpotič

Ljubljana, Slovenia, March 2013

Index

Abstract

Nuclear fusion offers a prospect of a safe, economical and environmentally friendly source of energy. For the advanced concepts of nuclear fusion, SiC-based fibre reinforced composites were proposed as a structural material for the first wall of the reactor vessel, enabling higher operating temperatures and efficiencies. Already developed techniques for fabrication of SiC_f/SiC composites are currently unable to achieve all of the design assumed values for these materials, therefore further development is needed. The main drawback in fabrication of SiC_f/SiC composites is densification of SiC matrix in 3D woven fabric preform using low activation elements and at temperatures at which the properties of the fibre reinforcement are preserved. Therefore, in this work, a novel combined process of electrophoretic (infiltration) deposition (EP(I)D) and polymer infiltration and pyrolysis (PIP) was introduced as a possible way to fabricate the SiC_f/SiC composites with reduced porosity and increased properties. The work was performed within the European fusion research programme (FP7, EURATOM – Fusion) and was coordinated and verified by European Fusion Development Agreement (EFDA).

Feasibility of densification by the combined process of EPD and PIP was initially evaluated on bulk SiC samples. By tailoring the electrokinetic properties of the suspensions and employing optimal electrical conditions, deposits with high packing density (~60 %TD) were obtained. Polymer infiltration and polymer-to-ceramic conversion was studied in order to optimise the infiltration and pyrolysis procedure. To ensure the formation of crystalline material, needed to achieve the desired properties, additional heat treatment at 1600 °C and 1700 °C was employed. Densification of EPD deposit by six polymer infiltration and pyrolysis cycles resulted in a matrix material with ~87 %TD, with uniform submicron porosity. The material was characterised by flexural strength of 337±75 MPa, hardness of 1740 HV and elastic modulus of 260 GPa. Thermal conductivity of the matrix material achieved nearly 60 $Wm^{-1}K^{-1}$.

Based on the results of comprehensive analysis of the EPD of bulk SiC, electrophoretic (infiltration) deposition was successfully utilised to infiltrate thick conductive SiC fibre preform. By separation of fibres from the deposition electrode, electric field penetration through the thickness of the preform was ensured in order to provide a driving force for migrating particles. Due to the same polarity of zeta potential of migrating SiC particles as for the fibres, the particles were able to penetrate throughout the 5.4 thick fabric preform and thus filled the voids within it. Best results were obtained from suspension with 50 wt. % of solids loading at current density of 2.5 $mAcm^{-2}$. After densification of the material by six polymer infiltration and pyrolysis cycles, a SiC_f/SiC composite was formed, composed of pure, crystalline SiC with a more favourable microstructure in terms of pore size and porosity distribution in comparison to other fusion-grade composites prepared by state-of-art techniques (CVI, PIP).

The resulting SiC_f/SiC composite was characterised by high thermal conductivity in achieving 60 $Wm^{-1}K^{-1}$ at room temperature and 30 $Wm^{-1}K^{-1}$ at 1000 °C, which is one of the highest thermal conductivities reported for such material. Initial mechanical properties characterisation of the composite material revealed a need for a more stable interphase layer between the matrix and the fibres.

Povzetek

Fuzija, tehnologija pridobivanja energije z zlivanjem (fuzijo) lahkih jeder, predstavlja varen, ekonomičen in okolju prijazen energetski vir za prihodnost. Napredni koncepti bodočih fuzijskih elektrarn predvidevajo uporabo z vlakni utrjenega kompozita na osnovi silicijevega karbida (SiC_f/SiC) v strukturnih delih prve stene reaktorja. Uporaba materialov na osnovi SiC bi namreč omogočila višje delovne temperature in s tem večji izkoristek elektrarne. Kompoziti, pripravljeni po znanih postopkih, ne dosegajo vseh zahtevanih lastnosti, zato je za uporabo teh materialov v bodočih fuzijskih elektrarnah nujen nadaljnji razvoj. Glavno oviro predstavlja težavno zgoščevanje matrice iz keramike na osnovi SiC v prazninah tridimenzionalne tkanine iz SiC vlaken. Zgoščevanje je potrebno doseči z uporabo le nizko aktivacijskih elementov in pri temperaturah pod 1800 °C, pri katerih vlakna obdržijo svoje začetne lastnosti. Predstavljeno delo je bilo izvedeno v okviru evropskega fuzijskega programa (7. OP, EURATOM – Fuzija) in je bilo vodeno in preverjano s strani združenja EFDA (European Fusion Development Agreement).

Kot nov način priprave kompozita SiC_f/SiC z izboljšanimi lastnostmi smo v tem delu predlagali kombiniran proces, ki vključuje infiltracijo tkanine s pomočjo elektroforetskega nanašanja (EFN) in zgoščevanje matrice z infiltriranjem in pirolizo polimera (PIP). Učinkovitost predlaganega procesa smo najprej preverili pri zgoščevanju matrice brez vlaken. Na osnovi študija elektrokinetičnih lastnosti suspenzije SiC prahu in izbire primernih pogojev elekroforetskega nanašanja smo pripravili surovce z visoko gostoto pakiranja delcev (~60 % teoretične gostote). Podrobneje smo preučili tudi proces pretvorbe tekočega polimera v keramiko. Po zgoščevanju nanosa iz SiC in šestkrat ponovljeno infiltracijo in pirolizo polimera smo uspeli pripraviti keramično matrico s 87 % gostoto in enakomerno poroznostjo z velikostjo por pod 1 μm. Material izkazuje relativno visoko termično prevodnost 60 $Wm^{-1}K^{-1}$, upogibno trdnost 337±75 MPa, trdoto 1740 HV in elastični modul 260 GPa.

Na osnovi dognanj raziskave elektroforetskega nanašanja SiC matrice brez vlaken smo EFN v nadaljevanju uporabili za infiltracijo debele prevodne tkanine iz SiC vlaken, prevlečenih s tankim slojem pirolitskega grafita. Z ločitvijo vlaken od depozicijske elektrode smo zagotovili penetracijo električnega polja skozi tkanino in s tem primerno gonilno silo za gibanje delcev. Zaradi enakega predznaka naboja delcev in vlaken in posledično elektrostatskega odboja med njimi so delci lahko prešli skozi celotno debelino tkanine in postopoma zapolnili praznine znotraj tkanine. Najboljše rezultate smo dosegli s suspenzijo s 50 ut. % vsebnostjo prahu in pri gostoti toka 2.5 $mAcm^{-2}$. S šestkratnim infiltriranjem in pirolizo polimera smo uspeli pripraviti SiC_f/SiC kompozit, sestavljen izključno iz kristaliničnega SiC in z ugodnejšo velikostjo in porazdelitvijo por v primerjavi s kompoziti pripravljenimi s postopkom CVI ali PIP. Kompozit ima sicer zaradi neustreznih lastnosti prevleke na vlaknih neustrezne mehanske lastnosti, vendar pa se odlikuje po visoki termični prevodnosti in sicer 60 $Wm^{-1}K^{-1}$ pri sobnih pogojih in 30 $Wm^{-1}K^{-1}$ pri 1000 °C, kar je ena izmed najvišjih vrednosti izmerjenih za podoben material.

Abbreviations

D	=	Deuterium
T	=	Tritium
EFDA	=	European Fusion Development Agreement
ITER	=	International Thermonuclear Experimental Reactor
EPD	=	electrophoretic deposition
EP(I)D	=	electrophoretic (infiltration) deposition
PIP	=	polymer infiltration and pyrolysis
% TD	=	percent of theoretical density
TMAH	=	tetramethyl ammoniumhydroxide
CVD	=	chemical vapour deposition
CVI	=	chemical vapour infiltration
RS	=	reaction sintering
NITE	=	nano-infiltration and transient-eutectoid
SITE	=	slip-infiltration and transient-eutectoid
SiC_f/SiC	=	silicon carbide fibre reinforced silicon carbide matrix composite
FE-SEM	=	field emission scanning electron microscope
TEM	=	transmission electron microscope
EDXS	=	energy-dispersive X-ray spectroscopy
XRD	=	X-ray diffraction
DSC	=	differential scanning calorimetry
TGA	=	thermogravimetric analysis
FTIR	=	Fourier transform infrared spectroscopy
λ	=	thermal conductivity
ρ	=	density
σ	=	electrical conductivity
ζ	=	zeta potential
ζ_i	=	induced zeta potential
P_e	=	Peclet number
λ_D	=	Damköhler number
2D	=	two-dimensional
3D	=	three-dimensional
PyC	=	pyrolytic carbon
FM	=	fibre-matrix

1 Introduction

1.1 Fusion energy

Fusion energy is one of the future prospects towards an unlimited, environmentally friendly power source. In the face of the increasing global energy and the economic, political and environmental risks of using fossil fuels, fusion energy, if successful, has the potential to make a major contribution to the world's energy needs in a more secure and sustainable way. Nuclear fusion, a process in which, under proper conditions, two light atoms combine to form a heavier atom, is the natural process in the Universe providing energy of the stars and the Sun. Under the proper conditions, the low atomic number elements react to convert mass to energy ($E=(\Delta m)c^2$) via nuclear fusion. There has been considerable research effort focused on achievement of a controlled thermonuclear fusion (CTF) to produce energy on Earth. This task, however, has proven to be a very challenging one, from understanding the basic physics on one hand, to development of new materials needed to ignite and contain the plasma on the other.

There are a few reactions possible to achieve controlled thermonuclear fusion (CTF) involving deuterium (D), tritium (T), helium (He), lithium (Li), boron (B) and even proton (p) or neutron (n). Due to the highest cross section (probability that a fusion reaction will occur) and high energy output, the reaction between hydrogen isotopes deuterium (D) and tritium (T) or the so-called D-T reaction is regarded as the easiest (occurs much faster and at lower temperatures in comparison to other reactions) and most immediately prominent reaction to achieve nuclear fusion [1].

$$ {}_1^2D + {}_1^3T \rightarrow {}_2^4He + {}_0^1n + 17.6MeV \quad (1) $$

The difference in mass between the reactants and the products is converted into energy according to Einstein's equation $E=(\Delta m)c^2$. Most of the energy is released as the kinetic energy of neutron (about 14 MeV for D-T reaction), which has to be captured and its energy transformed into heat which can then be used to form electrical power. The products of this fusion reaction are not radioactive by itself, however the neutron can induce radioactivity in the materials used in the structural and functional components of the reactor wall. By careful selection of the appropriate materials, the level of radioactivity should decrease quickly, so that after about 100 years, it is expected that the material can be recycled or stored relatively easily. The induced radioactivity can also be reduced or in some cases even avoided by choosing different fusion reactions (e.g. reaction between a proton (p) and the isotope of boron (B^{11}) resulting only in α particles), however they are more difficult to ignite and sustain [1, 2].

To achieve nuclear fusion of D and T, we must overcome the Coulomb barrier due to electrostatic repulsion between the protons. This can be achieved by accelerating a beam of D and T or by heating up the D-T mixture to such high temperature that a high-energy collision occurs. In the so-called "magnetic confinement fusion", D-T gas will require a temperature over 10^8 K (10 times hotter than the core of the Sun) in order to fuse. At these temperatures, the atoms

become ionised and matter is in the state of plasma. To reach temperatures of 100 million degrees Celsius, powerful heating of the plasma is required and the thermal losses must be minimised by keeping the hot plasma away from the walls of its container. This is achieved by placing the plasma in a toroidal chamber-tokamak (*rus. toroidal'naya kamera s magnitnymi katushkami* - toroidal chamber with magnetic coils), made by strong (superconducting) magnetic coils which prevent electrically charged plasma particles from escaping (the fusion neutron is not confined because it has no electrical charge) [1, 2].

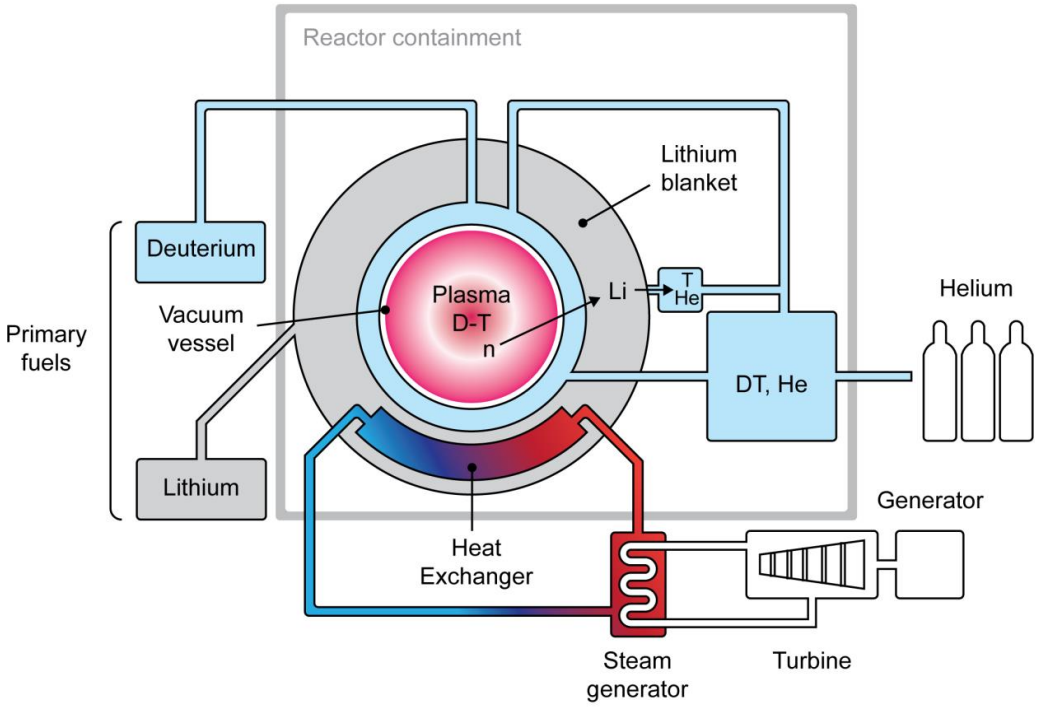

Figure 1: Fusion power plant concept [3].

A different approach is used in the so-called "inertial confinement fusion", where fusion reaction is achieved by compressing and heating of a very small D-T pellet (~2 mm in diameter) to a density of 1,000 gcm^{-3} and temperature 10 keV by ultra-high power lasers or ion beams. In order to have a steady power output, the pellet has to implode at least ten times a second, a condition not achievable with current state-of-art laser technology [1].

In order to demonstrate the feasibility of commercial use of fusion to produce electricity, several steps still have to be made. In order to demonstrate the "steady state" operation, power-plant-scale experimental reactor – ITER (International Thermonuclear Experimental Reactor) is being built at Cadarache near Aix-en-Provence in France by a consortium of the EU, Japan, Russia, USA, China, South Korea and India) [3]. To test the candidate materials at a relevant fusion irradiation conditions, the International Fusion Materials Irradiation Facility (IFMIF), a neutron source based on the D-Li stripping reaction, is planned within the framework of an international agreement between Japan and the European Union called "Broader Approach" [4]. The gathered knowledge will serve as a platform for the construction of a prototype (demonstrational) fusion power plant DEMO, a stepping stone towards commercial use of fusion.

1.2 Structural materials for fusion reactor

In order to achieve the demanding conditions required to achieve atomic fusion of deuterium and tritium and to minimise the effects of induced radioactivity (mitigate radioactive waste), a new set of materials with enhanced properties had to be developed. Fusion materials must operate in a very demanding environment which includes various combinations of high temperatures, chemical interactions, time-dependent thermal and mechanical loads and especially intense neutron fluxes. The first-wall neutron spectrum of a D-T reacting plasma contains a large 14 MeV component, which causes high-displacement rates (120 dpa per year at a neutron wall loading of 2 MWm^{-2}) but also causes higher transmutation rates than are experienced in fission reactors [5].

There are three main groups of materials considered as low-activation structural materials for fusion power plants; martensitic steels (RAFM - reduced-activation ferritic-martensitic steels, ODS - oxide dispersed steels…), vanadium alloys and silicon carbide (SiC) [6]. Martensitic steels are being used extensively in high-temperature applications, including fission reactors. The database on properties in a radiation environment is extensive. Based on high-temperature strength, the upper operational temperature limit is estimated to be 550 °C. The main constituents of martensitic steels, iron and chromium, have relatively good activation properties and the main source of activation comes from alloying elements. Low-activation martensitic steels are formed by reformulating the "standard" composition including niobium (Nb), molybdenum (Mo) etc. which are the main source of activation. These elements are replaced with low-activation ones such as vanadium (V), titanium (Ti) and tungsten (W). Vanadium alloys are composed of vanadium, titanium, chromium and silicon, which all qualify as low-activation elements. It has been found that vanadium alloys become brittle below 400 °C and above 650 °C leaving a rather narrow operating range. Interest in the use of SiC based materials stems not only from the low-activation properties, but also from the mechanical strength at very high temperatures (~1000 °C) [7], enabling higher operating temperatures and efficiencies. None of these material groups existed 20 years ago in their current form [6], however their development is crucial for successful operation of future fusion power plants.

There are several design concepts of a fusion power plant, differing on the used materials and consequently the operation temperature, efficiency, size of the reactor etc. The European Fusion Power Plant Conceptual Study (PPCS) from 2005 [8] considers four major types of fusion reactors. PPCS A and PPCS B conceptual designs are more conservative and are based on limited extrapolations in plasma physics performance compared to the design basis of ITER. The technology employed in these two models stems from the use of near-term solutions for the blanket. PPCS C and PPCS D are based on successively more advanced concepts in plasma configuration and in materials technology. In both cases the objective is to achieve higher operating temperatures and efficiencies. A summary of basic parameters and materials used in each concept is gathered in Table 1.

The most advanced concept – Model D is based on the Self-Cooled Lithium-Lead (SCLL) concept, drafted on the most attractive features of existing blanket designs such as European TAURO [9] and US ARIES-AT [10]. It assumes the maximisation of the coolant outlet temperature and the minimisation of the energy stored in the vacuum vessel (minimisation of afterheat, operating pressure and chemical radioactivity with water and air). In this concept, SiC_f/SiC was proposed as a structural material since it allows a high coolant temperature, shows very low short term activation and afterheat levels. In combination with Pb-17Li (Li enriched at 90% in ^{6}Li) as

a breeder/coolant, it offers a system capable of achieving high energy conversion efficiency and has a potential of achieving fusion energy economic competitiveness associated with high safety standards.

Table 1: Main parameters of the PPCS models [8].

Model	PPCS A	PPCS B	PPCS C	PPCS D
Design Concept	WCLL[a]	HCPB[b]	DC[c]	SCLL[d]
Parameter (plasma physics)				
Unit size (GW)	1.55	1.33	1.45	1.53
Fusion power (GW)	5.00	3.60	3.41	2.53
Aspect ratio	3.0	3.0	3.0	3.0
Major radius (m)	9.55	8.6	7.5	6.1
Plasma current (MA)	30.5	28.0	20.1	14.1
Parameters (engineering)				
Average neutron wall load	2.2	2.0	2.2	2.4
Divertor peak load (MWm^2)	15	10	10	5
H&CD Efficiency	0.6	0.6	0.7	0.7
Plant efficiency	0.31	0.37	0.42	0.6
Coolant blanket	water	He	LiPb/He	LiPb
T_{in}/T_{out} [°C]	285/325	300/500	480/700 300/480	700/1100
Coolant divertor	water	He	He	LiPb
T_{in}/T_{out} [°C]	140/167	540/720	540/720	600/900
Structural Material				
First wall	RAFM	RAFM	RAFM (ODS)	SiC_f/SiC
Divertor	W/Cu	W	W/ODS	$W/SiC_f/SiC$

[a] WCLL: Water-Cooled Lithium-Lead, [b] HCPD: Helium-Cooled Pebble Bed, [c] DCLL: Dual Coolant, [d] SCLL: Self-Cooled Lithium-Lead

SiC_f/SiC as a structural material is also proposed in the Japanese DREAM (DRastically Easy Maintenance) [11] concept, based on a helium-cooled ceramic breeder (HCCB) which assumes inlet/outlet helium-coolant temperatures of 600/900 °C with an approximate thermal efficiency of 50 %.

In addition to the application of SiC composites as a structural material, it was also proposed to use SiC_f/SiC for functional application as a flow channel insert (FCI) [8, 12]. However such application requires a completely different set of (functional) material properties (low electrical and thermal conductivity etc.)

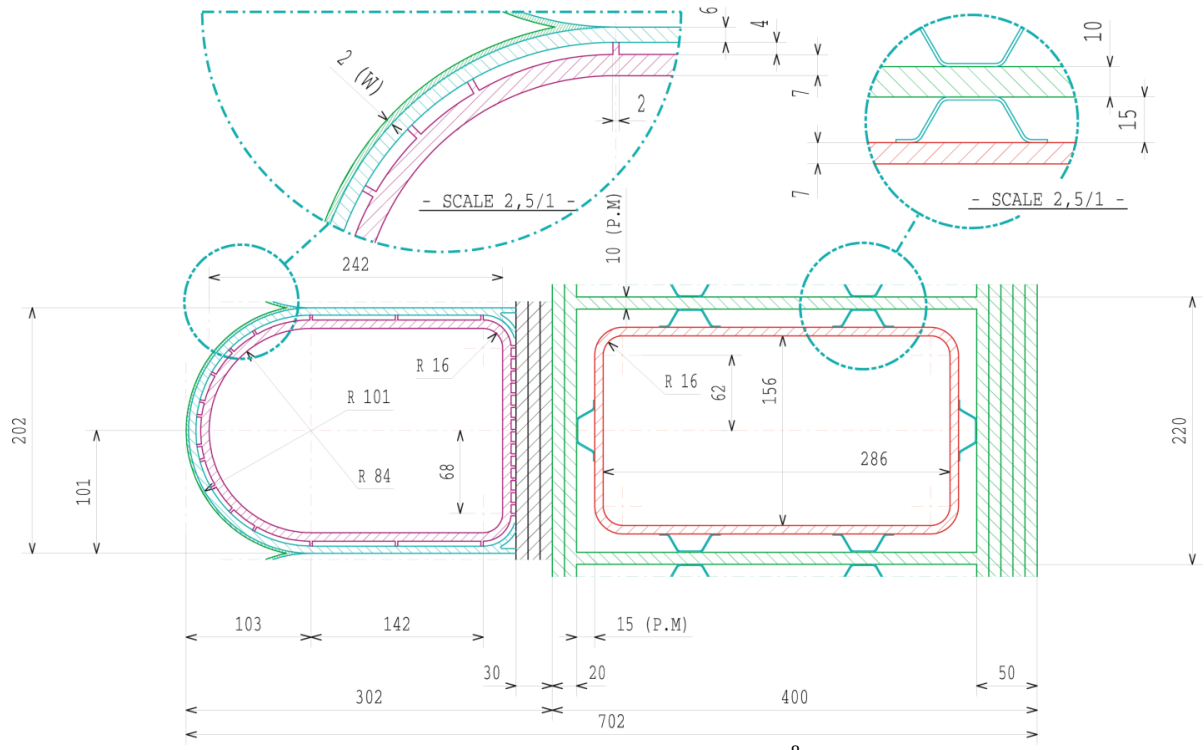

Figure 2: PPCS D - SCLL outboard blanket mid-plane cross-section [8]. All dimensions are in mm.

1.3 Silicon carbide composites for fusion application

Silicon carbide (SiC) was first proposed as a low activation fusion reactor material by Hopkins in 1975 [13], however serious development of this material did not begin until the early 1990's, driven by the emergence of composite materials that provided enhanced toughness and implied the ability to use this typically brittle materials in engineering application [14]. Selection of SiC as a structural material of a fusion reactor was based on its intrinsic properties of high temperature stability, high oxidation resistance, and very low activation and afterheat levels after being exposed to high energetic neutron irradiation.

Pure SiC is a covalent compound with exceptional properties, such as extremely high melting point (2730 °C), low specific weight (3.21 g/cm^3), oxidation resistance up to 1600 °C, excellent mechanical strength (> 500 MPa) and elastic modulus (>400 GPa) and high thermal conductivity (490 W/m-K) [15-17]. There are more than 200 known polytypes of SiC, where the cubic polytype is referred to as β-SiC and all other non-cubic structures (hexagonal and rhombohedral) collectively as α-SiC. These poly-types all consist of identical closely packed Si-C double layers, whose stacking sequence differs along a certain direction. The nearest neighbour arrangement of atoms is identical in all crystal structures. Each carbon atom is tetrahedrally surrounded by four Si atoms, and each Si atom is tetrahedrally bonded to four carbon atoms by sp^3 hybrid orbitals[15]. The strong directional bonding and the mass difference between Si and C atoms render the crystalline form of β-SiC exceptionally stable under neutron irradiation [18]. The main limitation of pure SiC is its inherent brittle nature (fracture toughness of 3 to 4 MPa m$^{1/2}$) and consequently high probability of catastrophic failure under load. Therefore, to ensure sufficient fracture toughness and reliability, the proposed material for structural parts is a SiC$_f$/SiC composite, composed of a SiC matrix reinforced with continuous SiC fibres woven into a two-dimensional

(2D) or, preferably, three-dimensional (3D) fabric.

Continuous SiC-fibre reinforced SiC matrix composites, SiC_f/SiC, have been already utilized in highly demanding engineering applications (aerospace, advanced friction systems, thermal protection, etc.). However, the severe environment of the fusion reactor dictates different set of requirements and a simple development of existing materials has proven to be futile. Various approaches have been used to produce a composite with acceptable properties; however, the overall materials properties are in many cases a compromise, where one characteristic goes on account of another. In recent literature two processes, used to produce SiC_f/SiC have been singled out as being "fusion grade"; chemical vapour infiltration (CVI) [19] and nano-infiltration and transient eutectoid (NITE) process [20]. In comparison to other fabrication techniques these two are most developed and even industrialised processes. CVI-SiC_f/SiC composites are being produced for several years industrially, mostly for aerospace applications. NITE-based composites are commercially available under its commercial name Cera-NITE [21]. Since both processes still have certain drawbacks (cost, inappropriate additives), other promising techniques also remain in consideration.

Continuous fibre reinforced ceramic matrix composites are typically comprised of a ceramic matrix, reinforcing (ceramic) fibres and a thin compliant interphase layer between the matrix and the fibres. The properties of a composite material are influenced by fibre weaving architecture, volume fraction of fibres (total volume fraction as well as fraction of fibres in different directions – dependent on the type of weaving), type and density of interface layer and matrix properties (density, pore size and distribution, etc.). The main obstacle in fabrication of dense SiC_f/SiC composite is difficulty to form a dense SiC within the SiC-fabric, in particular with 3D architecture.

1.3.1 SiC fibres

The high strength potential of ceramic matrix composites (CMC) is directly related to the use of small diameter high-strength, high-modulus ceramic fibres. Thermo-mechanical and thermo-chemical properties of fibres as well as their ability of weaving into complex shapes define in a great extent (together with the interphase layer), the overall properties of the composite. The main objective of introduction of high-strength continuous fibres into brittle ceramic matrix is to increase fracture toughness of the material. Toughening occurs primarily as a result of delamination and fibre pull-out (Figure 3), which can be described as a crack shielding process. As a crack passes through the matrix and intersects the fibre, it is deflected along the fibre-matrix (FM) interphase, so that the fibre slips within the matrix. Delamination of the fibre from the matrix continues until the fibre fractures and is pulled out from the matrix. Fibrous toughening in ceramic composites can be only achieved if the bond between fibre and the matrix is weak [22]. Types of weak FM interphase are discussed in more detail in continuation (Section 1.3.3).

Long ("continuous") fibres necessary to produce woven structures are produced by melt spinning of organo-metallic precursors, chemical vapour deposition (CVD), conversion of carbon fibres into SiC, etc. that results in different microstructures, chemical composition, geometry and thermo-mechanical properties. To ensure sufficient flexibility the fibres, their diameter has to be sufficiently low. To achieve comparable flexibility as a 25 μm nylon fibre (a typical flexible fibre) the diameter of crystalline SiC fibre (with Young's modulus E=420 GPa) has to be < 10 μm [23].

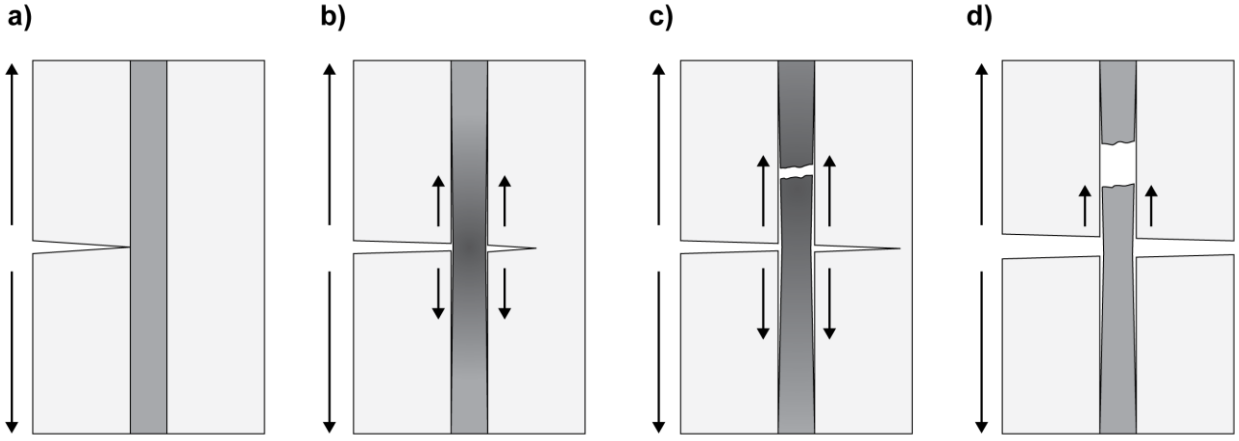

Figure 3: Sequence of steps involving fibre pull-out. Incoming crack momentarily stopped by the fibre (a), interfacial shearing and lateral contraction of fibre resulting in debonding and further increment of crack extension (b), breaking of fibre and further crack extension (c) and fibre pull-out (d) [22].

Pioneering work in the field of small diameter silicon carbide fibres was performed in Japan in the mid 1970 s', when Yajima et al. [24] developed a process for fabrication of the fibres by controlled pyrolysis of polymeric precursor. In the next decade, in 1982, Nicalon SiC fibres with diameter of 15 μm were commercially produced by Nippon Carbon Co. Ltd., Japan. Amorphous microstructure along with the presence of oxygen and free carbon in the first generations of SiC fibres (Nicalon, Hi-Nicalon of Nippon Carbon and Tyranno Lox M and Tyranno ZMI of UBE Industries Ltd.) was detrimental for the mechanical properties of composites; especially in

temperatures above 1200 °C or oxidizing environment.

The need for a more temperature stable and oxidation resistant SiC fibre for high temperature applications (e.g. gas turbine generator industry) was a major driving force for further development. The third generation near-stoichiometric SiC-fibres exhibit properties much closer to those of bulk SiC. Hi-Nicalon-Type-S (Nippon Carbon Co. Ltd.), Tyranno SA (Ube Industries Ltd.) and Sylramic (Dow Corning – ATK COI Ceramics Inc.) are currently considered as the most developed types [25, 26], however the current production of these fibres is rather low which contributes to their very high price.

The American company Dow Corning extended the approach adopted by Ube Industries Ltd. (Tyranno LOX-M fibre) using boron as a sintering aid for the development of polycrystalline Sylramic fibres with diameter of 10 μm and the grain size of 50 nm to 100 nm. This fibre is currently produced by ATK COI Ceramics, which further improved the Sylramic fibre by heating in presence of nitrogen. The so-called Sylramic-iBN is claimed to show reduced creep and increased oxidation resistance due to the BN-rich surface [26]. The use of both, Sylramic and Sylramic-iBN fibres is not suitable for fusion application due to the presence of boron and nitrogen, which are unstable under neutron irradiation.

Hi-Nicalon-S fibres have a diameter of 12 μm and they are composed of small β-SiC grains (50 nm to 100 nm) surrounded by pyrolytic carbon. To reduce the excess of free carbon, the starting compound - polymeric precursor (policarbosilane, PCS), is electron irradiated and pyrolysed in hydrogen atmosphere [26].

Tyranno SA fibres are produced from polymeric precursor grafted with aluminium (reaction of aluminium acetylacetonate with PCS), which promotes cross-linking of the precursor fibre and plays a role of a sintering agent during high-temperature heat treatment (up to 1800 °C). The Tyranno SA3 fibres are composed of cubic and hexagonal SiC phases with minor amount of residual free carbon whose concentration increases near the centre of the fibre [27]. There are two grades of Tyranno SA fibre available (Tyranno SA1, Tyranno SA3) with diameter of 10 μm and 7.5 μm, respectively, and the crystallite (grain) size around 200 nm [26]. Due to high thermal conductivity and better thermal stability in comparison to other types of SiC fibres, Tyranno SA fibres are preferred for nuclear application [27].

An alternative approach to producing polymer derived SiC fibres is the fabrication of the "SCS" fibres by Specialty materials Inc. (USA) [28] and "Sigma" fibres by Tisics Ltd. (United Kingdom), by chemical vapour deposition (CVD) [29]. Fibres with diameter in the range of 100 to 140 μm are fabricated by deposition of SiC onto 15 μm tungsten core (Sigma fibre) or onto 33 μm carbon monofilament (SCS fibre). The main problem with these fibres is large diameter, which does not allow the fibres to be knitted or woven. Additionally, a drawback of the Sigma fibres is a reaction between the W-core and SiC-rim at processing as well as at operating temperatures [30], while the carbon core represent the main limitation of the SCS-fibres to be used in fusion applications.

The fibres contribute not only to the mechanical properties of the composite, but also to its thermal conductivity, which significantly depend on the crystallinity, oxygen content and porosity. As a consequence of amorphous structure, first and second generation of SiC fibres are characterised by low thermal conductivity (1.5 – 8 $Wm^{-1}K^{-1}$) and are not suitable for high-temperature application also due to high oxygen content and tendency to recrystallize and consequently deteriorate mechanical properties. More advanced (third generation) fibres are crystalline and therefore exhibit higher values of thermal conductivity. Thermal conductivity of Hi-Nicalon-S fibres and Tyranno SA3 is 18 $Wm^{-1}K^{-1}$ and 65 $Wm^{-1}K^{-1}$, respectively [26]. The

properties and elemental composition of commercially available silicon carbide based fibres are summarised in Table 2 and the cross-section of Tyranno SA 3 fibre is illustrated in Figure 47.

1.3.2 Fibre architecture of the composites

The reinforcement of the matrix with continuous fibres is primarily selected with the aim to minimize the probability of catastrophic fracture. The type of weaving affects the volume ratio of the fibres and matrix, and may significantly affect the physical properties of the composite [31]. We can distinguish between two-dimensional (2D) and three-dimensional (3D) woven architectures (Figure 4).

When using textile structures as reinforcement in composites it is important to realize the yarn position that is as straight as possible, because non-crimped fibres can bear the highest loads and induce the highest stiffness [32]. In order to obtain sufficiently high shear strength and through-thickness thermal conductivity, the proposed optimal fibre architecture for a fusion relevant SiC_f/SiC is a 3D orthogonal woven fabric preform (Figure 4b). In comparison to 2D reinforced material where individual (2D) sheets (Figure 4a) are infiltrated with matrix material and then stacked to obtain the desired thickness, the introduction of the third fibre direction in 3D reinforced materials makes it more difficult to fabricate a composite with a homogeneous dense matrix throughout the thickness.

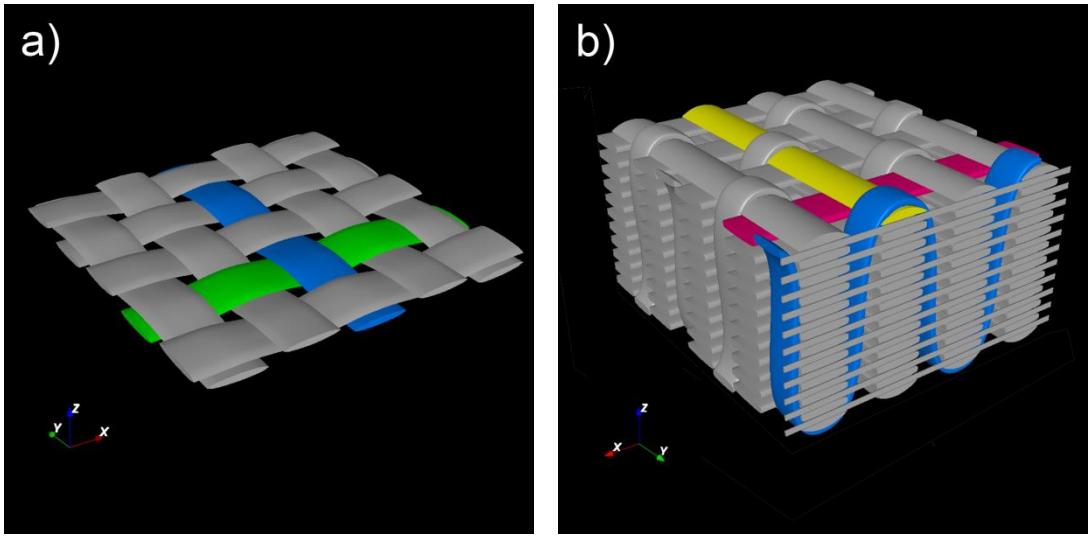

Figure 4: Comparison of representative models of a 2D plain woven and 3D orthogonal fibre reinforcement architecture rendered with TexGen [33]. Different colours represent major weaving directions of fibre bundles.

Table 2: Details of manufacture, composition and properties of commercially available advanced SiC based fibres [25, 26, 28, 29].

Trade mark	Manufacturer	Production process	Production temperature [°C]	Composition [wt. %]	Density [g/cm³]	Average diameter [µm]	Thermal expansion coefficient (to 1000 °C) [ppm/°C]	Axial thermal conductivity RT [W/mK]	Tensile strength RT [GPa]	Young's modulus RT [GPa]
Hi-Nicalon-S	Nippon Carbon	Crosslinking with electron irradiation	> 1500	68.9 Si 30.9 C 0.2 O	3.05	12	N/A	18	2.5	400
Tyranno SA-1	Ube Industries	Crosslinking with oxygen	> 1700	67.8 Si 31.3 C 0.3 O <2 Al	3.02	10	N/A	65	2.8	375
Tyranno SA-3	Ube Industries	Crosslinking with oxygen	> 1700	67.8 Si 31.3 C 0.3 O <2 Al	3.1	7.5	N/A	65	2.9	375
Sylramic	COI Ceramics	Crosslinking with oxygen	> 1700	67 Si 29 C 0.8 O 2.3 B 0.4 N 2.1 Ti	3.05	10	5,4	46	3.2	400
Sylramic iBN	COI Ceramics	Crosslinking with oxygen	> 1700	SiC/BN	3.05	10	5,4	> 46	3.5	400
SCS-Ultra	Specialty Materials	CVD on C filament	N/A	SiC on C	3.0	140 [a]	N/A	N/A	5.9	415
SigmaTM	TISICS	CVD on W filament	N/A	SiC on W	3.4	100-140	N/A	N/A	4	400

1.3.3 Interphase layer

Interphase layer is defined as a thin compliant layer between the fibres and the matrix material, designed to impede or deflect propagating cracks, allowing predictable pseudo-plastic deformation [6].

The interphase layer between matrix and fibres must be optimised in order to deflect propagating cracks and thereby to prevent catastrophic failure associated with brittle materials, which can be achieved by a weak fibre-matrix bonding [34-36]. If the strength of the bonding is too high, the formation and the propagation of the first matrix micro-crack may induce the failure of the brittle fibres by a notch effect [34]. For a weak interphase, a crack in the matrix can lead to debonding or crack deflection at the interface, crack bridging, fibre fracture, and finally fibre pull out. All these additional energy absorbing phenomena lead to enhanced fracture toughness and a non-catastrophic failure [37].

However, the role of the interphase is not only to deflect propagating cracks, but also to maintain a good load transfer between the fibres and the matrix. Therefore the interphase should be neither too strong nor too weak [34].

Several types of fibre-matrix interphase layer structures (Figure 5) were proposed to achieve the desired effect: a) simple weak interphase between fibre and matrix, b) layered structure, with layers parallel to the fibre surface and weakly bonded to each other, c) a multi-layered interphase, consisting of interchanging layers of different materials (e.g. $(X\text{-}Y)_n$), strongly bonded to the fibre surface, but with weak internal interfaces and d) porous interphase layer [34].

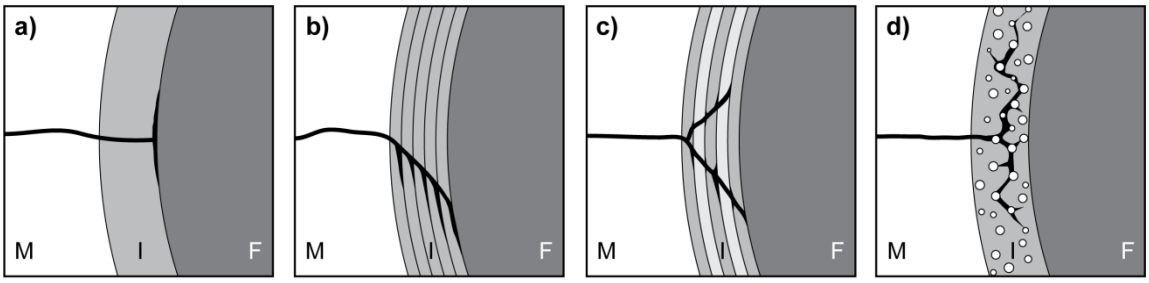

Figure 5: Schematic illustration of crack deflection in different type of interphase layer (I) between fibre (F) and matrix (M): a) weak interphase, b) interphase with a layered crystal structure, c) multi-layered interphase, d) porous interphase [34].

Most frequently used interphase materials in SiC-based ceramic-matrix composites are chemically vapour infiltrated (CVI) layers of pyrolytic carbon (PyC) [38-40] or boron nitride (BN) [41, 42], which have a layered crystal structure (the layer being roughly parallel to the fibre surface and weakly bonded to one another to promote crack deflection) [43]. Due to dimensional changes of PyC [44] and helium generation in BN under neutron irradiation, multi-layered CVD PyC-SiC ((PyC/SiC)n) and pseudo-porous SiC interphase were suggested as a better alternative in order to increase irradiation stability [19, 45]. The multi-layered PyC-SiC interphase appears to offer the best irradiation stability and post-irradiation fracture strength [45].

The thickness of the interphase in ceramic matrix composites usually varies between 0.1 – 1 μm [34]. Katoh et al. [38] reported on the insensitivity of ultimate fracture strength on PyC interphase layer thickness in CVI-SiC_f/SiC, however due to irradiation effects (especially in C-based interphases) a thin interphase layer (~100 nm) is preferred for nuclear application.

1.3.4 SiC matrix

Matrix formation is the final stage in the fabrication of ceramic matrix composites. Ideally the SiC matrix in SiC_f/SiC composite for structural fusion application would consist of pure, dense, stoichiometric β-silicon carbide, with sufficiently high mechanical and thermal properties. However, a fibre-reinforced composite with such a matrix material is extremely difficult to fabricate. Typically matrix phase in SiC based ceramic matrix composites is formed by one of the following processes: Chemical Vapour Infiltration (CVI), Polymer Infiltration and Pyrolysis (PIP), also refferd to as Liquid Polymer Infiltration (LPI) or by reaction sintering (RS), typically by melt infiltration (MI), also called Liquid Silicon Infiltration (LSI) or by Vapour Silicon Infiltration (VSI).

Chemical vapour infiltration (CVI) is one of the most developed processes for fabrication of continuous fibre reinforced composites. In the case of CVI-SiC_f/SiC, SiC-matrix is deposited on SiC-fibres woven in 2D or 3D preform from a vapour phase, typically a mixture of hydrogen and methyl-trichloro-silan [46, 47]. CVI process yields high-crystalline β-SiC matrix with a fine-grained microstructure at modest temperatures (< 1200 °C) [48], but its drawbacks are high-cost, slow deposition rate and above all, high residual porosity, usually higher than 10 %. Composites fabricated by CVI, although characterised by crystalline SiC matrix, have relatively large gradients of density and residual porosity. Large pore size in CVI-SiC_f/SiC limits the through-thickness thermal conductivity and is a concern from the mechanical properties point of view (e.g. fracture toughness).

In Polymer infiltration and pyrolysis (PIP) process, the matrix material is formed through infiltration of fabric preform with liquid polymer precursor (e.g. polycarbosilane), which after heat treatment transforms into SiC ceramic [49, 50]. It has to be stressed that various pre-ceramic polymers (Si-C-based, Si-C-O-based and Si-C-O-N-based) are used that result in ceramics with various chemical compositions and various behaviour. In the past, several disadvantages of the PIP process such as low thermal conductivity and poor radiation stability resulting mainly from the non-stoichiometric amorphous-like polymer-derived SiC temporarily hindered the development of fusion grade composites. Later, improved polymeric precursors (e.g. StarPCS™, SMP-10 by Starfire Systems Inc. [51]) yielded in near stoichiometric crystalline SiC that leads to much improved properties of SiC-ceramics [52]. Higher temperature stability of third generation of SiC fibres also enabled higher processing temperatures, resulting in a crystalline matrix material. The main drawback of the process, however, still remains the incomplete filling of the voids within the preform and crack formation due to dimensional changes during polymer-to-ceramic conversion. A more detailed description of the process is given in section 1.4.

Reaction sintering (RS) is yet another possible route for fabrication of SiC_f/SiC composites. The matrix material is produced by reaction between C and Si. Silicon can be introduced in carbon-based composite either by liquid silicon infiltration (melt-infiltration) [53, 54] or by vapour silicon infiltration [55]. The composites fabricated by reaction sintering exhibit relatively high densities and good mechanical properties, however, the presence of the matrix secondary phases such as silicon, carbon and silica and consequently, thermal and irradiation instability of the composite render reaction sintered materials unsuitable for fusion application.

1.3.4.1 Ceramic processing

SiC matrix can also be fabricated according to ceramic processing routes, by slurry infiltration and high temperature/high pressure sintering. However densification of SiC is a challenging task, due to its covalent nature and low self-diffusivity. Near theoretical

densification of pure SiC can only be achieved at high temperatures (2500 °C) and pressures (50 MPa) [56]. Pressureless solid state sintering of SiC can be achieved by addition of sintering aids (B, C, Al, B_4C etc.) at temperatures exceeding 2000 °C [57]. The main limitation of the solid-state sintered SiC for structural applications is its low fracture toughness (3–3.5 $MPam^{1/2}$) [58]. Densification can be achieved also at lower temperatures (1700-1850 °C) by liquid phase sintering (LPS). Y_2O_3-Al_2O_3 or Y_2O_3-AlN sintering aid compositions were found to be the most effective and pressureless or pressure-sintered (Hot-pressed, Hot-Isostaticaly Pressed) materials with near theoretical densities were produced. Pressure is normally used to reduce the sintering temperature and to prevent mass loss during sintering, due to decomposition of Al_2O_3 and SiO_2, which results in inadequate and irreproducible densification [59, 60]. Other type of additives based on rare-earth (La_2O_3, Ce_2O_3…) and metal oxides (BeO, CaO, MgO, P_2O_5…) were also investigated [61, 62]. Fracture toughness of LPS-SiC (6–7 $MPam^{1/2}$) and strength (>700 MPa) are higher than for solid-state SiC, on the other hand the oxidation resistance is lower due to the presence of the intergranular phase.

Standard additives used for sintering SiC, however, involve elements (e.g. boron, aluminium) that should be avoided in fusion-grade materials due to their adverse effects on properties of the composite under operation conditions (extensive absorption of neutrons, formation of long-lived radioactive isotopes, etc.). Boron, with its 20 % of the isotope ^{10}B, is one of the strongest thermal neutron absorbers and is transformed into stable helium and ^{7}Li already at very moderate neutron fluences. Transmuted He segregates at grain boundaries causing embrittlement of the material [18, 63]. On the other hand aluminium, whose isotope ^{26}Al is long lived (726,000 years half-life and emits a 1.8 MeV gamma ray), is a major contributor to materials radioactivity [14]. Same consideration has to be taken into account when using Al_2O_3 as a sintering aid in the case of liquid phase sintering. Next to high neutron activation, secondary phases formed from oxide additives are also less stable under neutron irradiation and are more prone to swelling [64]. Furthermore, densification of the SiC-matrix within a SiC-fibre preform appears even much more challenging than for the monolithic SiC-ceramics since high temperatures associated with sintering of SiC may degrade the properties of the fibres (stable up to 1800 °C [37]). Standard sintering processes are also not suitable for densification of SiC matrix material due to shrinkage (~20%) associated with densification. Densification is constrained by the reinforcing phase (fibres), which leads to the formation of crack like voids [65]. Therefore a densification process resulting in a pure SiC (at moderate temperatures) is required to achieve all the potential advantages of SiC over other materials.

A modified liquid phase sintering (LPS) is used in the NITE (nano-infiltration and transient eutectoid) process [20, 66, 67]. 2D pyrolytic carbon-coated fibre preforms are infiltrated with mixture of nano-sized β-SiC powder with 10–20 % of sintering additives such as Al_2O_3 and Y_2O_3 by tape casting. Polycarbosilane (PCS) is added to enhance densification of matrix inside fibre bundles. Infiltrated fibre preforms are stacked to obtain desired thickness and densified by hot-pressing at high temperatures (1750–1800 °C) under pressures ranging from 15 to 20 MPa. The SiC_f/SiC composites fabricated by NITE exhibit high densities and sufficiently high strength, however due to its 2D reinforcement architecture and the presence of secondary oxide phase (YAG) which lowers its thermal conductivity, is not resistant to radiation damage [64] and contributes greatly to neutron-activation of the material, it's use in fusion environment is questionable.

1.3.5 Requirements

Fusion reactor core is among the most challenging material environments. High operating temperature, high heat flux and especially high energy neutrons, which cause degradation of material through atomic displacements and transmutation products, make material requirements very demanding. Certain material properties for the design of the reactor were set in the PPCS Model D concept [8]. The design assumed properties and typical measured values of "fusion grade" materials are composed in Table 3.

Table 3: Design assumed values for SiC_f/SiC composites for structural application and measured literature values of "fusion grade" materials [8, 21, 64, 68].

Property	Unit	Assumed design requirement	Typical measured value	
		SCLL structures	3D CVI	NITE
Density	[gcm^{-3}]	> 3.0	2.8–2.9	2.77–2.93
Porosity	[%]	< 5	> 10	2.4–9.2
Young's Modulus	GPa	200-300	~200	300–400
Poisson's ratio		0.16–0.18		
Thermal expansion cooefficient	/°C	4 x 10^{-6}		
Thermal conductivity (through thickness)	[$Wm^{-1}K^{-1}$]			
Non-irradiated RT		> 20	25–40	15–40
Non-irradiated, 1000 °C		> 20	20–30	10–30
Irradiated, RT		> 20	5–8*	
Irradiated, 1000 °C		> 20	12–18*	
Ultimate tensile stress, 500-1000 °C	[MPa]	300	100–200	300–400
Matrix cracking stress, 500-1000 °C	[MPa]	-	-	200–250
Oxygen content	%	< 0.5		
Swelling (1000 °C)	%	< 0.2	> 0.5	> 1
Specific contact dose (after 100 years)	$mSvh^{-1}$	< 0.25		
Cost	€kg^{-1}	<300		>100000

* Based on model calculation

1.4 Polymer infiltration and pyrolysis (PIP)

As was already previously stated, the Polymer infiltration and pyrolysis (PIP) process is one of the standard techniques for formation of ceramic matrix in fibre reinforced composites.

The major advantages of polymer derived materials is their intrinsic homogeneity at the atomic level, low processing temperatures (polymer precursor is transformed into amorphous ceramic material at temperatures between 800 and 1000 °C) and the applicability of established polymer processing techniques. The resulting composition of polymer derived matrix depends primarily on the selected polymer precursor and processing atmosphere.
At heating, polymer precursor cross-links into an unmeltable, pre-ceramic polymer network (thermoset), followed by an organic-inorganic transition which results in amorphous ceramics, which crystallises at temperatures exceeding 1000 °C [49].

The main problem of the PIP process is the significant weight loss of the precursor polymer during pyrolysis (up to 40 %, depending on the polymer), due to the evaporation of low weight oligomers and structural rearrangement with evolution of gases (hydrocarbons, hydrogen). Weight loss, together with the transformation of liquid polymer precursor (density ~ 1 gcm^{-3}) into a ceramic material of higher density (2.5–2.7 gcm^{-3} for SiC precursors) implies the volume reduction of the matrix (> 50 %), with formation of macro and micro pores in the matrix. After crystallisation additional micro-cracks are formed within the bulk matrix material. To achieve a reasonable densification of the material the process of polymer infiltration and pyrolysis process has to be repeated several times. This leads to a significant reduction in porosity and simultaneously hardening of the matrix. Mechanical characteristics of the composite are improved with the number of PIP cycles until reaching a maximum of strength. Nevertheless, the porous microstructure (inevitable formation of large voids) compromises the integrity of the material [49].

In order to overcome the need for several PIP cycles and minimise residual porosity (and pore size), ceramic powders, such as SiC, B_4C, Si_3N_4, BN are used as passive (inert) fillers, which do not undergo any volume shrinkage during heat treatment and are compatible with the matrix. The use of passive fillers enables faster infiltration and reduction of the number of necessary PIP cycles. To achieve a homogeneous distribution of passive filler material nano-metric powders are desired, especially in processing of three-dimensional fabric preforms. The homogeneous dispersion of such nano-metric powders into an initially amorphous matrix can also act as a crystallisation nucleus for the matrix formation [49]. However, only limited amount of SiC powder can be added to the polymer, since higher amounts of filler powder result in higher viscosity of the slurry, thus lowering the impregnation efficiency. Moreover, during infiltration the preform may act as a filter to the SiC particles resulting in a inhomogeneous distribution of the SiC filler within the preform [69].

Another approach to reduce the need for multiple PIP cycles is the use of active filler controlled pyrolysis (AFCOP) proposed by Greil [70]. Active filler material (typically metal or metallic silicide) expands during reaction with decomposition products of a polymer phase or the reactive atmosphere (N_2, NH_3…) and thus compensate for the shrinkage of the polymer during pyrolysis (Figure 6).

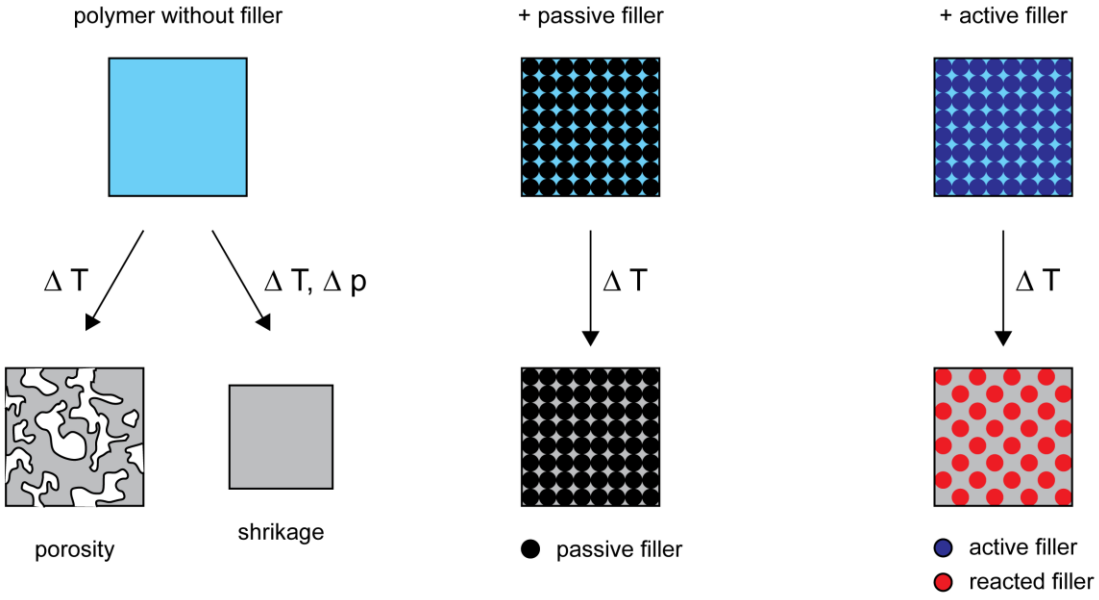

Figure 6: Microstructural changes during polymer-ceramic conversion [70].

1.5 Infiltration of fibrous preform

In order to minimise processing time and formation of large voids in the CVI or PIP processing of SiC_f/SiC composites infiltration of SiC fibre preforms with SiC powder prior to densification was proposed. Infiltration of fibrous (or any porous) preform can be achieved by infiltration of particles in a suspension into the porous structure. To achieve infiltration an external force acting on the suspension or particles in the suspension has to be applied. The driving force for infiltration can be achieved by application of a pressure difference, by applying an external pressure (e.g. pressure-assisted infiltration [69, 71, 72]) or by vacuum-assisted infiltration [73].

Alternatively, electrophoretic (infiltration) deposition was suggested as a possible technique for the fabrication of fibre reinforced composites, where the electrophoretic force exerted on the charged particles in the suspension is the driving force for the infiltration. The process was already successfully utilized for fabrication of oxide-oxide composites and 2D reinforced SiC composites.

1.5.1 Electrophoretic deposition

1.5.1.1 Origin of surface charge

When a surface is immersed into a polar (e.g. aqueous) medium, it acquires a surface charge by one, or the combination of processes of ionisation, ion adsorption and ion dissolution. Surface charge influences the distribution of ions in the polar medium. Counterions (ions of opposite charge) are attracted towards the surface and co-ions (ions of same charge) are reppeled away from the surface. Together with the mixing tendency of thermal motion, this leads to the formation of an electric double layer (Figure 7), made up of the charged surface and a neutralising excess of counter ions over co-ions distributed in a diffuse manner in the polar medium [74]. At the surface there is a immobile Stern layer, which consists of layer of specifically adsorbed ions and solvent dipoles (the plane which passes through the centres of these ions is called the inner Helmholtz plane-IHP), followed by a layer of solvated, non-specifically adsorbed ions (the plane which

passes throuhg the centres of the solvated and non-specifically adsorbed ions is called the outer Helmholtz plane-OHP). Ions outside the Stern layer form a diffuse layer or Gouy layer (also, Gouy-Chapman layer), where there is free interchange of ions and solvent molecules. In electrophoresis (or electroosmosis), an applied external electric field causes tangential fluid flow along a charged solid surface. In such tangential motion a thin layer of fluid adheres to the surface forming a hydrodynamically stagnant layer, which extends from the surface to some specific distance, where the so-called hydrodynamic slip plane is assumed to exist. The potential at the slip plane between the stagnant layer and bulk solution is extremely important in electrokinetic effects and is called the electrokinetic or zeta potential, ζ [75, 76].

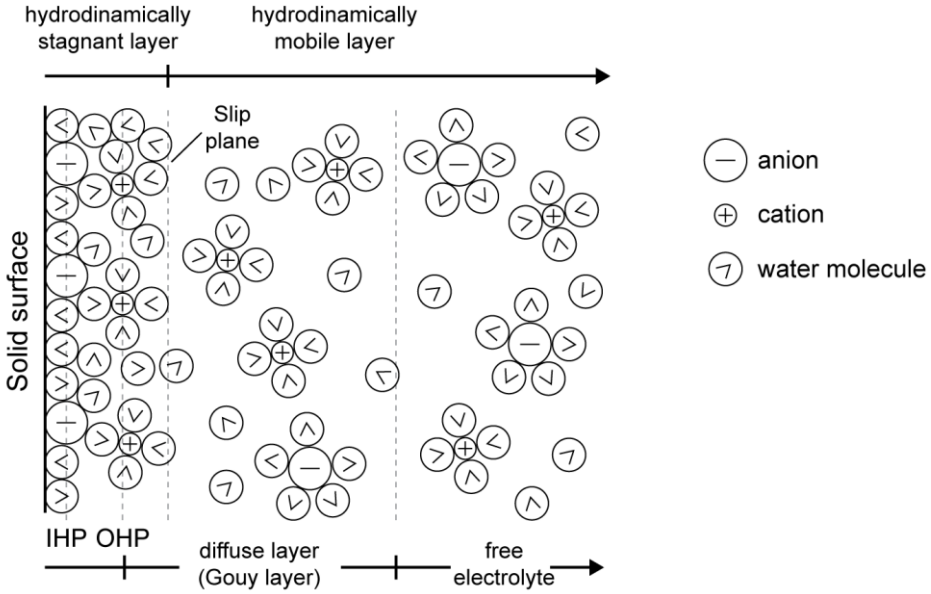

Figure 7: Schematic representation of the electric double layer according to Bockris, Devanathan, and Müller model [75, 76].

The surface of SiC powders is typically oxidized by a thin passivation layer of SiO_2. After dispersion of powder in aqueous medium the surface SiO_2 is hydrated resulting in the formation of silanol groups (Si-OH) on the surface of SiC particles [77]. Silanol groups are amphoteric in nature, relatively strongly acidic and weak alkalescent [78]. At pH above the isoelectric point silanol groups react with OH^- to form $Si\text{-}O^-$ with negative charge on the surface of the SiC powders. At lower pH, silanol groups react with H^+ ions and form $Si\text{-}OH_2^+$,with positive charge on the surface of SiC powders. The reactions are expressed as:

$$[SiOH_2]^+ \overset{H^+}{\leftarrow} [SiOH] \overset{OH^-}{\longrightarrow} [SiO]^- + H_2O$$

The resulting pH of the isoelectric point (pH_{iep}) is related to the amount of surface oxide layer which shifts the isoelectric point of SiC to that of silica (pH_{iep} = 2–3.5).

1.5.1.2 Electrophoresis

Electrophoretic deposition (EPD) is a colloidal forming technique where charged colloidal particles from a stable suspension are deposited onto an oppositely charged substrate by the application of electric field [79, 80]. EPD offers the ability to easily fabricate dense homogeneous green bodies, enabling fabrication of a variety of composite materials (particulate, laminates, fibre-composites, functionally graded materials, etc.). The process is composed of two steps; electrophoresis and deposition. Electrophoresis is an electrokinetic phenomenon, where the external applied field induces the movement (electrophoresis) of charged solid particles through the liquid. The forces acting on the suspended particle under the application of electric field are electrostatic Coulomb force (F_C), Stoke's frictional force (F_d, viscous drag of the liquid), relaxation force (F_{eB}, due to the action of the electric field on ions of opposite charge to that of particle within the double layer) and retardation force (F_R, induction forces in the double layer caused by the electric field) (Figure 8). The velocity of the charged particles under applied electric field (v_e) can be calculated by

$$v_e = u_e \cdot E \tag{2}$$

where u_e is electrophoretic mobility of the particles and E is the strength of the applied electric field. The electrophoretic mobility of a particle, u_e , depends linearly on the dielectric constant of the fluid (ε), and the zeta potential of the particles (ζ_p) and is inversely proportional to the fluid viscosity (η). The relation between these quantities is given by Henry equation:

$$\mathrm{u_e} = \frac{2}{3}\frac{\varepsilon\varepsilon_0\zeta_\mathrm{p}}{\eta}\mathrm{f}(\kappa r) \tag{3}$$

where ε_0 is the permittivity of vacuum and $f(\kappa r)$ is Henry's function, where r is the particle radius and κ^{-1} the Debye length (double layer thickness), defined as

$$\kappa = \sqrt{\frac{\sum_{i=1}^{N} e^2 z_i^2 n_i}{\varepsilon\varepsilon_0 kT}} \tag{4}$$

where e is the elementary electric charge, z_i, n_i the charge number and number concentration of ion i (the solution contains N ionic species), k is the Boltzmann constant and T the thermodynamic temperature.

Henry's function varies according to which of the forces acting on a particle above have to be considered (depending on particle size and double layer thickness). For small particles in dilute solution, the double layer is thick and $f(\kappa r) \rightarrow 1$ (negligible relaxation effect). For large particles in concentrated solutions, where the double layer is thin, $f(\kappa r) \rightarrow 1.5$ (negligible electrophoretic retardation). All other situations lead to intermediate numerical factors [76, 79]

For aqueous suspensions, typically the Debye screening layer is much smaller than particle size ($f(\kappa r)$ = 1.5) and Equation 2 is reduced to the Helmholtz-Smoluchowski equation, where electrophoretic velocity is expressed as:

$$v_e = u_e \cdot E = \frac{\varepsilon_s\varepsilon_0\zeta}{\eta} \cdot E \tag{5}$$

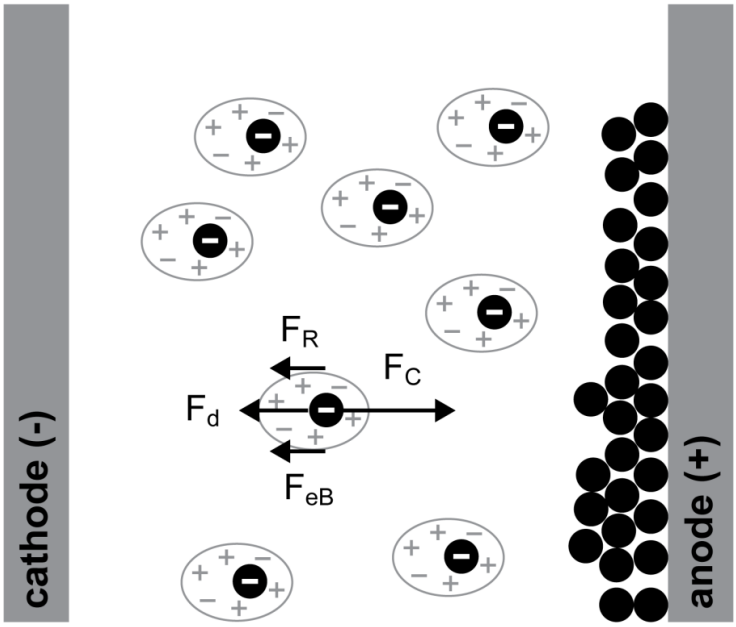

Figure 8: Schematic representation of EPD process. Negatively charged particle migrates toward the anode (positively charged) due to Coulomb electrostatic force (F_C), the forces opposing electrophoresis are Stokes frictional force (F_d), electrophoretic relaxation force (F_{eB}) and retardation force (F_R).

Equations describing electrophoretic transport were derived for infinite dilute particle suspension. However situation is more complex if we consider a concentrated colloidal suspension. Particles in colloidal suspension will exhibit a reduced electrophoretic mobility due to the presence of neighbouring particles which affect the fluid velocity in the immediate vicinity of each particle and modify the structure of particles double layer (ion distribution). Several models were developed describing the reduction of electrophoretic mobility as a function of particle concentration and Henry's function. Electrophoretic mobility is reduced with increasing particle concentration and/or smaller κr. The reduction in mobility is even more pronounced in the case of high surface potentials ($|\zeta_p|$ > 100 mV) However for aqueous systems, where the double layer thickness is typically very small relative to particle size (κr >>1) it is expected that electrophoretic velocity of a given particle ($|\zeta_p|$ < 100 mV) is not effected by the presence of other particles and therefore the Helmholtz-Smoluchowski equation (Equation 3) holds [81].

1.5.1.3 Deposition

Although the electrophoretic deposition as a process is known since late 1920's and has been explored extensively to form different materials deposits [82], the exact mechanisms of the deposition process are still not entirely understood. Several mechanisms were proposed to explain experimental results, however a general understanding of deposition of charged particles is lacking. Proposed mechanisms, (focused mainly on cathodic deposition), can be divided into three major cathegories; particle aggregation due to the pressure exerted by incoming particles, electrocoagulation (charge neutralisation at the electrode) and electrochemical coagulation (flocculation of

particles due to lowering of ζ) [83].

In 1940, Hamaker and Verwey [84] suggested that deposition of particles at EPD is akin to sedimentation and that deposit is formed by particles accumulation. It was supposed that applied electric field exerts sufficient force to overcome particle mutual repulsion and particles deposit due to the pressure exerted by those incoming and in the outer layers. This concept is feasible when deposition does not occur at the electrode (deposition on a porous membrane). Observation made by Vandeperre that zeta potential of the particles shifts towards the isoelectric point with increasing solids loading supports this mechanism [83].

Grillion et al. [85] suggested that precipitation (deposition) of particles occurs by particle charge neutralization upon contact with the opposite charge of the electrode. Such explanation is only valid for monolayer deposits at the electrode, and does not provide any explanation for deposition of thick deposits or deposition when particle-electrode processes are prevented.

Koelmans proposed that deposition is governed by electrochemical coagulation of particles by an increase in ionic strength near the depositing electrode, which decreases the interparticle repulsion (lowers the particle zeta potential) and induces flocculation [83]. This theory however is only applicable in aqueous systems where electrode reactions generate OH^- ions which causes increase in electrolyte concentration near the electrode. For systems where there is no increase of ionic strength near the electrode, Sharkar and Nicholson [82] offered an explanation involving distortion of the double layer (thinner ahead and thicker behind) due to applied electric field and fluid dynamics. Counterions in the extended double layer behind the particle may interact with ions in the suspension (also migrating toward the counter electrode) and thus reduce the thickness of the double layer. The next incoming particle with thin (leading-edge) double layer can now approach close enough to favour van der Waals attractive forces and induce coagulation (deposition). De and Nicholson [86] showed that, in contrast to the claim by Sharkar and Nicholson, for suspensions involving H^+ (or H_3O^+) ions, H^+ are not in excess in the vicinity of the cathode but are depleted by electron discharge in the cathodic reaction. This increases the local pH towards the isoelectric point (pH_{iep}), decreasing zeta potential and thus facilitating coagulation.

1.5.1.4 Electrophoretic (infiltration) deposition

The process of electrophoresis can also be used to infiltrate porous substrates. In the process of electrophoretic (infiltration) deposition, an electric potential gradient between the electrodes is used to drive the charged particles in the solution into the porous preform. Three driving mechanisms influencing particle penetration are identified [87]: the electrophoretic force exerted on the particles, the hydrodynamic drag force exerted on the particles due to the electroosmotic flow of the solvent inside the pores, and the random Brownian force due to thermal fluctuations of the solvent molecules. The particles subjected to these forces migrate through the porous substrate, until they reach the walls of the pore and are captured and deposited onto the walls by the short range van der Waals forces. According to the work of Haber and Gal-Or [87, 88], the penetration of colloidal ceramic particles into porous substrate based on probability distribution function, is enhanced at large values of Peclet number ($P_e >> 1$) and low values of Damköhlers number (λ_D). Peclet number is a non-dimensional parameter in fluid dynamics which determines the relative significance of the convective process in relation to the diffusive process:

$$P_e = \frac{v \cdot b}{D} = \frac{(v_o + v_e) b}{D} \qquad (6)$$

where v is the particle velocity (sum of electroosmotic (v_o) and electrophoretic velocity (v_e) of a charged particle), b is the mean pore radius, and D is the diffusion coefficient of the particle. According to Stokes-Einstein, relation diffusion can be expressed as:

$$D = \frac{kT}{6\pi\eta r} \tag{7}$$

where k is the Boltzman constant and r is particle radius.

On the other hand, the Damköhler number (λ_D) determines the ratio between diffusion and deposition time scales, namely:

$$\lambda_D = \frac{\delta b}{D} \tag{8}$$

where δ stands for local deposition rate. Large Damköhler number represents a process where the deposition of particles is governed mainly by diffusion, whereas small values correspond to a process controlled by the local deposition rate. As was stated by Haber and Gal-Or [87] very low or zero value of Damköhlers number (e.g. no deposition) would result in the deepest particle penetration through porous substrate, which might be achieved by the introduction of a repelling force (stronger than van der Waals attraction forces) between the particles and the pore walls. When electrostatic forces are used to prevent particle deposition, according to Bowen et al. [77], there is a critical filtration velocity below which the particles are excluded from the pore due to electrostatic repulsion, therefore the electric field acting on the particles (and resulting electrophoretic velocity) has to be sufficiently high to overcome the effect of electrostatic repulsion between the pore wall and the penetrating particle.

The movement of particle inside a porous substrate is a combination of electrophoretic and electroosmotic velocity. The direction of electroosmotic flow depends on the ζ of the wall and can either contribute or oppose the motion of the particle through the substrate [87].

For the simple case of electroosmotic flow parallel to a charged plane (or straight capillary wall), the electroosmotic velocity of the electrolyte solution under the applied electric field parallel to a plane wall is given by Helmholtz-Smoluchowski equation

$$v_o = -u_o \cdot E = -\frac{\varepsilon_s \varepsilon_0 \zeta}{\eta} \cdot E \tag{9}$$

which is of the same form (with opposite sign) as Equation 3 for electrophoresis (assuming the pore radius is much larger than the wall double layer thickness) [76, 89]. However, the straight capillary model of porous media is not a realistic model for fibrous systems, for it does not consider the effects of pore orientation, geometry, tortuosity, etc. [89]. Several authors have used unit cell models to predict the electroosmotic mobility of electrolyte in fibrous porous media [89-91]. As was determined by Kozak and Davies [91] and Ohshima [90], for moderate surface potentials and large κr (> 10^2) electroosmotic velocity reduces to Helmholtz-Smoluchowski equation and for small values of κr, the electroosmotic velocity decreases as the porosity decreases.

As was determined by Keh and Chiou [92] in their analysis of electrophoresis of a colloidal sphere in a circular cylindrical pore, the direction and velocity of particle motion is determined by the difference in particle and wall zeta potentials (ζ_p - ζ_w). The migrating particle is also affected by the electrophoretic enhancement due to electrostatic interaction between the particle and the pore wall and by the hydrodynamic retardation of the pore wall resulting in a decrease in electrophoretic mobility as a function of particle-pore size ratio.

1.5.1.5 Use of EP(I)D for fabrication of SiC_f/SiC

The use of EPD in the infiltration of fibrous preform was reviewed by Boccaccini [93]. Most of the previous research has been focused on the fabrication of oxide based composites in particular with 2D reinforcement [94, 95]. Since oxide fibres are non-conductive, they are placed in front of the electrode and the particles migrating towards the electrode with the opposite charge, gradually fill the fibrous preform. In the case of conducting substrates, the substrate (porous structure, fibres) is used as depositing electrode [96, 97].

Literature on fabrication of SiC based composites by electrophoretic deposition is very scarce and limited to infiltration of 2D reinforcement. Boccaccini et al. [96] infiltrated 2D plain woven SiC fibre mats with silica and alumina from aqueous suspension to form a SiC_f/ mullite composite. They reported on a full infiltration of fabric preform indicating a possibility to use EPD to infiltrate 2D and possibly also 3D fabric preforms. Streckert et al. [98] reported on infiltration of a thick Nicalon-HVR-fabric with SiC powder from acetone suspension. A very porous "green" composite with density of approximately 30 % TD was obtained. Due to inefficient particle infiltration macro voids and virtually no particle infiltration between the fibre tows were observed. Müller et al. [99] infiltrated 2D carbon fabric by SiC particles in ethanol suspensions. They noted a significant improvement of the infiltration with suspension containing 10 vol. % of solid content (in comparison to 1 vol. %), which was attributed to the collective movement of particles. In a more recent research, Lee et al. [100] infiltrated 2D SiC reinforcement with mixture of SiC powder and sintering aids in a toluene/ethanol solvent mixture. SiC fabric was used as an anode or cathode (depending on the surface charge of SiC particles) and placed between two oppositely charged electrodes in order to increase infiltration by deposition from both sides. In a related study, Gil and Yoon [101] reported on an increased infiltration of intra-bundle areas by combination of EPD and ultrasonification of ethanol suspensions containing SiC with Al_2O_3-Y_2O_3-MgO sintering additives. Same principle of infiltration of a 2D fabric from both sides, was also demonstrated by Yoshida et al. [102] in an aqueous system.

The feasibility of electrophoretic (infiltration) deposition for infiltration of 3D conductive fibre reinforcement was not yet demonstrated and such reinforcements were even termed "not suitable for fabrication of fibre reinforced ceramic matrix composites by electrophoretic deposition" [95].

2 Aims and Hypothesis

Silicon carbide based ceramic matrix composites are among the candidate structural materials for nuclear fusion application. The intrinsic properties of SiC (high temperature stability, low neutron activation and after heat levels etc.) have rendered SiC the material of choice for advanced fusion concepts envisioning higher operating temperatures and higher efficiencies of the fusion reactor. However, currently available processing techniques have not been able to satisfy all the requirements imposed on SiC composites for fusion application; therefore further development is essential for successful implementation of this material in future fusion power plants.

The desired process should enable fabrication of dense SiC matrix within the 3D fibre preform at moderate temperatures (<1800 °C) and pressures. Higher temperatures might cause degradation of SiC fibres. In order to preserve the advantages of SiC in nuclear environment (low neutron activation, low afterheat levels), material should consist only of low-activation elements such as Si, C, Cr, Fe, V, Ti and W, while standard sintering additives, such as Al_2O_3 or B should be avoided. Additional drawbacks of densification by standard sintering are high temperatures and pressures normally employed and large shrinkage associated with densification. Materials produced by state-of-art processes, such as chemical vapour infiltration (CVI) or polymer infiltration and pyrolysis (PIP), suffer from inherent porosity with large pore size due to the nature of densification process. On the other hand reactive sintering (RS) or nano-infiltration and transient eutectoid (NITE) processes, although successful in densification, result in a material with secondary phases (Si, SiO_2, C in the former and YAG in the latter) which deteriorate the stability and low activation properties of the material under neutron irradiation.

The aim of the composed work was to define and develop an alternative, low-temperature, low-pressure processing route for fabrication of SiC fibre reinforced SiC composite materials (SiC_f/SiC) intended for structural application in future fusion reactor. The proposed concept envisages the use of electrophoretic (infiltration) deposition process for the infiltration of the SiC fabric preform with SiC powder, which would be densified at temperatures below 1800 °C by polymer infiltration and pyrolysis process. The combined process would produce a dense, highly crystalline SiC matrix. Introduction of large amount of crystalline SiC powder prior to densification would enable more efficient densification and would prevent the formation of large voids during densification, which is one of the main drawbacks of the existing state-of-art process.

The use of electrophoretic deposition for fabrication of ceramic matrix composites have already been demonstrated, however the relatively small volume of work performed has been focused mainly on non-conductive substrates and 2D reinforcements such as fibre mats. In order to utilize electrophoretic (infiltration) deposition, appropriate suspension properties and infiltration conditions should be determined. By studying the infiltration kinetics of a thick conductive porous substrate, improvement to the existing concept of infiltration of conductive fibrous preforms by use of electrophoresis has to be made. Determination of optimal condition for densification of fibrous preform infiltrated by large amount of powder material, which acts as a passive filler, with appropriate preceramic polymer precursor and establishing a suitable heating regime in order to yield a crystalline ceramic with desired properties is needed. Alternative approach of active

filler controlled pyrolysis can be used during polymer pyrolysis to reduce the processing time and increase densification.

3 Materials and Methods

3.1 Materials

Aqueous suspensions of submicron β-SiC powder with d_{50}=0.6 μm (BF12, H.C.Starck, Germany), nanosized β-SiC powder with d_{50}=50 nm (Hefei, Keier nano, China) and $CrSi_2$ with d_{50}=4.539 μm (ChemPur, Germany) were prepared by dispersing the powder in deionised water. The surface charge of ceramic particles was modified with 2.8 M tetramethyl-ammonium hydroxide (TMAH, Sigma-Aldrich Chemie GmbH, Germany) or 1 M hydrochloric acid (HCl, Sigma-Aldrich, Germany). W powder (Secco), with average grain size of 1 μm, was dispersed in absolute ethanol (Sigma-Aldrich Chemie GmbH, Germany) with the addition of citric acid (CA, Johnson Matthey GmbH, Germany).

For the EP(I)D experiments, Tyranno SA Grade 3 (UBE Industries Ltd., Japan) fibres of 7.5 μm in diameter were used as fibre reinforcement (Figure 47). The fibres were orthogonally woven into 3D fabric preform of 5.4 mm in thickness by Shikobo Ltd., Japan and a thin layer of pyrolytic carbon (PyC) of thickness of approximately 100 nm was applied as an interphase layer at Italian National Agency for New Technologies, Energy and Sustainable Economic Development - ENEA. The ratio of fibres oriented in the x, y and z direction was 1:1:0.1 with total fabric fibre volume fraction of 0.35. To study the infiltration conditions, PAN based carbon fibres with 7 μm in diameter (Toho Tenax America Inc., USA), woven into a non-crimp 3D orthogonal fabric preform of thickness 4.5 mm (3TEX, USA), were used. Unless stated otherwise, the fibres were treated with sodium dioctyl sulfosuccinate (SDOSS, Sigma-Aldrich Chemie GmbH, Germany) to increase the wetting of fibre preform with the suspension.

For the polymer infiltration and pyrolysis process, allyl-hidridopolycarbosilane (AHPCS) (StarPCS^{TM} SMP-10, Starfire Systems, USA) was used. SMP-10 is a hyperbranched partially allyl substituted polycarbosilane, with compositional formula $[Si(CH_2CH{=}CH_2)_2CH_2]_x[SiH_2CH_2]_{n-x}$ (where x = 0.5 %) [103]. AHPCS average structure and SMP-10 polymer basic properties are shown in Figure 9 and Table 4 respectively.

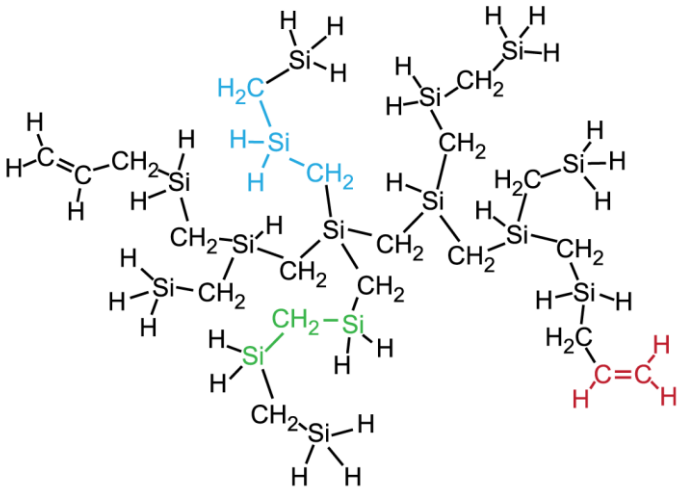

Figure 9: AHPCS “average” structure [104].

Table 4:Basic properties of StarPCS^{TM} SMP-10 [51].

Property	Value
Density	0.998 gcm^{-3}
Appearance	clear, amber liquid
Viscosity (25 °C)	0.04–0.10 Pas
Flash Point	89 °C
Moisture Absorption	< 0.1 % in 24h at room temperatures
Surface Tension	30 mN/cm
Odour	none
DOT/IATA Regulations	non hazardous

3.2 Electrophoretic deposition

3.2.1 Suspension

Aqueous suspensions of submicron SiC and nanosized SiC were prepared with various solids loading of 10–70 wt. % and 1–50 wt. % respectively. Nanosized SiC powder was heat treated at 650 °C for 30 min to remove the surface carbon layer. Mixed suspensions of submicron and nanosized SiC powder and submicron SiC and $CrSi_2$ were also prepared with 5–80 vol. % of nSiC and 5–30 vol. % of $CrSi_2$ respectively. Suspensions of submicron SiC with 1–10 vol. % of W were prepared in absolute ethanol. Electrokinetic properties of powders in suspensions were measured using a Zeta Probe analyser (Colloidal Dynamics, USA). Conductivity and pH of the suspension were also evaluated using conductivity meter (Portamess 910, Knick, Germany) and pH meter (Metrohm 744, Switzerland) with Polyclave 120 electrode (Hamilton, USA). The pH levels in aqueous suspensions were adjusted using tetramethyl-ammonium hydroxide (TMAH) and hydrochloric acid (HCl). Suspensions were homogenised using ultrasonic processor (UP400S, Hielscher Ultrasonics, Germany) with power of 400 W at 50 % amplitude, for 3 min at 0.5 s pulse before each characterization measurement. Zeta potential of used fibres was measured in a dilute aqueous suspension using Phase Analysis Light Scattering (ZetaPals, Brookhaven Instruments Corporation, USA). Fibres were crushed in a B_4C mortar and approximately 0.1 g was dispersed in 100 mL of distilled water. pH was adjusted using 0.01–1 M HCl and 0.01–1 M NaOH.

3.2.2 Electrophoretic deposition

EPD experiments were conducted in a glass beaker with suspension in which two flat graphite electrodes were immersed at a mutual distance of 2 cm using a power source (0–64 V, Thrulby Thandar Instruments, United Kingdom). Constant current depositions with current density of 2–10 $mAcm^{-2}$ were applied for 5–20 minutes. A cellulose membrane was placed in front of the depositing electrode to prevent bubble incorporation due to water electrolysis. For the EP(I)D experiments, fibre preform was either used as an anode or was placed in front of the anode, separated from it by a cellulose membrane. Prior to infiltration, the fibres were immersed in 0.005 M solution of sodium dioctyl sulfosuccinate (SDOSS) in water and dried in air. The deposits were carefully dried in humid atmosphere.

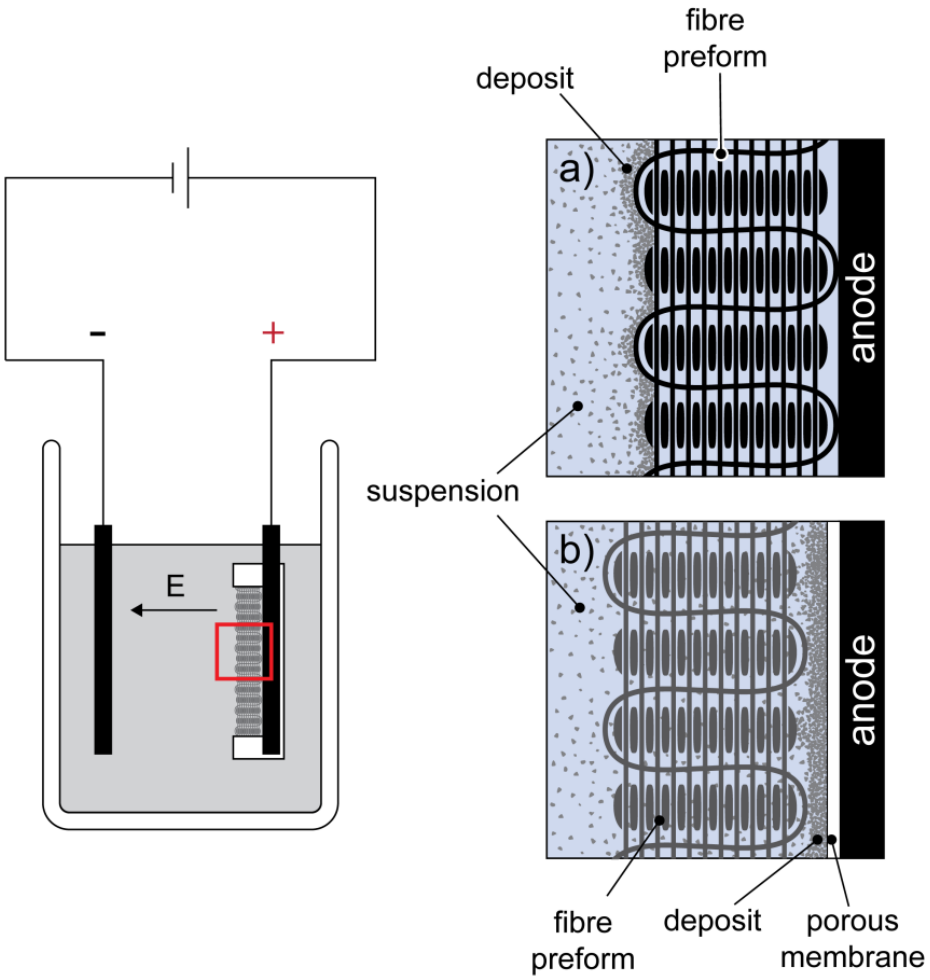

Figure 10: Scheme of electrophoretic deposition cell where a) fibres are in contact with the electrode and b) fibres electrically isolated from the electrode.

3.3 Polymer infiltration and pyrolysis

EPD and EP(I)D samples were infiltrated with polymer precursor either as-deposited, or after being pre-sintered at 1600 °C–1700 °C in vacuum.

Prior to infiltration, the preceramic polymer was agitated with a magnetic stirrer in order to degas the polymer and heated to 90–100 °C. All samples were evacuated to 1000–500 Pa (unless stated otherwise) and then infiltrated with the polymer using a pressure difference between the chambers with the polymer and the sample. Rate of infiltration was monitored by visual examination of fracture surface of infiltrated samples after infiltration under various conditions (temperature, time, evacuation).

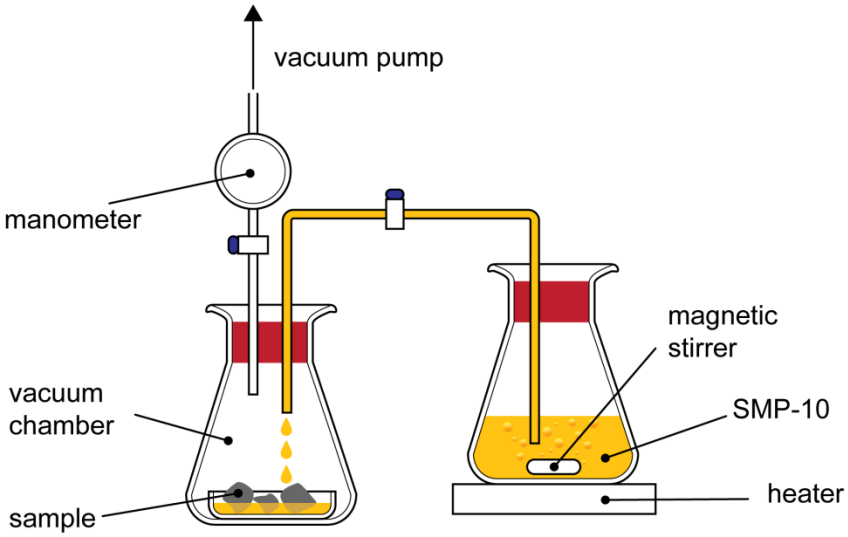

Figure 11: Schematic representation of the preceramic polymer infiltration system.

The infiltrated samples were heat-treated to 1000 °C in argon in a high-temperature tube furnace (RHTC 80-230/15, Nabertherm, Germany) in order to pyrolyse the preceramic polymer. Heating profile was adjusted in order to minimize the effect of dimensional changes during polymer to ceramic transformation. After pyrolysis, the samples were further heat-treated at 1600 °C or 1700 °C in vacuum in a high temperature Astro furnace (Thermal Technologies Inc., USA). To study the polymer-to-ceramic transformation the as-received polymer was pyrolysed and additionally heat-treated at various temperatures up to 1800 °C.

The entire experimental procedure is schematically presented in Figure 12.

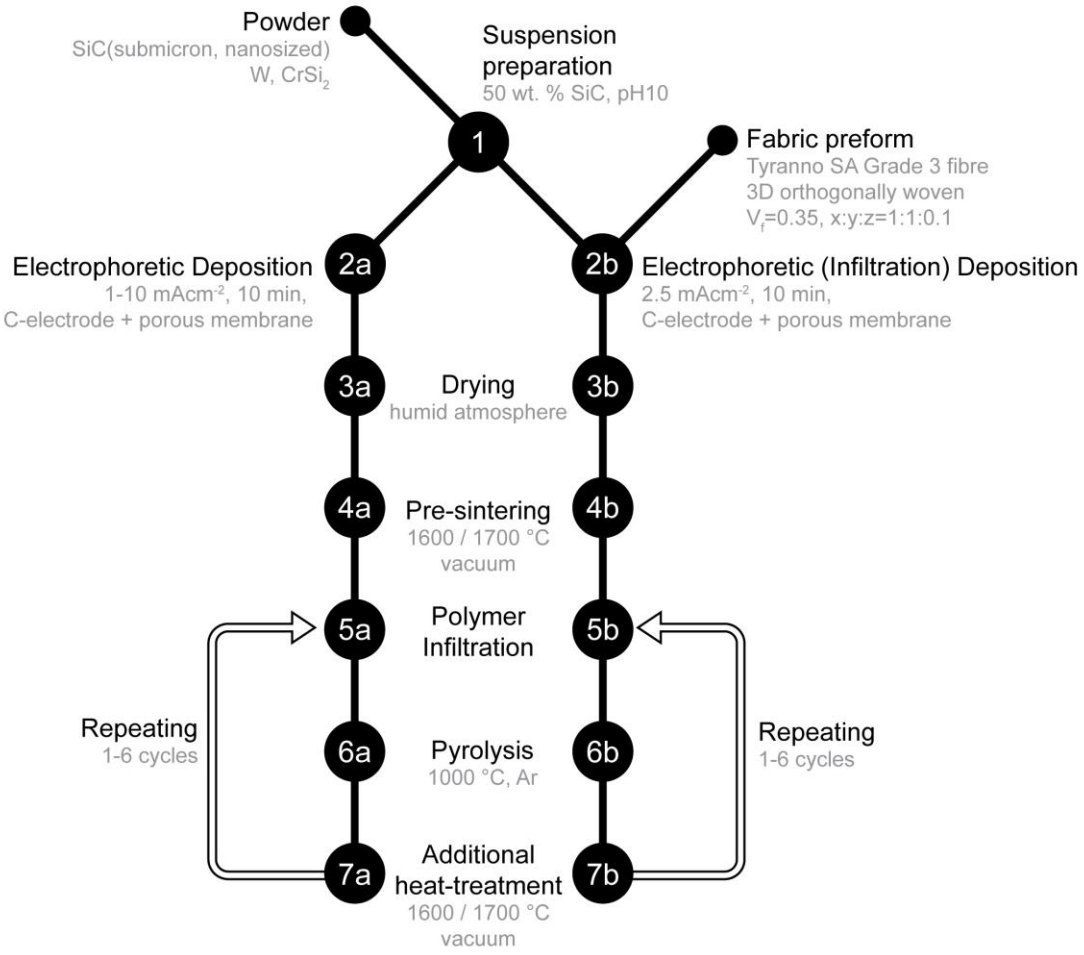

Figure 12: Workflow chart of the entire experimental process.

3.4 Characterisation

3.4.1 Viscosity

The rheological properties SiC suspensions with different solids loading and SMP-10 polymer and polymer-SiC powder mixtures, were measured using a Physica Modular Rheometer MCR301 (Anton Paar Gmbh, Austria) using a cone (CP50-2, CP20-2) and plate method. Viscosity was measured at temperature of 30 °C as a function of shear rate in the interval of 1–100 s^{-1}. Temperature–dependent viscosity measurements were performed at shear rate of 5 s^{-1} in the temperature range of 20–110 °C.

3.4.2 Wetting angle

Wetting angle on pre-sintered SiC and PyC substrates was measured with Theta Lite optical tensiometer (Attension, Biolin Scientific, Finland) using distilled water or SMP-10 polymer. Substrates were washed with acetone and distilled water prior to measurements. In the case of water wetting angle measurements, the effect of surfactants was evaluated by immersion of substrate into aqueous solutions of SDOSS or DBSA. Wetting angle was determined approximately 3 s after the droplet was released to the surface of the sample.

3.4.3 Thermal analysis

To determine the curing temperature of the SMP-10 polymer, differential scanning calorimetry (DSC200 F3, Netzsch, Germany) was employed up to 400 °C with heating rate of 10 $Kmin^{-1}$. Thermal gravimetry analysis (TGA, Mettler Toledo, Switzerland) of the polymer was preformed in a nitrogen atmosphere up to 1000 °C with a heating rate of 3 $Kmin^{-1}$.

3.4.4 Electron microscopy

Morphology and size of used powders and the microstructures of the fracture surfaces or polished cross-sections of the samples were examined using a field-emission scanning electron microscope (FEG-SEM) (JEOL JSM-7600F, Tokyo, Japan) equipped with an energy-dispersive X-ray spectroscopy (EDXS) system INCA (Oxford Instruments, United Kingdom). A quantitative, standardless EDXS method with a virtual standards data library, combined with a spectral acquisition time of 60 s and beam energy of 6.5 keV, was used to analyse the composition of SiC-matrix and SiC-fibres in the composite.

For the transmission electron microscopy (TEM) studies, the specimens were cut, ground and polished into 100 μm discs, which were further prepared according to standard procedures for TEM specimen preparation by dimpling and ion milling (BAL-TEC, RES 010) using 4-kV Ar^{+} ions at an incidence angle of 10 °C to obtain large electron-transparent areas. Powder specimens were placed on a copper grid. The morphology and crystallinity of the samples were studied using 200-keV transmission electron microscopes (JEOL JEM 2100 and JEOL JEM 2010F, Jeol Inc., Tokyo, Japan).

3.4.5 X-ray diffraction analysis (XRD)

Phase composition and crystallinity of powders, fibres, pyrolysed polymer ceramic residue and bulk materials was evaluated by X-ray diffraction (XRD) using a diffractometer (D4 Endeavor, Bruker AXS, Karlsruhe, Germany) with Bragg-Brentano geometry, a Cu Kα radiation source and a Sol-X energy-dispersive detector. Polymer

derived ceramic residue samples and ceramic fibres were crushed into powder prior to XRD analysis. An estimate of the crystallite size of the pyrolysis residue after heat treatment in the temperature range of 1000–1800 °C was obtained from peak broadening using Debye-Sherrer equation [105].

3.4.6 Fourier transform infrared spectroscopy (FTIR)

A PerkinElmer 2000 FT-IR spectrometer (PerkinElmer, Waltham, MA) was used to record IR spectra of the as-received polymer and crushed powder residue after heat treatment at different temperatures. The spectrometer is equipped with Specac Golden Gate Diamond ATR (Specac Ltd., Orpington, U.K.) as the sample support. The data were collected in the wave number range of 600–4000 cm^{-1} using spectral resolution 2 cm^{-1} and 8 scans.

3.4.7 Density & Porosity

Densities of green deposits and samples after densification were measured using Bulk Density Measurement System (Densitec, Exelia AG, Switzerland) based on the Archimedes principle in silicone oil (M350, Carl Röth Gmbh, Germany). Porosimetry measurements were performed using a Hg-intrusion porosimeter (Pascal 140 / 440, Thermo Scientific, USA) in the range of 100 kPa–400 MPa. Pore size and distribution of the material was also characterised by 3D X-ray computed tomography (CT) at Henry Moseley X-ray Imaging Facility at University of Manchester. Imaging was performed on disk shaped sample with diameter of 10 mm and 4 mm thickness, using the Nikon Metris 320 kV custom bay.

3.4.8 Thermal conductivity

Room temperature thermal conductivity of bulk samples was measured on a Physical Property Measurement System (PPMS, Quantum Design Inc., USA) with a 9 T magnet using the standard four-probe lead configuration. Measurements were performed in the temperature range between 300 and 400 K. The samples were in the form of small bars with the maximum size 4 mm × 4 mm × 15 mm.

Composite samples for thermal diffusivity measurements were in the shape of disks, 10 mm in diameter and 4.0–4.8 mm in thickness. Thermal diffusivity was measured through thickness by laser flash analysis system (LFA457, Netzch, Germany) in the temperature range from room temperature to 1050 K in vacuum. The thermal diffusivity values were determined using the Cowan algorithm and pulse correction. Measurements were performed partially at Nuclear Research And Consultancy Group (NRG) in Petten and partially at the National Institute of Materials Physics in Bucharest. Thermal conductivity of the samples was calculated according to the equation:

$$\lambda = \alpha C_p \rho, \tag{10}$$

where α is measured thermal diffusivity, C_p specific heat and ρ density of the material. Specific heat of the material was measured directly or was calculated following the mathematical approximation suggested by Snead [16]:

$$C_p = 925.65 + 0.3772\ T - 7.9259 \times 10^{-5}\ T^2 - 3.1946 \times 10^{-7}\ T^{-2} \tag{11}$$

Changes in density with increasing temperature due to thermal expansion of the material were also approximated according to equation:

$$d\rho / \rho = -3adT \quad (12)$$

where thermal expansion due to temperature increase can be expressed according to approximation derived for 3C-SiC high-purity CVD SiC as:

$$a = -1.8276 + 0.0178\,T - 1.5544 \times 10^{-5}\,T^2 + 4.5246 \times 10^{-9}\,T^3\ (10^{-6}\,K^{-1}) \quad (13)$$

3.4.9 Mechanical characterisation

3.4.9.1 Hardness & Elastic modulus

Hardness was measured using Vickers nanoindentation (Fischeroscope H100C, Helmut Fischer, Sindelfingen-Maichinigen, Germany). The instrument records instantaneous measurements of indentation depth and load, from which microhardness and modulus of elasticity can be calculated. Samples were polished and indentation force of 1 N was used for 10 s.

3.4.9.2 Strength

Strength of the bulk matrix material was measured on disk samples of 17.4 mm in diameter and thickness of 2–4 mm. The samples were grinded and polished in order to minimise the effect of surface imperfections. The strength was measured using piston-on-three ball biaxial strength testing (Galdabini Quasar 50, Italy). The measured sample is supported on the bottom (flexural) side by three balls equidistant from its centre. The upper face of the specimen is centrally loaded with a piston of radius 1.4 mm, as shown in Figure 9. The supporting balls are made of stainless steel with radius of 1.4 mm and are equally spaced along a concentric circle with radius of 11 mm.

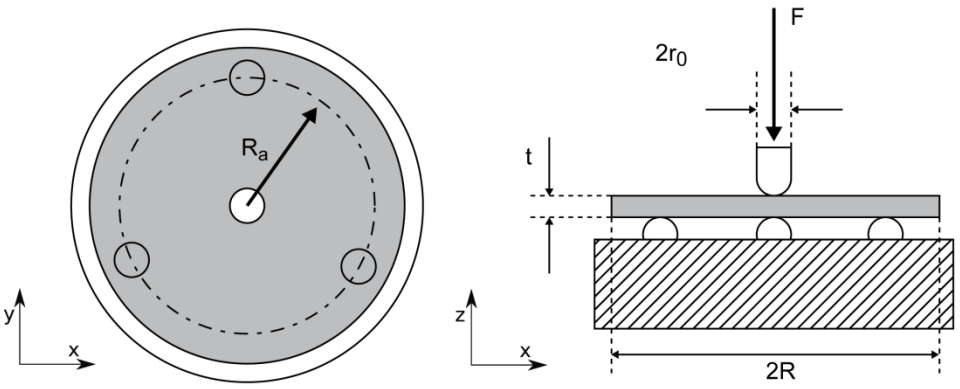

Figure 13: Schematic of fixture for testing biaxial flexure properties using piston on three ball configuration.

In the area underneath the piston, there exists an equibiaxial tensile stress state where initialization of fracture is expected. The flexure strength was determined from the peak load at failure according to [106].

$$\sigma_{max} = -\frac{3F(1+\nu)}{4\pi t^2} \cdot \left[1 + 2 \cdot ln\frac{R_a}{b} + \frac{(1-\nu)}{(1+\nu)} \cdot \left(1 - \frac{b^2}{2R_a^2}\right) \cdot \frac{R_a^2}{R^2}\right], \quad (14)$$

where

$$b = \frac{t}{3}, \tag{15}$$

where v is the Poisson ratio of the specimen (assumed to be 0.19 for SiC (ref)), b is the radius of the loaded area (e.g. contact radius of the loading piston), R_a is the radius of the support and R and t are the radius and the thickness of the disc specimen, respectively.

Strength of composite samples was measured at Universidad Politécnica de Madrid using standard three-point bending technique with 35 mm span, and free rollers. Samples were cut into bar shape of 3×3×35 mm and grinded on all surfaces. Flexural strength of composite material was measured from room temperature up to 1400 °C in vacuum and in air atmosphere.

4 Results

4.1 Suspension

For a successful electrophoretic deposition (and electrophoretic (infiltration) deposition), suitable suspension properties (zeta potential, conductivity, viscosity) are of key importance. To determine basic electrokinetic behaviour of SiC powder in aqueous media, zeta potential (ζ) and conductivity (σ) of 25 wt. % aqueous suspension of submicron SiC powder were evaluated.

The pH dependent values of ζ and σ are shown in Figure 14. Isoelectric point (IEP) of SiC in aqueous suspension was established at pH 3.8. The natural pH of aqueous SiC suspension was very near the IEP, which explains why the initial suspension was very unstable. With decreasing pH, ζ was increased up to 20 mV and by increasing pH, absolute value of ζ was increased up to 80 mV. Conductivity of the suspensions linearly slightly increased with addition of TMAH up to pH~10. Further increase in pH caused exponential increase in conductivity up to 4 $mScm^{-1}$ at pH 12. With HCl addition, the conductivity of suspension was also exponentially increased.

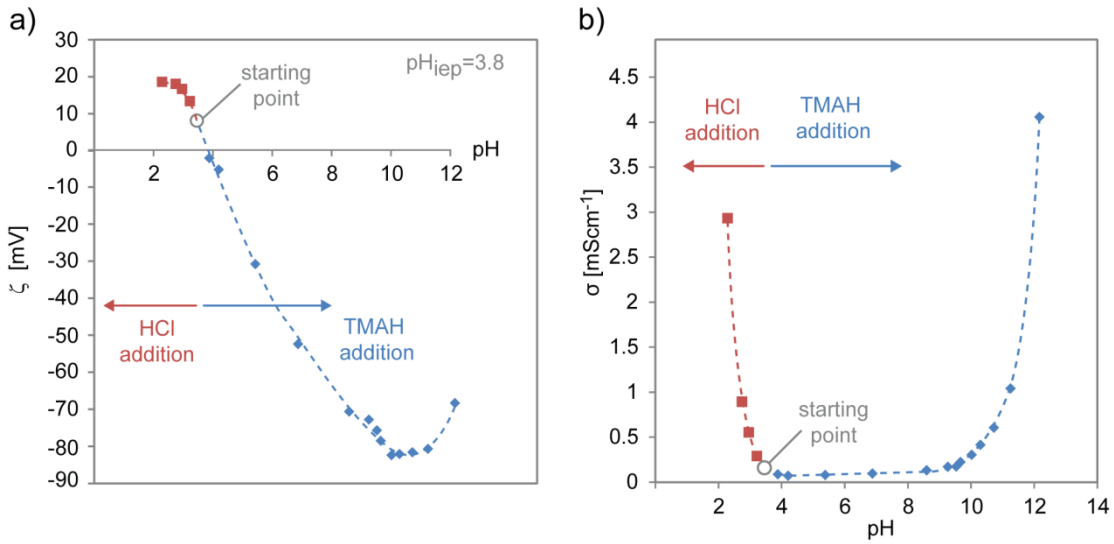

Figure 14: Dependance of ζ and conductivity (σ) as a function of pH for 25 wt. % aqueous SiC suspension.

The effect of solids loading on electrokinetic properties of SiC powder in aqueous suspensions was evaluated with aqueous suspensions with 10–70 wt. % of SiC powder in water without additives and at pH10 with addition of TMAH (suspension containing 70 wt. % of solids loading without additives could not be prepared, due to high viscosity). The effect of solids loading had a minor effect on the zeta potential (Figure 15a) for suspensions with (~-65 mV) or without additives (~20 mV). Slightly lower values were measured for suspensions containing low (< 20 wt %) or high (> 60 wt. %) solids loading.

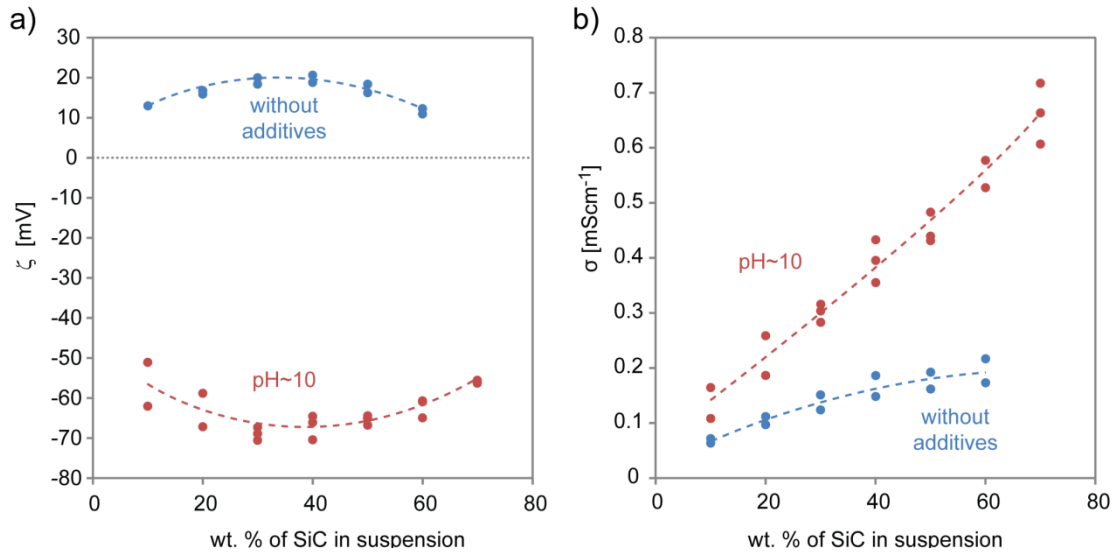

Figure 15: Zeta potential (ζ) and conductivity (σ) of aqueous SiC suspension as a function of solids loading.

By increasing the solids content in the suspension, also the conductivity increased from ~ 0.1 $mScm^{-1}$ for suspension with 10 wt. % solids loading to ~0.2 $mScm^{-1}$ at 60 wt. % solids loading for suspensions without electrolyte addition (pH ~4). The increase in conductivity was more pronounced in suspensions with addition of TMAH (pH10), where from initial 0.15 $mScm^{-1}$ the conductivity was linearly increased up to ~0.6 $mScm^{-1}$ for suspensions containing 70 wt. % of SiC powder.

To enable full infiltration of the suspension in the fibrous preform, the viscosity of the slurry should be minimised. Viscosity of dispersed SiC suspensions at pH10 gradually increased with solids loading from 0.001 Pas for suspension containing 10 wt. % of SiC powder, to 0.007 Pas for 50 wt. % of solids loading. Suspension containing 70 wt. % of solids loading exhibited a large increase in viscosity to 0.119 Pas. Due to high viscosity, suspensions with > 60 wt. % of solids loading are not suitable for electrophoretic (infiltration) deposition.

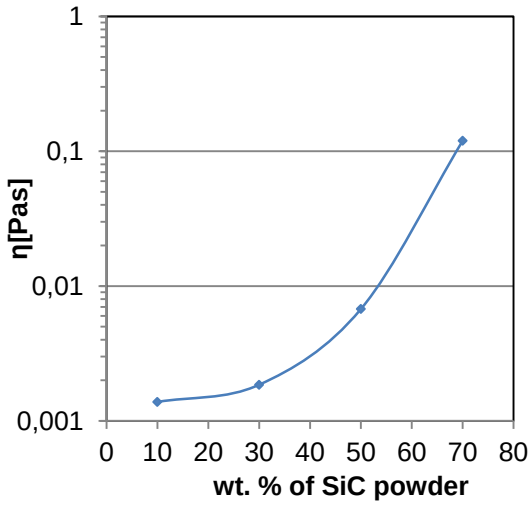

Figure 16: Viscosity of aqueous SiC suspensions at pH10 as a function of solids loading.

4.2 SiC matrix

4.2.1 Electrophoretic deposition (EPD)

Due to high price of reinforcing fibre and limited availability of the fibre preform, the processing conditions were initially determined for deposition of bulk SiC matrix and later transferred to fabrication of composite material.

The effect of suspension properties on the properties of EPD green deposits was evaluated by measuring density of dried green bodies. Regardless of the solids content in the suspension, the highest deposit densities (for individual solids loading) were obtained in the pH range of 9–11, (Figure 17 a). To determine the optimal concentration of powder in suspension, depositions were preformed from suspensions with pH10. Densities of dried green deposits increased with the amount of powder in suspension up to 50–60 wt. % where the measured density was > 60 % TD (Figure 17b). Further increase in solids loading resulted in deposits with lower packing densities. Figure 18 illustrates as deposited bulk SiC matrix formed from a suspension with 50 wt. % of solids loading at pH10, and its fracture surface (Figure 18b).

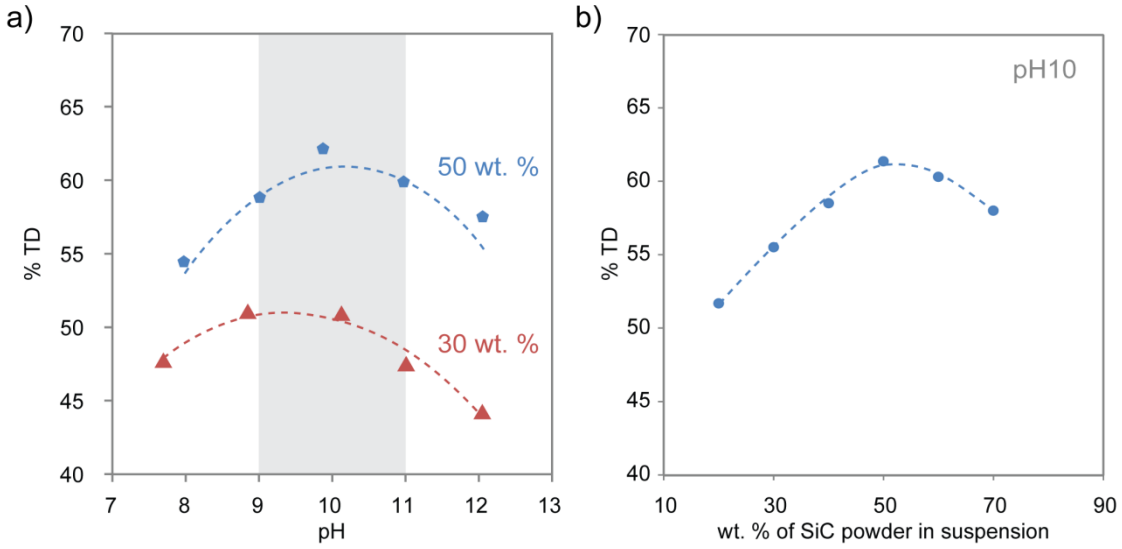

Figure 17: Green densities of deposits formed by EPD as a function of pH and solids loading.

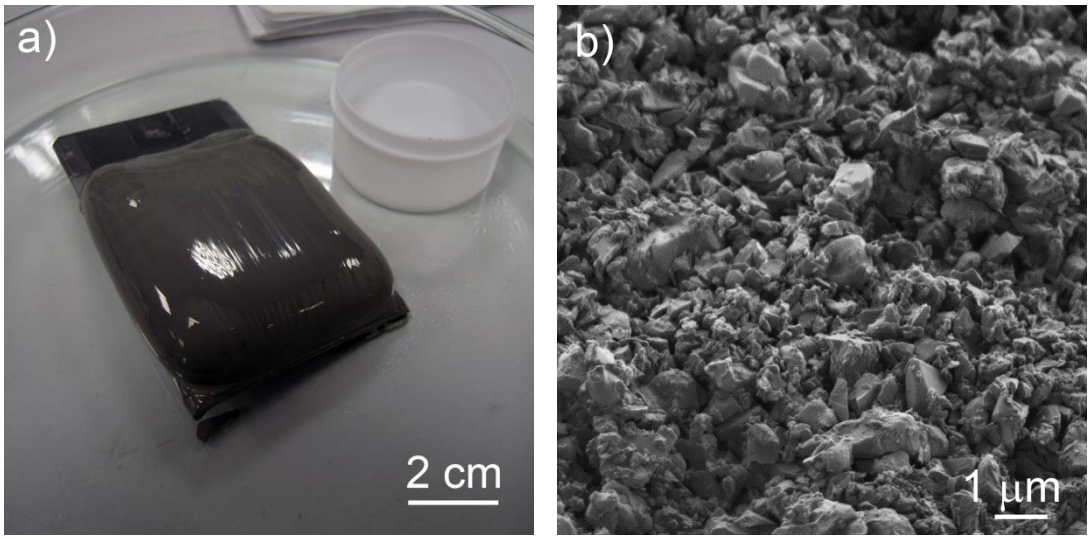

Figure 18: EPD green deposit formed from suspension with 50 wt. % of SiC powder (a) and scanning electron micrograph of its fractured surface after drying (b).

As it is evident from Figure 19a, applied current density (*j*) had no effect on the density of the deposits, however, for depositions below 2 $mAcm^{-1}$, the rate of deposition was much slower and longer times had to be employed to yield a deposit with thickness > 5 mm. Thickness of the formed deposit increased with time and applied current density (Figure 19b). At the applied current density of 4 $mAcm^{-2}$, a 9 mm thick deposit was formed in 10 min.

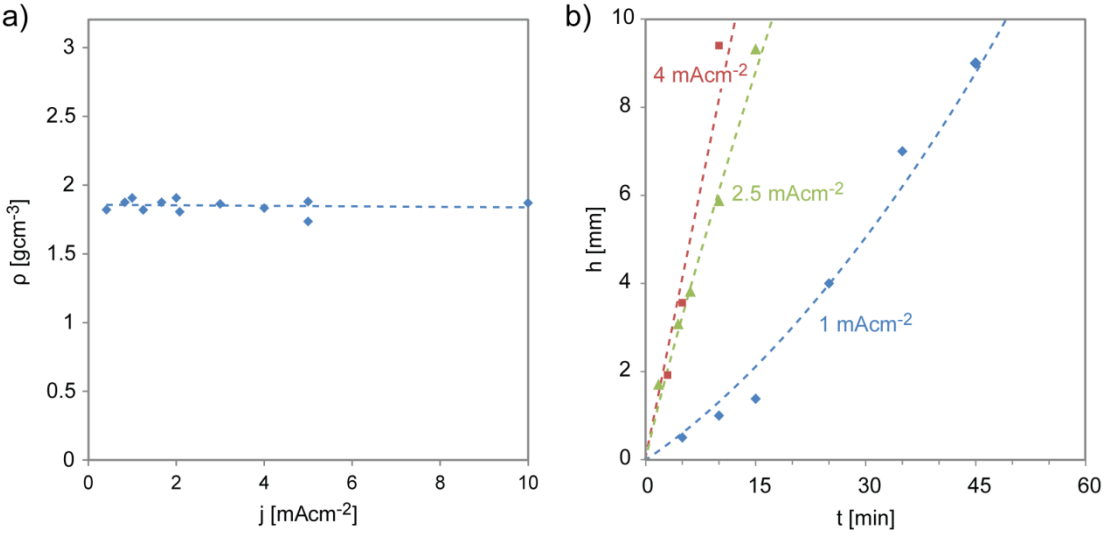

Figure 19: Green deposit density as a function of current density a) and thickness of formed deposit (h) as a function of current density and time.

In order to increase the density of green deposits, an attempt was made also by using a bimodal particle packing of submicron and nanosized SiC (nSiC) powder. The as-received nanosized SiC powder was hydrophobic and thus could not be dispersed in water. TEM examination of fibres surface revealed that the surface of nSiC powder is coated with a thin (~ 2 nm) layer of carbon (Figure 20a). Since carbon is hydrophobic in nature, the layer was burnt-off by heating the powder at 650 °C, for 30 min in air. Carbon surface layer was removed and an amorphous SiO_2 passivation layer (typical for SiC

surface, present also on submicron SiC) was formed (Figure 20b).

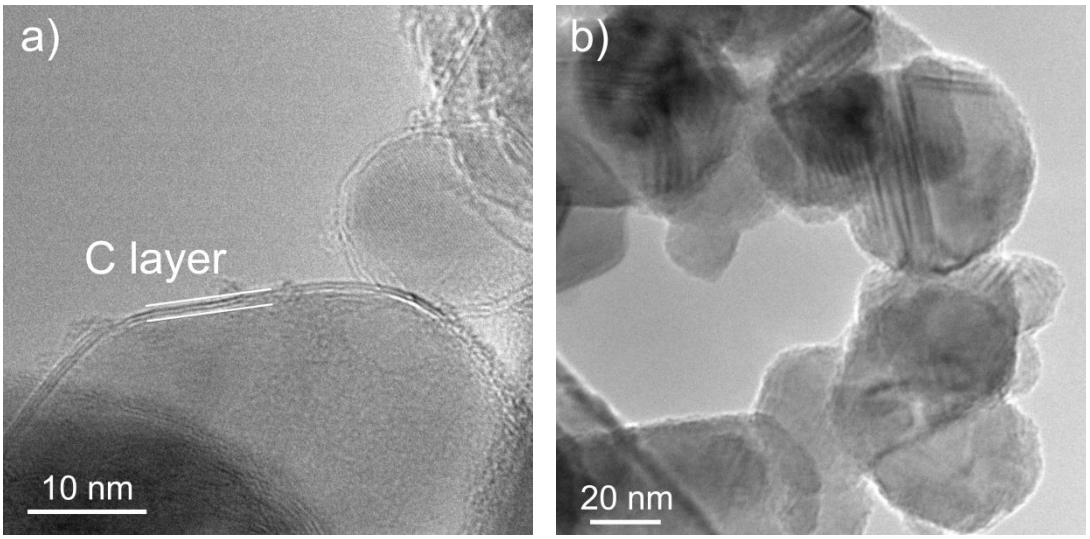

Figure 20: Transmission electron micrographs of as-received nSiC powder (a) and after heat treatment at 650 °C in air (b).

Electrokinetic properties of nanosized SiC powder (nSiC) were evaluated with aqueous suspension containing 5 wt. % of powder. Due to similar surface chemistry, the electrokinetic behaviour was comparable to the submicron powder (Figure 21). Isoelectric point was determined to be at pH 3.6, and natural pH of the suspension was 5.4. Maximum value of ζ was observed between pH 9–10, where absolute value of ζ was above 70 mV. In the same range, σ was between 0.15 and 0.5 mS/cm.

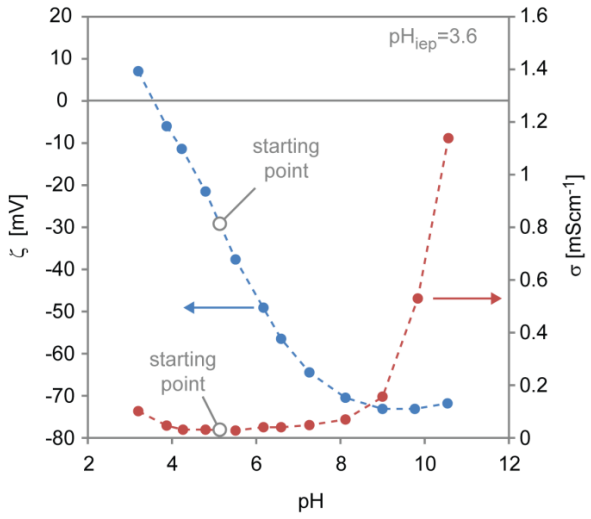

Figure 21: Dependence of ζ and conductivity (σ) as a function of pH for 5 wt. % aqueous nSiC suspension.

Electrophoretic deposition of SiC-nSiC mixtures was conducted at pH ~10. Effect of nanosized SiC addition on packing density was evaluated by measuring bulk density of green deposits. On the contrary to the expectations, the addition of nanosized powder had an adverse effect on deposit density (Figure 22). At smaller additions (up to 15 %), measured densities were only slightly lowered in comparison to deposits formed from only submicron powder, whereas at higher concentrations of nSiC, the densities were

significantly lower (< 50 %TD). Deposition of only nSiC resulted in a deposit with 43 % TD.

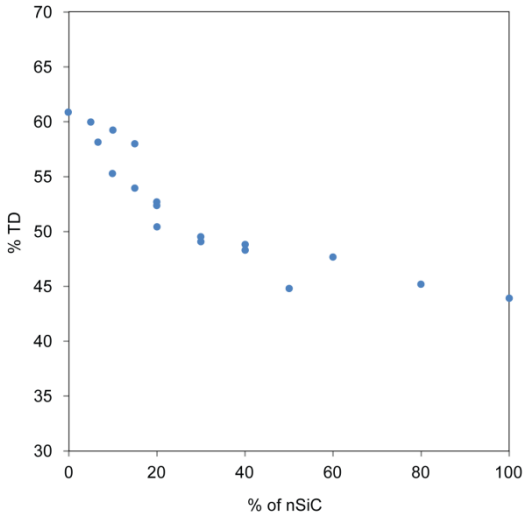

Figure 22: Density of SiC EPD green deposits as a function of amount of nSiC in the SiC-nSiC mixture.

Fracture surface of dried green deposit revealed that the nSiC powder is homogeneously distributed through the deposit and no gradient structures were observed (Figure 23). After heat treatment at 1600 °C, the nanosized powder is no longer observed and the resulting microstructure is comparable to samples without nSiC addition after pre-sintering.

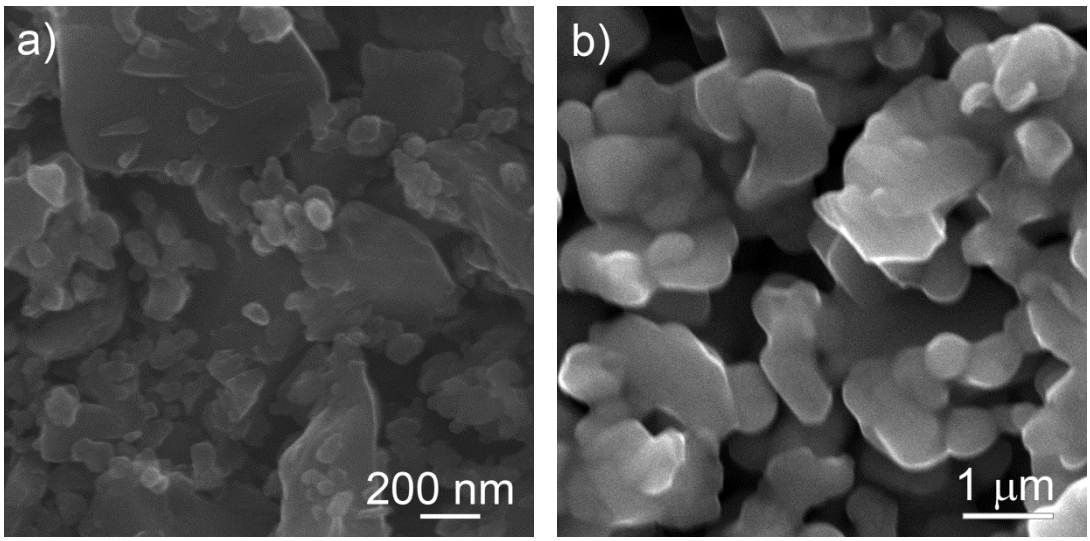

Figure 23: Fracture surface of SiC EPD deposit with 10 wt. % of nSiC a) as deposited and b) after sintering at 1600 °C.

4.2.2 Polymer infiltration and pyrolysis (PIP)

4.2.2.1 Infiltration

In order to promote the infiltration of the liquid preceramic polymer precursor into porous substrate (EPD deposit), it is desirable that there is a good wetting of the substrate with the liquid (low wetting angle) and that the liquid viscosity is as low as possible. Therefore, to reduce the viscosity, the SMP-10 polymer was heated. Shear stress measured at 30 °C as a function of shear rate in the range of 0.1 -10 s^{-1} exhibited a Newtonian fluid behaviour with viscosity of 0.086 Pas (Figure 24a). As it is evident from (Figure 24b), the viscosity of SMP-10 polymer decreased with increasing temperature up to 110 °C. Measured room temperature viscosity of as received polymer was 0.10 Pas, which decreased to 0.015 Pas at 100 °C. After heating above 110 °C, there is a sharp increase of viscosity to 0.259 Pas, most likely due to the onset of cross-linking reactions.

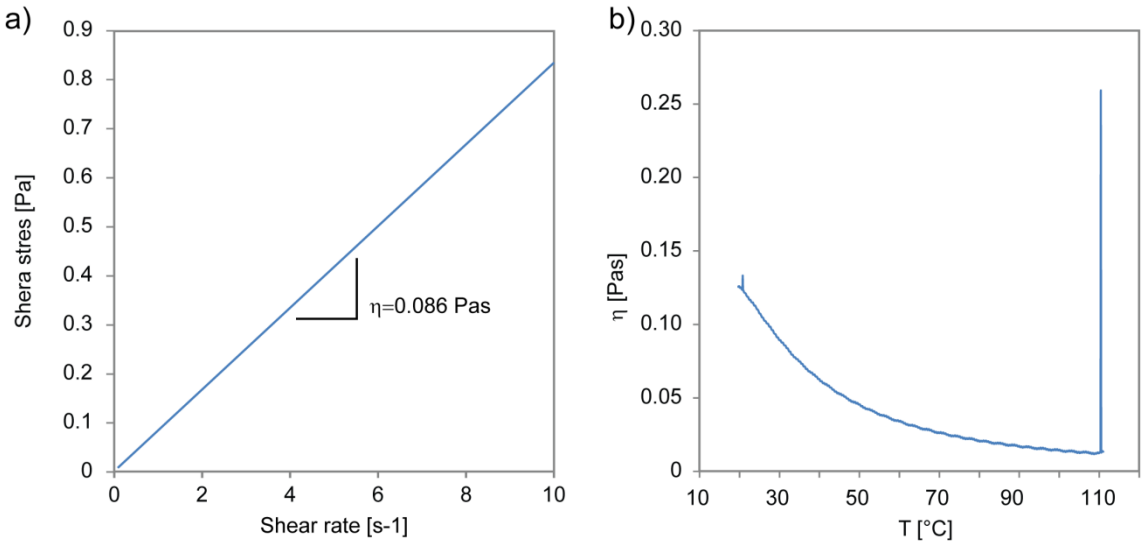

Figure 24: a) Shear stress of SMP-10 polymer as a function of shear rate measured at 30 °C and b) viscosity (η) as a function of temperature measured at shear rate of 5 s^{-1}.

SMP-10 polymer readily wets the SiC substrate with wetting angle of 19±4° (Figure 25). Comparison of wetting angle of the as-received polymer at room temperature and polymer heated at 100 °C did not show any noticeable change.

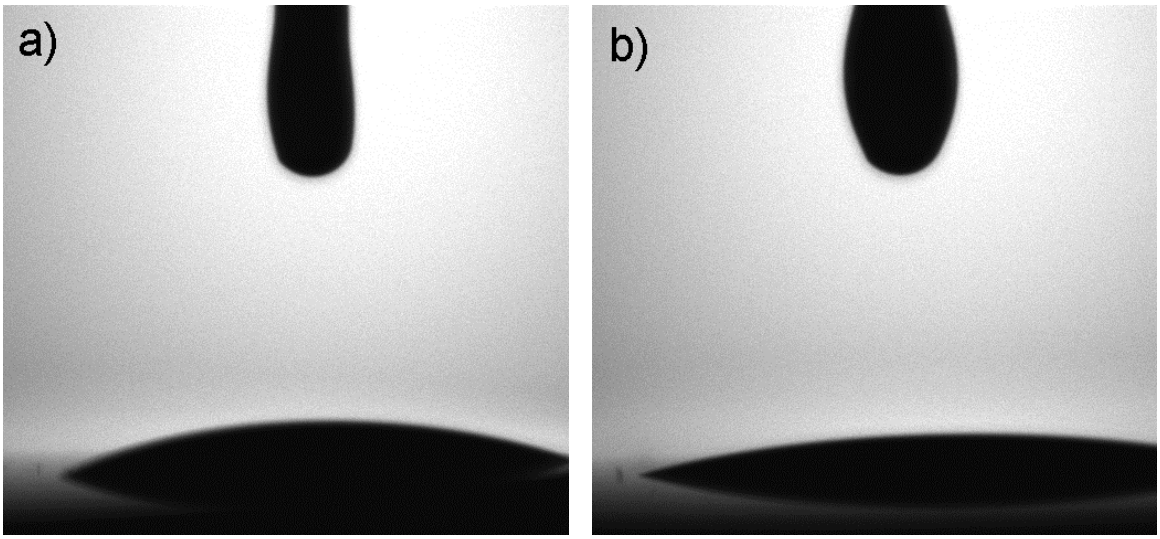

Figure 25: Wetting angle measurement of SMP-10 with SiC substrate at a) room temperature and b) 100 °C.

The effect of polymer heating and evacuation prior to infiltration on infiltration depth was examined to determine the conditions needed for full infiltration. As is evident from Figure 26, depth of infiltration was time dependent. By longer infiltration, the depth of infiltration was increased. Enhanced infiltration was observed at the edge of samples.

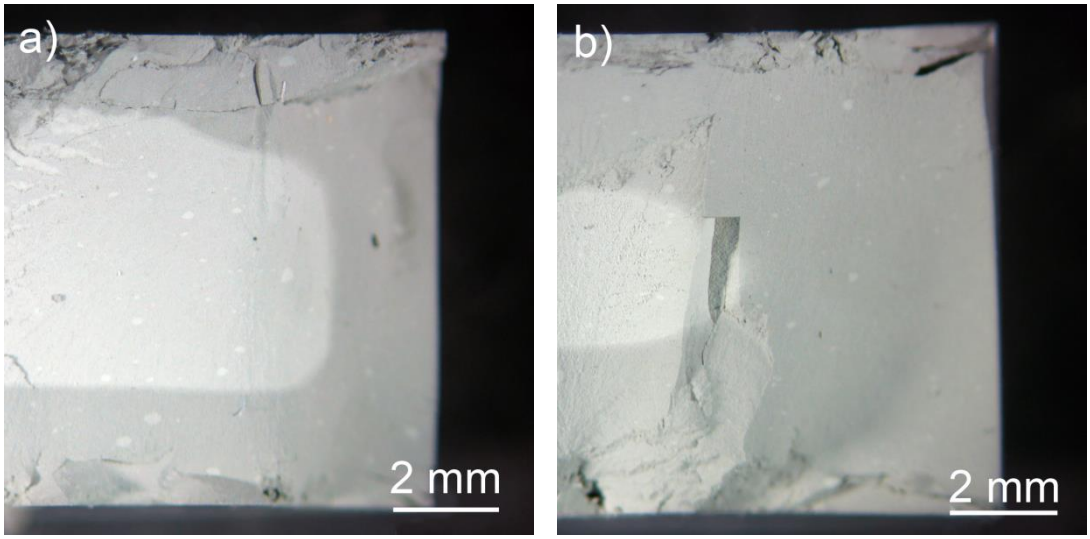

Figure 26: Fracture surface of infiltrated substrate after a) 5 min and b) 15 min of infiltration with polymer heated at 100 °C.

Figure 27 shows the influence of temperature and evacuation on infiltration depth as a function of time. Full infiltration of 1 cm thick bulk samples pre-sintered at 1700 °C with polymer heated to 100 °C was achieved after 45 minutes. Infiltration rate was reduced in the case when samples were additionally evacuated prior to infiltration, most likely due to increase in polymer viscosity, since the samples were not heated. If the polymer was not heated, infiltration was much slower and full infiltration was not achieved (even with prolonged infiltration time of 24 h).

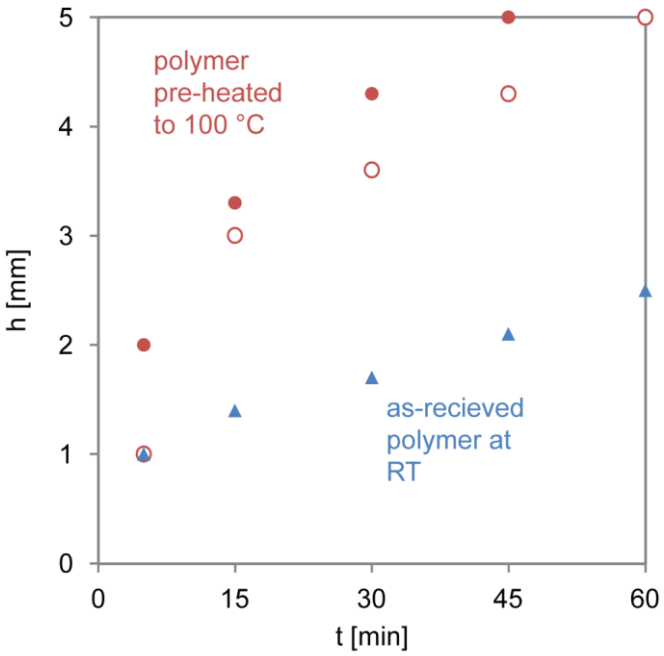

Figure 27: Infiltration depth (h) of SMP-10 polymer into pre-sintered SiC samples as a function of time (t) for as received polymer (▲) or polymer pre-heated to 100 °C, with (○) or without (●) evacuation of samples.

4.2.2.2 Polymer-to-ceramic transformation

To minimise the effect of dimensional changes during pyrolysis, the polymer-to ceramic conversion of SMP-10 polymer was studied by thermal analysis. The onset of cross-linking was observed with DSC analysis of as-received polymer precursor at 116 °C with a sharp exothermal peak at 230 °C (Figure 28). Thermo gravimetric analysis (TGA) revealed that during heat treatment up to 1000 °C in nitrogen atmosphere, there is a 28 % weight loss, which corresponds to 74.6 vol. % (taking into account the density of as-received polymer is 0.998 gcm^{-3} and density of amorphous SiC residue is 2.83 gcm^{-3}). Weight loss occurs in three major steps. From room temperature to 280 °C, there is a 10 % weight loss mainly in the region between 110 °C and 280 °C corresponding to the initial cross-linking and formation of a thermoset. Between 280 °C and 500 °C, there is major, 14 % weight loss, followed by additional 4 % weight loss after heating to 1000 °C.

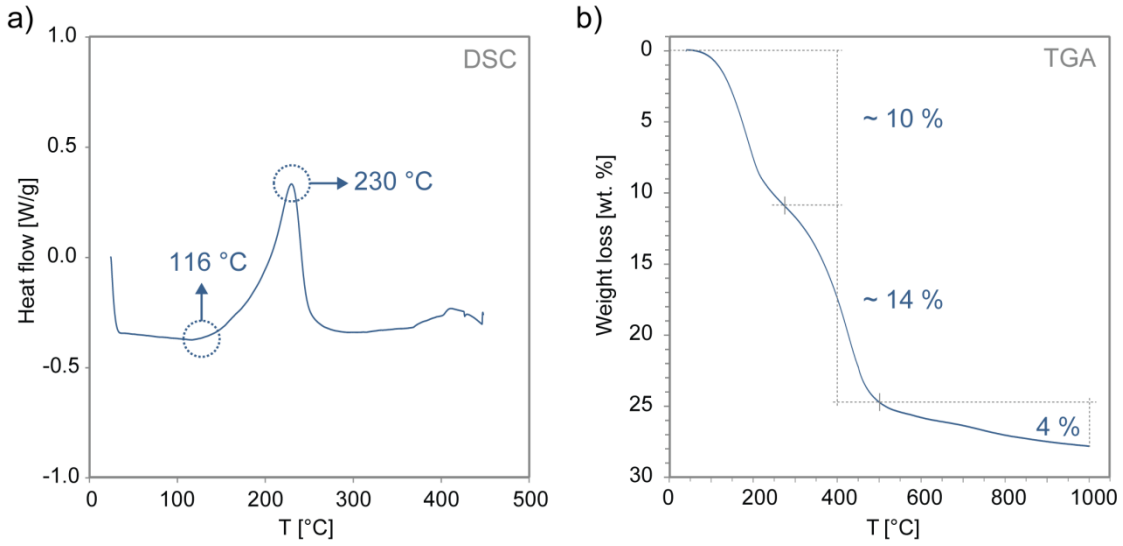

Figure 28: DSC of SMP-10 in argon and TGA analysis of SMP-10 during pyrolysis up to 1000 °C in nitrogen atmosphere.

Fourier transform infrared spectroscopy (FTIR) was performed on polymer derived material heated to 400, 600, 800, 850, 1000 and 1200 °C to study the reactions during polymer-to-ceramic transformation. The observed peaks in the ranges of 2800–3000 cm^{-1}, 2000–2140 cm^{-1} and 870–1070 cm^{-1} were attributed to C-H, Si-H and Si-C bonds (Figure 29). With increasing temperature also the intensity of the peaks increases due to higher degree of cross-linking and gradual formation of ceramic network structure. C-H and Si-H bonds are reduced with increasing temperature and disappear upon heating above 1000 °C.

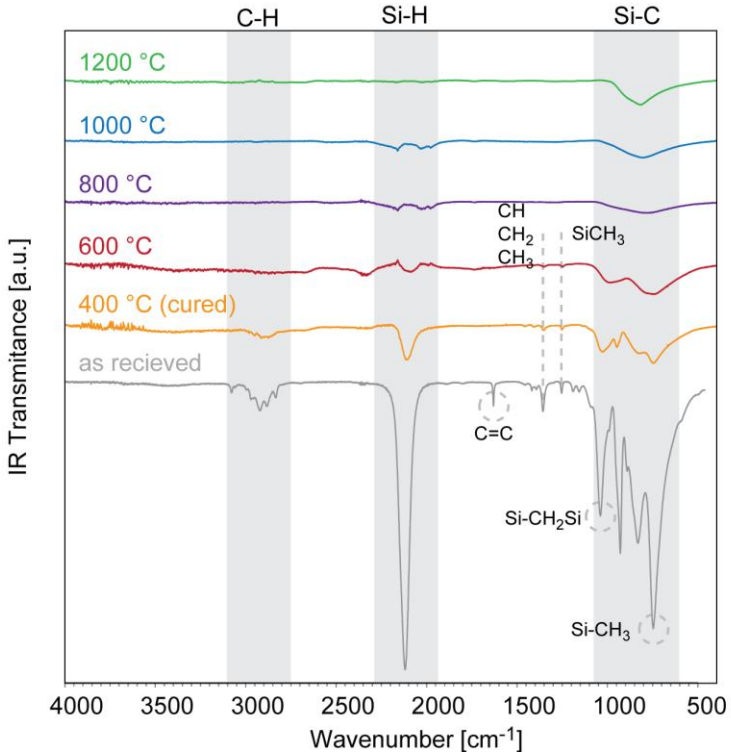

Figure 29: FTIR spectra for SMP-10 heated at 400 °C, 600 °C, 800 °C, 1000 °C and 1200 °C. The data is offset for comparison.

Figure 30 shows XRD spectra of polymer after pyrolysis and additional heat treatment at 1400 °C, 1500 °C, 1600 °C, 1700 °C and 1800 °C. After pyrolysis at 1000 °C, greatly diffused peaks indicating amorphous structure of the ceramic are seen. After additional heat treatment of amorphous polymer derived SiC, the peak intensity increases. The crystallite size of samples heat-treated at temperatures above 1500 °C was calculated using the Debye-Scherrer equation. The crystallite sizes were found to be approximately 4, 10, 30 and 50 nm at 1500 °C, 1600 °C, 1700 °C and 1800 °C respectively. In the diffraction pattern of powder residue after heating to 1800 °C contains also a minor peak at 2θ 33.65 °, which corresponds to the 100 plane of 6H Moissanite (α-SiC).

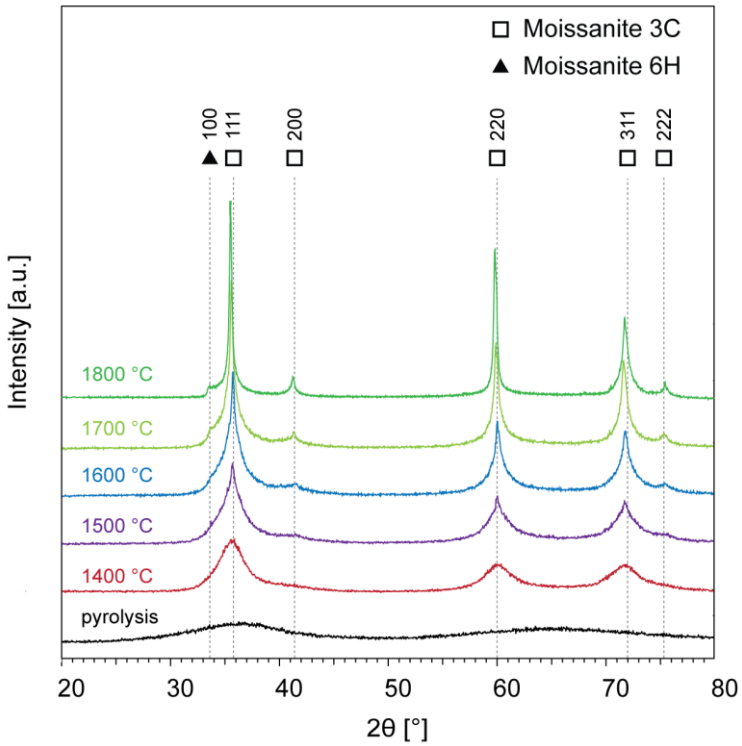

Figure 30: XRD of SMP-10 polymer and SiC matrix infiltrated with SMP-10, heat-treated at different temperatures. The data is offset to aid comparison.

Amorphous nature of pyrolysed SMP-10 after heat treatment at 1000 °C was also confirmed by transmission electron microscopy (TEM) (Figure 31a). TEM of SMP-10 polymer heat-treated at 1600 °C reveals large areas of well-ordered nanocrystalline β-SiC (Figure 31b). A rough estimate of the crystal size supports the crystal size determined by powder diffraction.

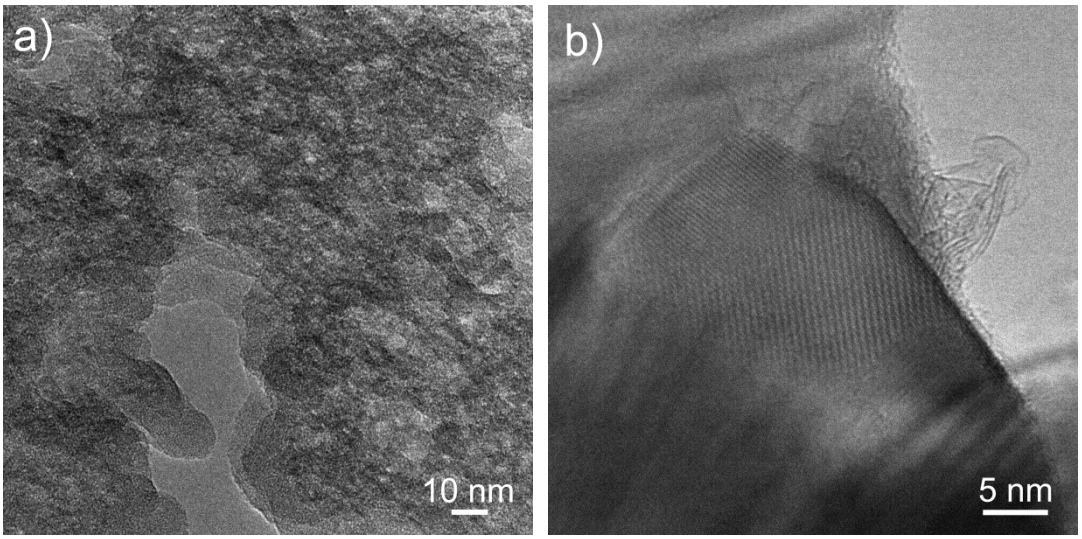

Figure 31: Transmission electron micrographs of SMP-10 polymer heat treated at a) 1000 °C and b) 1600 °C.

Microstructure of the EPD deposit infiltrated with SMP-10 after pyrolysis and crystallization shows that the space between the initial SiC grains is filled with amorphous polymer-derived SiC after pyrolysis (Figure 32a). After crystallization at 1600 °C, the microstructure reveals well-faceted, connected SiC grains (Figure 32b). The contrast change in SiC grains under transmission electron microscope (TEM) indicates the presence of stacking faults.

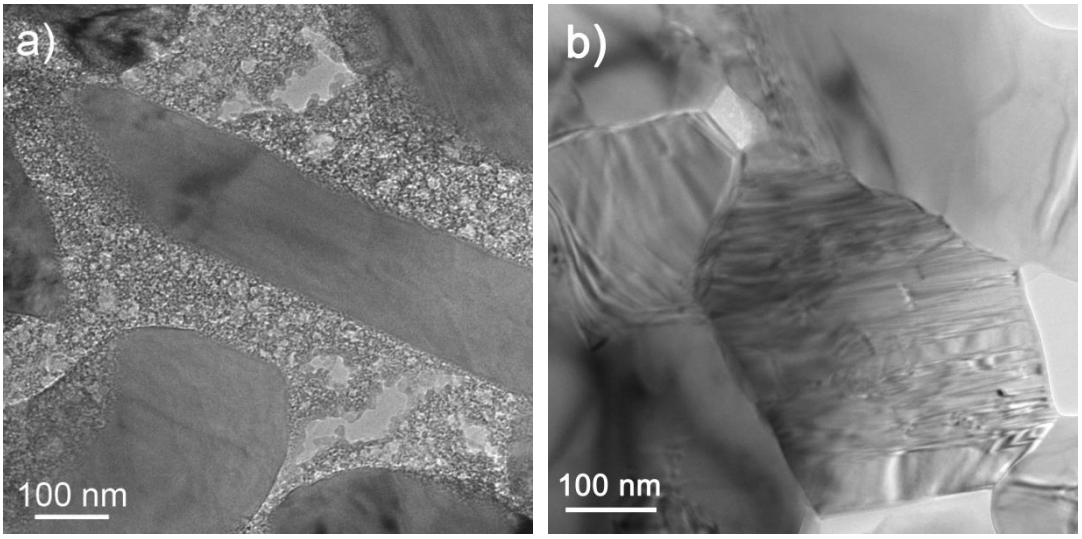

Figure 32: Transmission electron micrograph of EPD sample infiltrated with SMP-10 polymer after a) pyrolysis and b) crystallization.

In addition, the comparison of the appearance of the fracture surfaces of the green EPD-formed part and the body after the first PIP cycle (EP1) confirms that the preceramic polymer deposits onto the SiC particles, resulting in SiC grain growth to form well-faceted SiC grains. The transmission electron micrographs of the EP1 sample (Figure 33c) in comparison to the SiC (BF12) powder (Figure 33a) also indicate a minor increase in grain size, which appears to be the result of the epitaxial crystallization of the polymer precursor on the surface of the SiC particles.

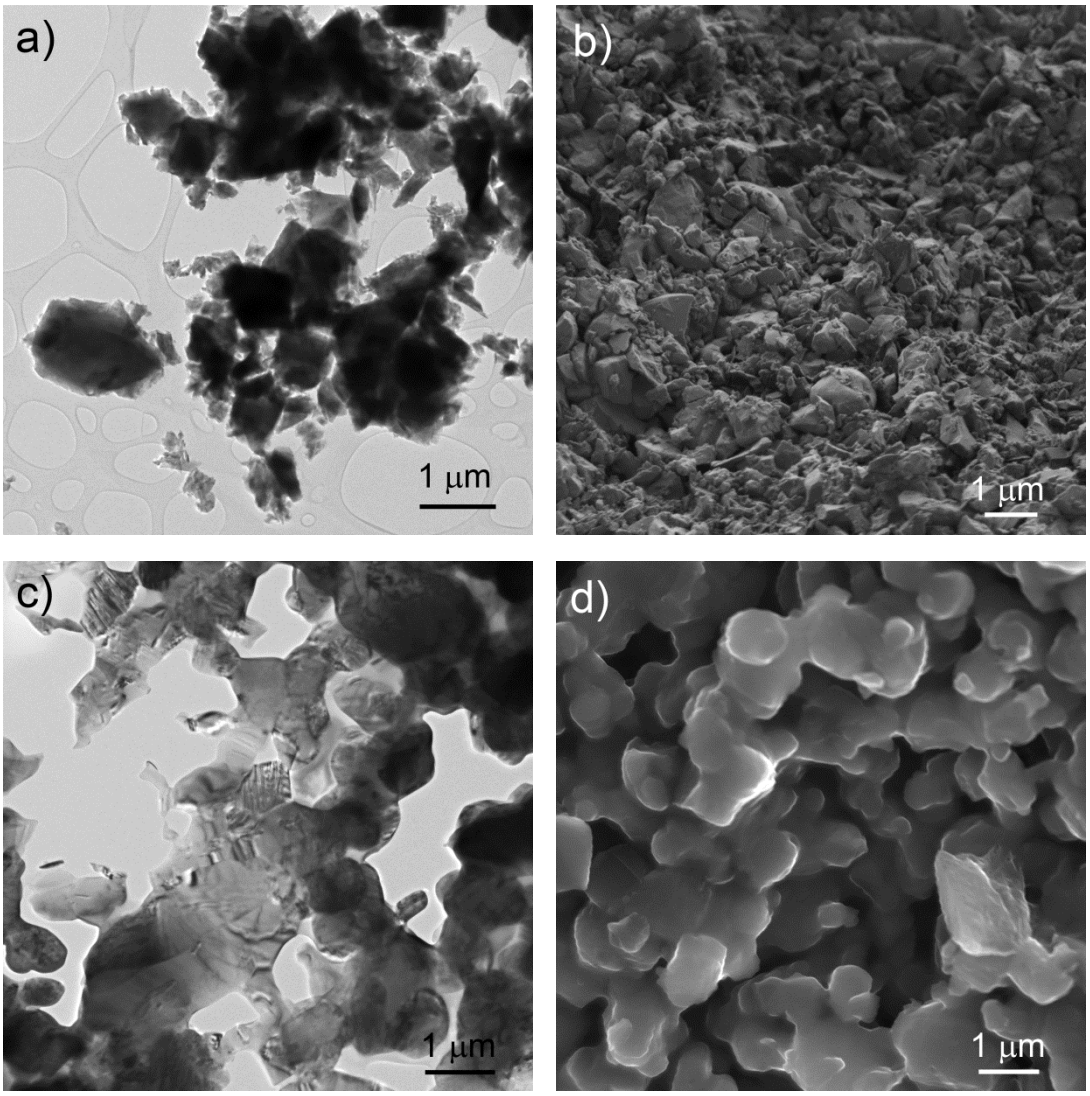

Figure 33: Transmission electron micrograph of BF12 powder (a); scanning electron micrograph of a fracture surface of EPD green deposit (b); transmission and scanning electron micrographs of EP1 sample fracture surface after crystallization (c), (d), respectively.

Even though the infiltration and the resulting densification and increase in strength were achieved, the samples after pyrolysis were extensively cracked after first PIP cycle. In order to overcome this drawback, the samples were pre-sintered prior to PIP processing. Figure 34 shows that extensive cracking during PIP processing observed at samples without pre-sintering (Figure 34a) was avoided by pre-sintering of EPD samples at temperatures above 1600 °C.

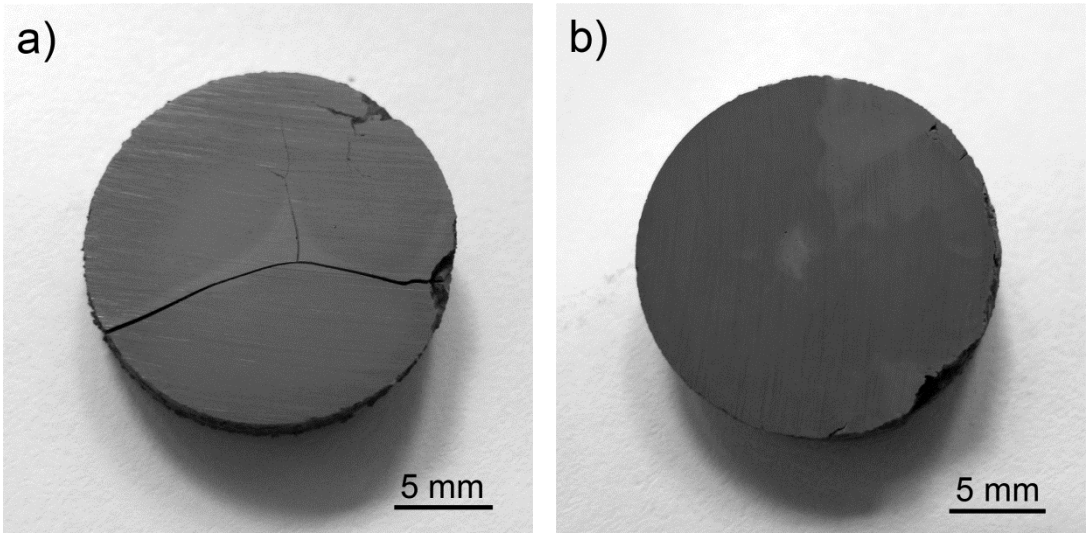

Figure 34: Optical micrographs of sample after densification with one PIP cycle (EP1), without a) and with pre-sintering b).

Pre-sintering resulted in neck-formation (Figure 35) which provided sufficiently high strength to withstand the stresses during polymer-to-ceramic conversion. By pre-sintering, the particles coalesced together and facetation of grains (Figure 35b) occurred resulting in increased pore size beneficial for further infiltration with polymer precursor.

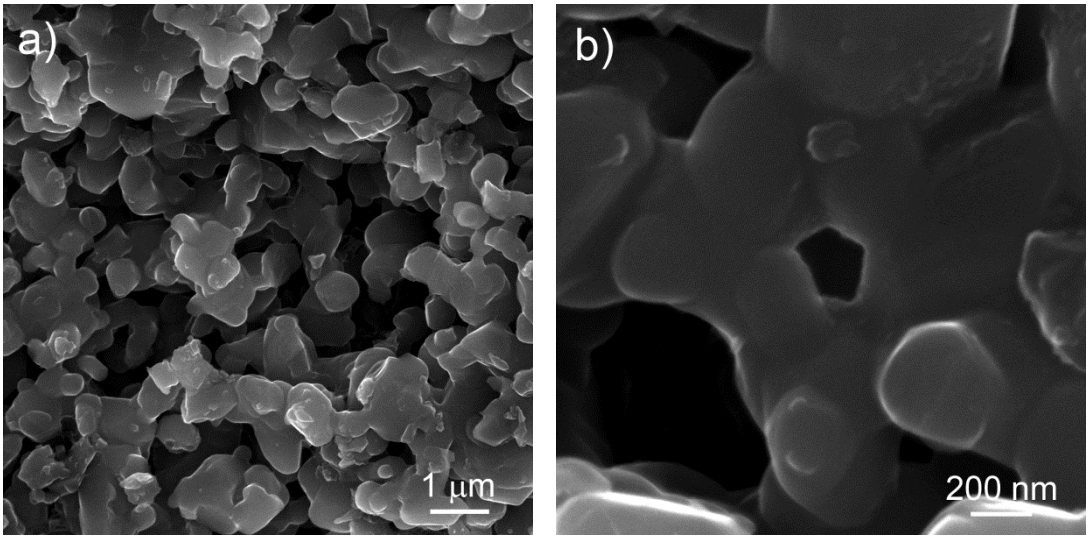

Figure 35: Fracture surface of pre-sintered EPD deposit at different magnifications.

4.2.3 Density & porosity

For successful densification of SiC matrix, several PIP cycles were needed due to large shrinkage of the polymer during heat treatment. As it is evident from Figure 36, density of the sample densified by one PIP cycle (EP1) increased from initial density of 62 %TD of EPD deposit to ~ 67 %TD. Gradual increase in density was observed after each PIP cycle up to six cycles (EP6) when it reached a plateau. After nine PIP cycles (EP9), there was no noticeable increase in density in comparison to samples densified only by six cycles. Due to this fact and the fact that multiple PIP cycles are associated with very long processing times, in further experiments only six PIP cycles were employed for densification.

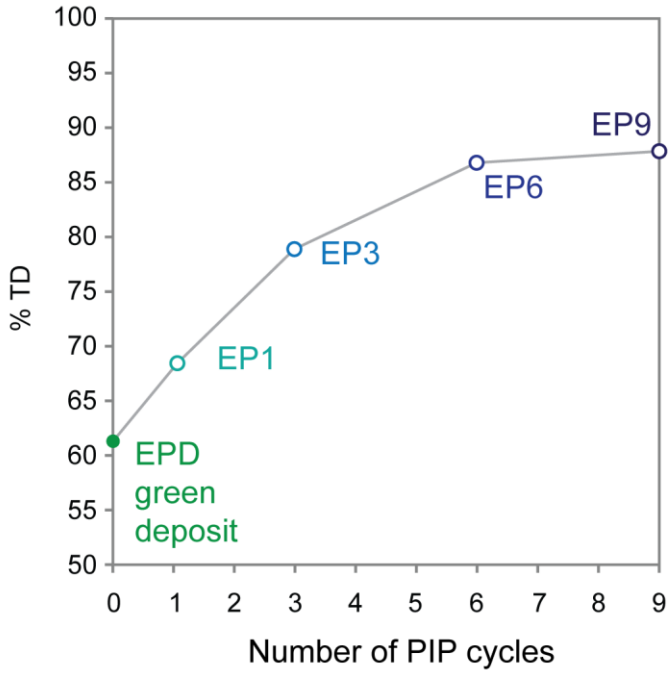

Figure 36: Densification of SiC matrix with number of PIP cycles.

Increase in density was also observed by microstructural investigation of polished cross sections of samples densified with different number of PIP cycles. By comparison of the microstructures of samples after one (EP1) or six PIP cycles (EP6) (Figure 37) it is evident that the density is increased and the amount of porosity is reduced.

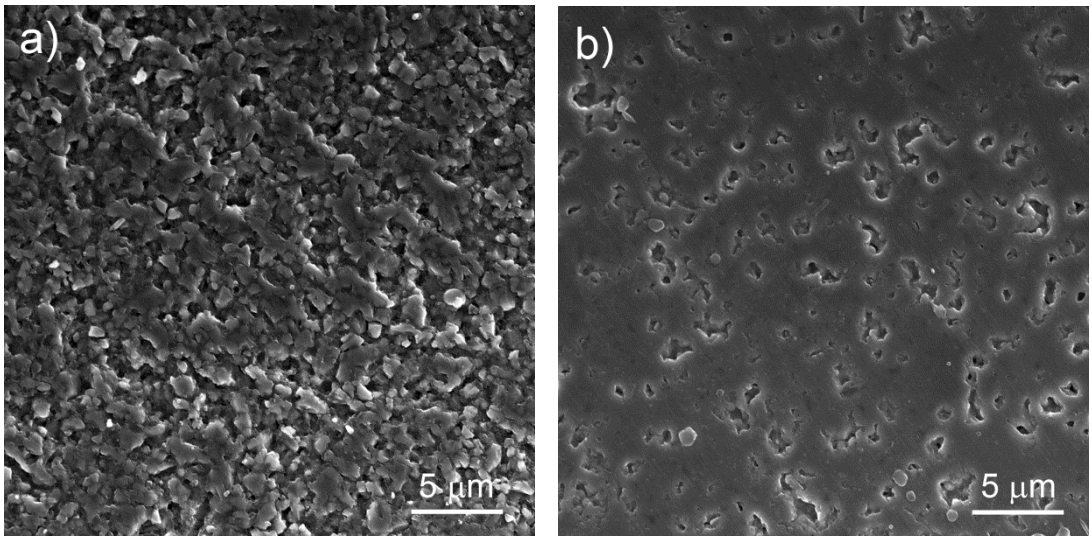

Figure 37: Microstructure evolution with densification after a) one PIP cycle (EP1) and b) six PIP cycles (EP6).

Porosity evolution in the densification steps reveals that during pre-sintering at 1600 °C and 1700 °C, the median pore size increased from initial 60 nm to 144 nm and 224 nm, respectively. During each consecutive PIP cycle, porosity and pore size were reduced achieving ~13.5 % porosity with pore size 80 nm after 6 PIP cycles.

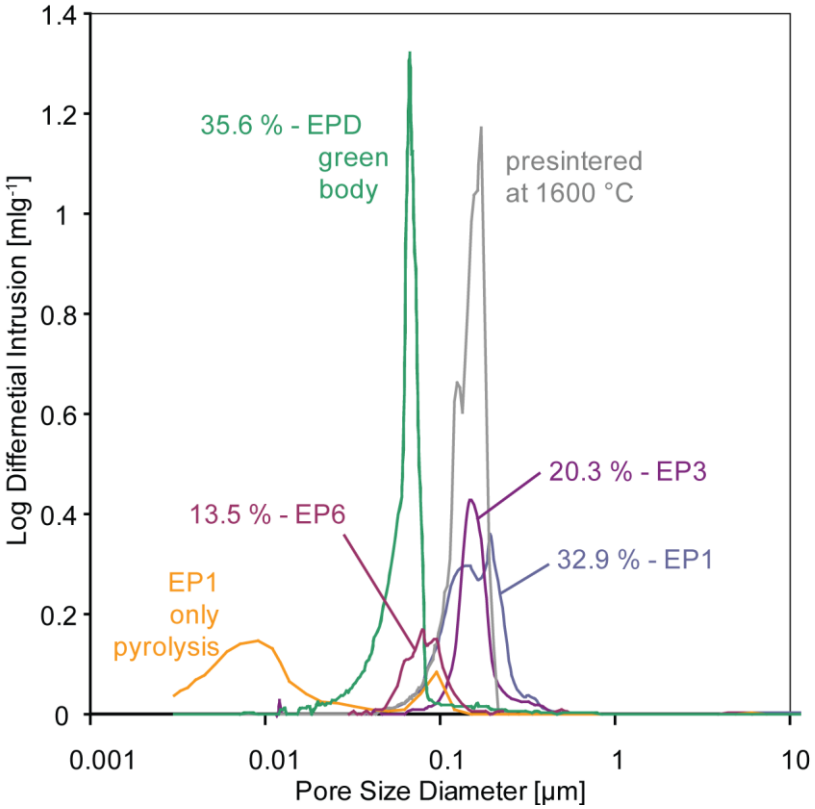

Figure 38: Evolution of porosity during densification with maximum heating temperature of 1600 °C.

4.2.4 Active filler controlled pyrolysis (AFCOP)

Since further processing of samples densified with six PIP cycles did not result in a sufficient increase in density of the material and in order to avoid long processing times associated with repetition of several PIP cycles, faster and a more efficient densification would be desirable. One of the possible paths towards this goal is the use of active filler controlled pyrolysis, which suggests the use of so-called active filler materials which react with pyrolysis byproducts and thus compensate for the shrinkage of the polymer during pyrolysis. Due to limited selection of elements that ensure low neutron activation of fusion relevant material, W and $CrSi_2$ were selected.

4.2.4.1 Chromium silicide ($CrSi_2$)

In order to utilize active filler in the densification of SiC matrix, it has to be electrophoretically co-deposited with SiC. To assess the feasibility of co-deposition, ζ of aqueous suspension of $CrSi_2$ was measured and compared to ζ of SiC. $CrSi_2$ exhibited similar electrokinetic behaviour in aqueous suspensions as SiC, achieving the highest ζ of -73 mV at pH11.5 (Figure 39). Suspensions with active filler to SiC ratio of 15/85 and 30/70 were prepared. The solids content of powders in the suspensions was kept constant at 50 wt. %. Aqueous solution of tetramethylammonium hydroxide (TMAH) was used to increase the pH of the suspensions. The SiC suspensions containing $CrSi_2$ were deposited at pH10 where both used powders exhibited high ζ and conductivity of the mixed suspension was 0.6 $mScm^{-1}$. Scanning electron micrographs of the fracture surface of deposit reveal a good dispersion of $CrSi_2$ within the SiC matrix (Figure 40).

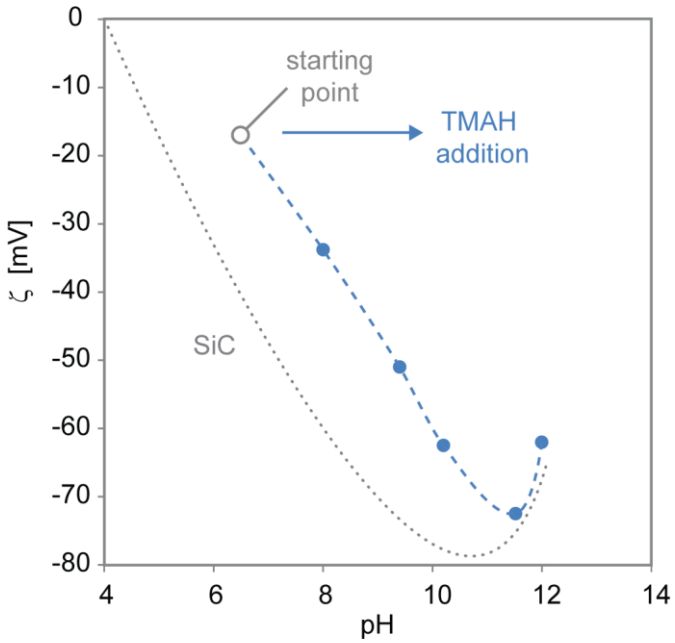

Figure 39: Zeta potential (ζ) as a function of pH for 5 wt. % $CrSi_2$ aqueous suspension.

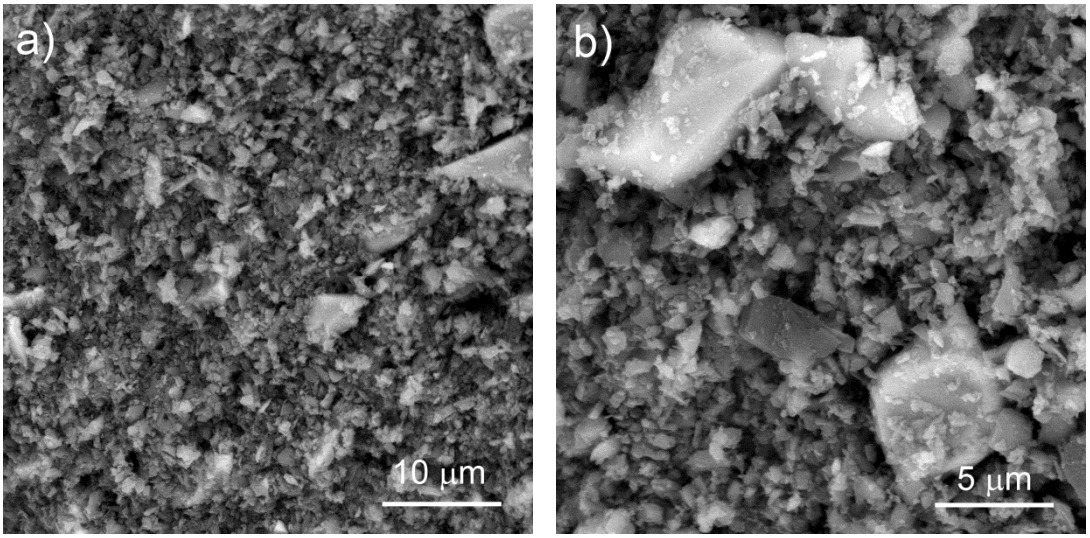

Figure 40: Backscattered scanning electron micrograph of co-deposited $CrSi_2$-SiC composite fracture surface. Larger, light grey particles represent $CrSi_2$.

Since the melting temperature of $CrSi_2$ is 1475 °C [107] and the molten $CrSi_2$ formed clusters within the matrix after heat treatment at 1600 °C, the samples containing $CrSi_2$ were pre-sintered at 1400 °C. Microstructural investigation of fracture surfaces after PIP revealed that $CrSi_2$ acted only as passive filler and did not react with pyrolysis byproducts. However during additional heat treatment 1600 °C the $CrSi_2$ reacted with SiC to some extent. At the surface of the sample there was a formation of a ~ 50 µm relatively dense layer with larger areas of SiC and Cr_3C_2. $CrSi_2$ inside the sample also formed larger clusters of a Cr-Si-C phase which could not be identified. The XRD analysis of the sample showed mostly SiC, however there were a few peaks that could not be resolved with available XRD library.

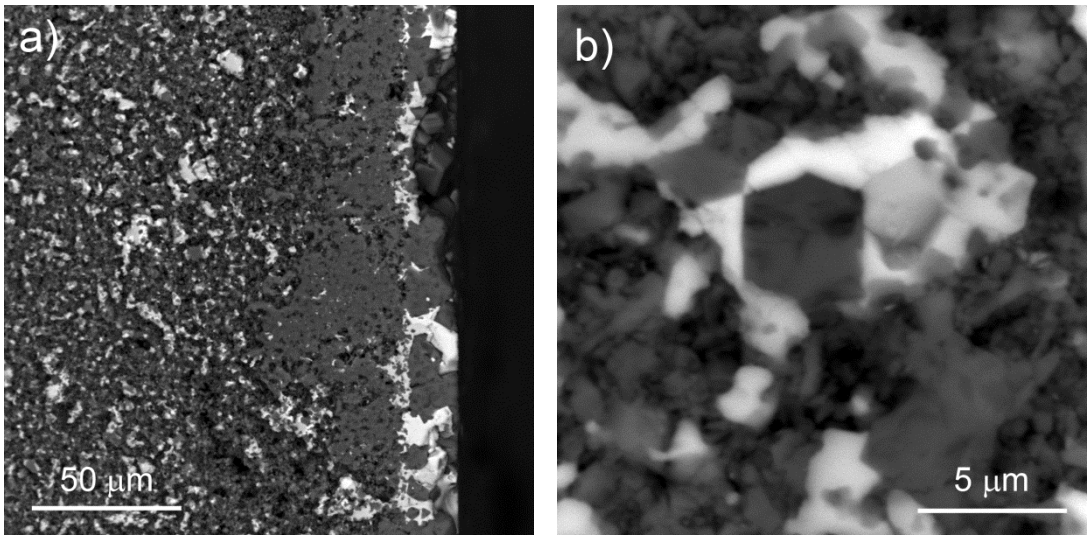

Figure 41: Backscattered scanning electron micrograph of co-deposited $CrSi_2$-SiC composite after crystallisation at different magnifications. Light colour represents chromium rich areas.

4.2.4.2 Tungsten (W)

The use of tungsten as active filler material was initially evaluated using dry-pressed samples with different W-SiC ratios. W reacted with preceramic polymer and polymer derived SiC and formed a composite matrix material, composed of W, SiC, WSi_2, W_5Si_3, WC and W_2C. Samples with high W concentration (> 90 wt %) resulted in a nearly fully dense material composed of W, W_5Si_3 and W_2C, already after one PIP cycle, however during densification there was also ~ 10 % shrinkage of the sample. At lower W concentrations (< 50 vol. %), the resulting material was composed of WSi_2, WC and SiC and no shrinkage was observed. Material with high tungsten concentration exhibited good mechanical properties (flexural strength of 340 MPa, hardness of 1100 HV and E-modulus of 269 GPa) and increasing thermal conductivity from room temperature (15 $Wm^{-1}K^{-1}$) to 1000 °C (25 $Wm^{-1}K^{-1}$). The increase in thermal conductivity with temperature could be especially beneficial in combination with SiC since its thermal conductivity at high temperatures is decreased.

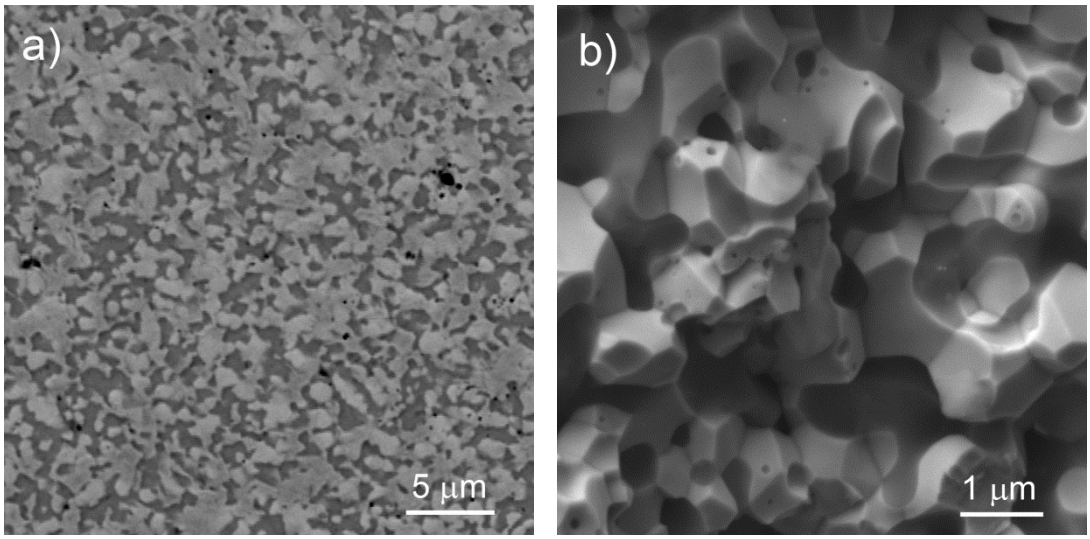

Figure 42: Polished cross section and fracture surface of a pressed W after densification by PIP at different magnifications.

In the case of tungsten it is impossible to use an aqueous suspension for EPD, due to tungsten oxidation [108], therefore, ethanol was used to prepare the suspensions. Since W is a metal, only relative values of ζ_p could be measured using arbitrary value of dielectric constant, therefore electrophoretic mobility (independent of dielectric constant) was used to evaluate probability of deposition. Without additives W and SiC exhibited electrophoretic mobility with opposite sign (-0.23×10^{-8} and 0.59 SI$\times10^{-8}$ $m^2V^{-1}s^{-1}$, respectively). Citric acid (CA) was used to reverse the surface charge of W, since it was already demonstrated that addition of citric acid yields a high density deposits of SiC from ethanol suspension [109]. After the addition of 0.1 wt. % of citric acid, the electrophoretic mobility of W and SiC were 0.022×10^{-8} $m^2V^{-1}s^{-1}$ and 0.202×10^{-8} $m^2V^{-1}s^{-1}$, respectively. Cathodic deposition of mixed suspension with the addition of CA resulted in a successful co-deposition with homogeneous distribution of W particles in SiC matrix (Figure 43), however deposition from ethanol resulted in lower green densities in comparison to aqueous deposition of SiC and resulting porosity after PIP processing was higher than in the samples without W.

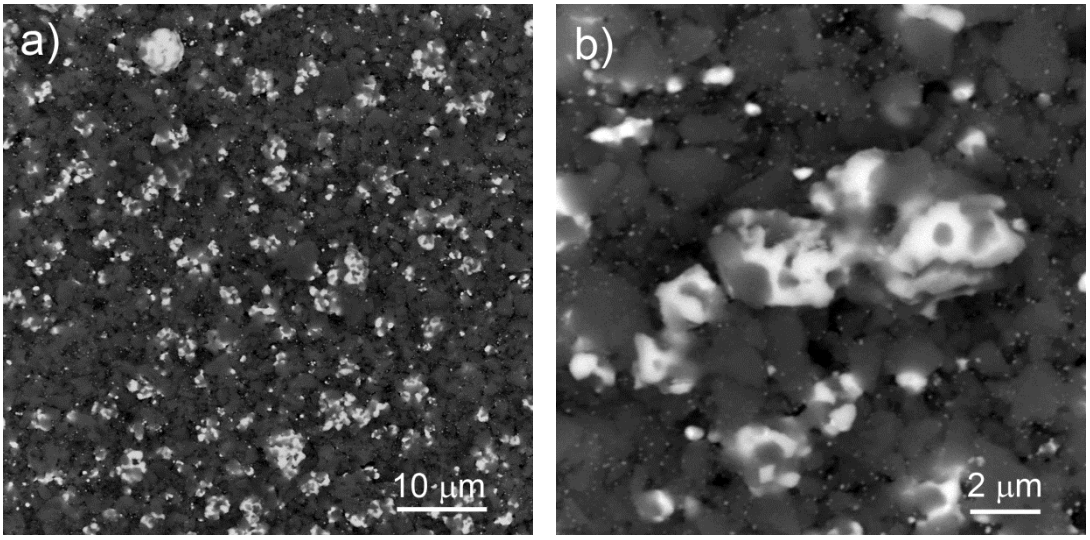

Figure 43: Backscattered scanning electron micrograph of co-deposited W-SiC composite after heat treatment at 1600 °C at different magnifications. Light colour represents W-rich areas.

4.2.5 Mechanical properties of SiC matrix

Mechanical properties of SiC matrix were evaluated after one, three and six PIP cycles. With increasing the density of the material also the mechanical properties were increased (Figure 44). Samples densified with maximal heating temperature of 1600 °C (temperature of pre-sintering and additional heat treatment), exhibited a large scattering in measured values, especially after more PIP cycles were performed. After six PIP cycles (EP6) the measured values varied from 62.7 MPa to 391.4 MPa. Samples densified at 1700 °C showed more uniform failure behaviour. After three PIP cycles (EP3) average measured value was 277.12±113.1 MPa with the highest measured value of 390.2 MPa. After six PIP cycles (EP6) the average strength of the samples was 336.6±74.6 MPa, with highest measured value of 411.2 MPa.

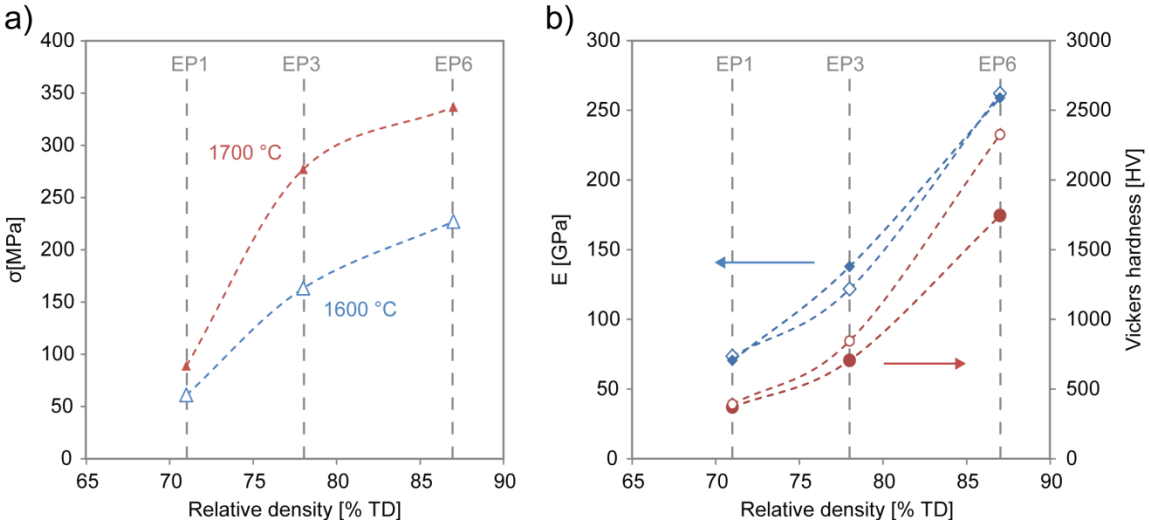

Figure 44: Evolution of flexural strength, Young's modulus and Vickers hardness measured at room temperature. Open symbols represent samples densified at 1600 °C and full symbols represent samples densified at 1700 °C.

In majority of the cases fracture was initiated at or very near the tensile surface plane underneath the loading ball (Figure 45). In the case of samples densified at lower temperature (1600 °C), the fracture was also initiated at defects deeper in the samples. Failure with two-fold symmetry was the most dominant (Figure 45), however disks broke also into three or more pieces. The number of fracture pieces increases with measured strength, due to stored elastic energy [106].

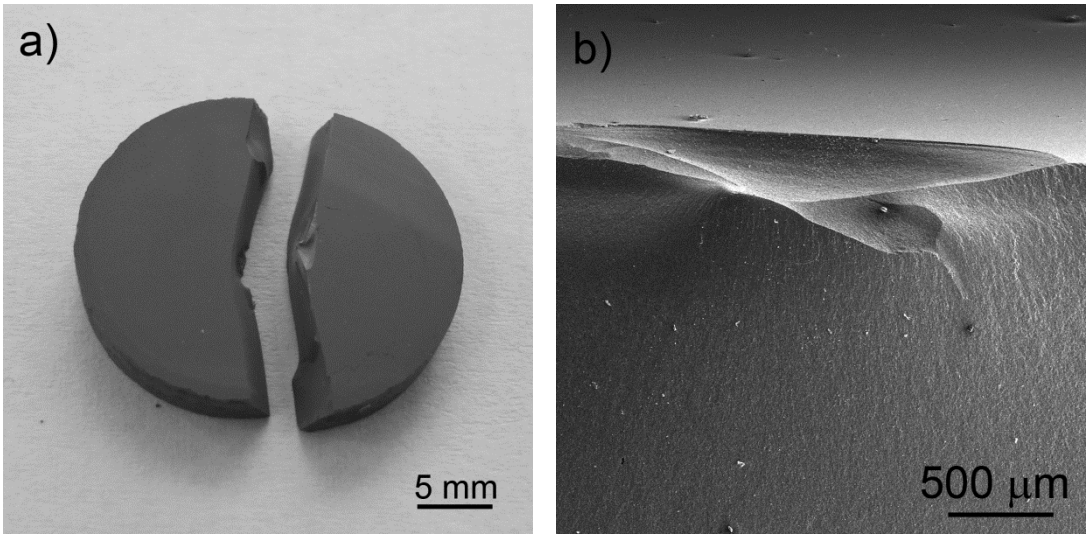

Figure 45: Fracture pattern and the fracture origin.

Samples densified at 1600 °C or 1700 °C exhibited nearly the same values of elastic modulus (Figure 44). From initial value of 70 GPa after one PIP cycle, elastic modulus was increased up to 260 GPa after six PIP cycles. Microhardness measurements of samples heat treated at 1600 °C also show an increase with density. From initial value of ~390 HV after one PIP cycle the value was increased to 845 HV and 2300 HV after three and six PIP cycles respectively. In the case of samples densified at 1700 °C, hardness values after one PIP cycle were comparable to the ones densified at 1600 °C. After additional densification, values of microhardness were slightly lower than for the samples

densified at 1600 °C achieving 706 HV and 1740 HV after three and six PIP cycles respectively.

4.2.6 Thermal properties

Effect of densification and crystallinity of samples on thermal transport properties was evaluated by measuring thermal conductivity of the matrix at room temperature. The sample, which was subjected only to densification by pyrolysis at 1000 °C (polymer derived SiC is amorphous) without pre-sintering or crystallisation exhibited a low thermal conductivity of 8 $Wm^{-1}K^{-1}$. By additional heat treatment at 1600 °C and crystallisation of the polymer derived SiC, the conductivity increased to 34 $Wm^{-1}K^{-1}$ already after one PIP cycle (EP1). Further densification with consecutive PIP cycles further resulted in a gradual increase in the thermal conductivity, achieving nearly 60 $Wm^{-1}K^{-1}$ after six PIP cycles (EP6) (Figure 46).

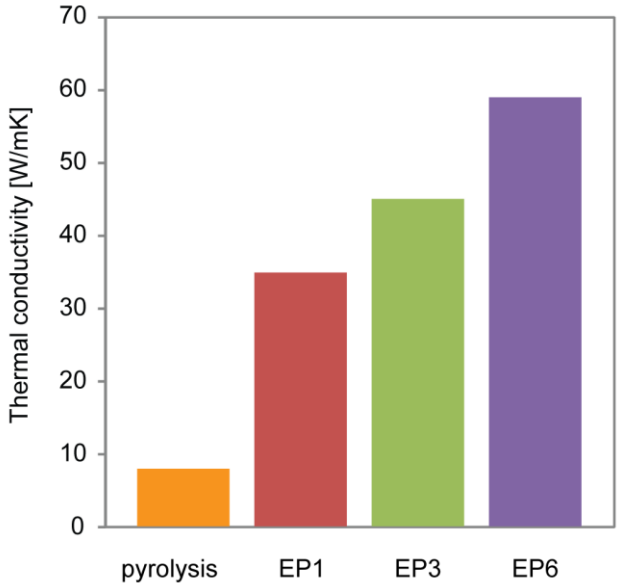

Figure 46: Increase in room temperature thermal conductivity as a function of densification.

4.3 Silicon carbide fibre reinforced silicon carbide composite

4.3.1 Electrophoretic (infiltration) deposition (EP(I)D)

Findings obtained in the densification of bulk SiC matrix material prepared by combination of electrophoretic deposition and polymer infiltration and pyrolysis were used as starting point for the fabrication of SiC_f/SiC composite.

The goal of electrophoretic (infiltration) deposition is to successfully fill the voids between the fibres (intrabundle area) and fibre bundles (interbundle area) with SiC powder prior to densification by polymer infiltration and pyrolysis process. The procedure of suspension optimisation and electrophoretic deposition for the fabrication of bulk SiC described above, was adapted to form SiC matrix within porous fabric preform. Further infiltration specific issues were addressed in order to optimise the infiltration of powder into fabric preform.

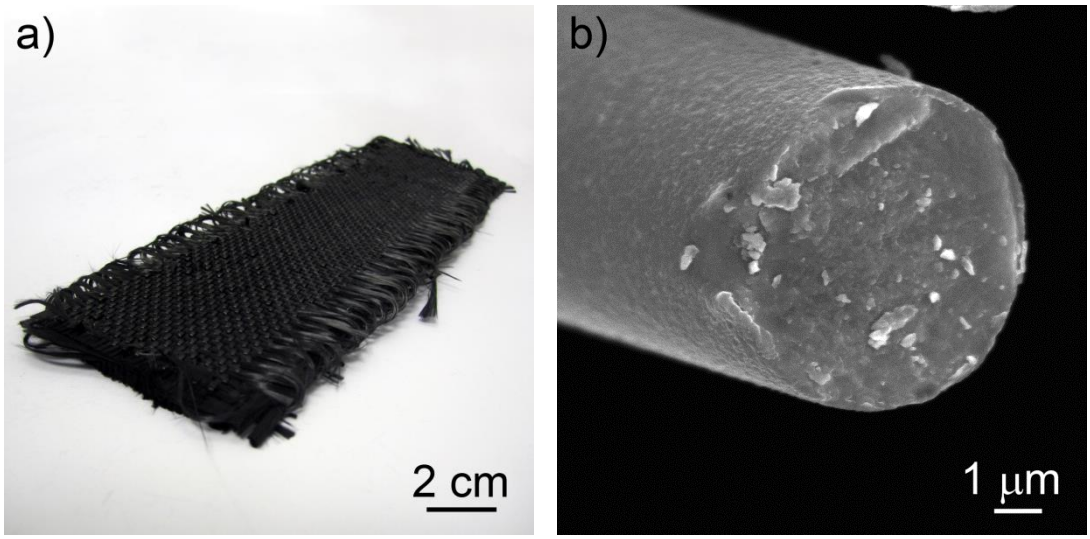

Figure 47: 3D orthogonally woven fabric preform a) and scanning electron micrograph of Tyranno-SA 3 (UBE Industries Inc.) fracture surface b).

The term SITE was introduced to describe the use of electrophoretic (infiltration) deposition combined with a low temperature densification process for the fabrication of ceramic matrix composites [110, 111]. Such nomenclature will be used in continuation for composites fabricated by the combination of EP(I)D and PIP.

Due to hydrophobic nature of (PyC coated) fibres and consequently the poor wettability with aqueous suspensions, fibre preform was treated with anionic surfactant. The effect of anionic and non-ionic surfactants on wettability of SiC fibres was also investigated in a related study [112]. Effect of dodecylbenzensulfonic acid (DBSA) and sodium dioctyl sulfosuccinate (SDOSS) addition on wetting of fibres with aqueous suspension was evaluated by measurement of wetting angle. Untreated sintered SiC substrate was compared to SiC substrate previously immersed aqueous solutions of SDOSS and DBSA. Both surfactants improved the wetting of the substrate with the suspension, however SDOSS had a more pronounced effect. Wetting angle decreased from 58.1° for the untreated substrate to 30° and 28° for substrate immersed into DBSA or SDOSS, respectively. SDOSS was used for EP(I)D experiments. Since surface of the fibres is covered by a thin layer of PyC, wetting angle was also measured on PyC substrate. Wetting angle decreased from initial value of 70° for the untreated substrate to 31° for substrate immersed in SDOSS (Figure 48).

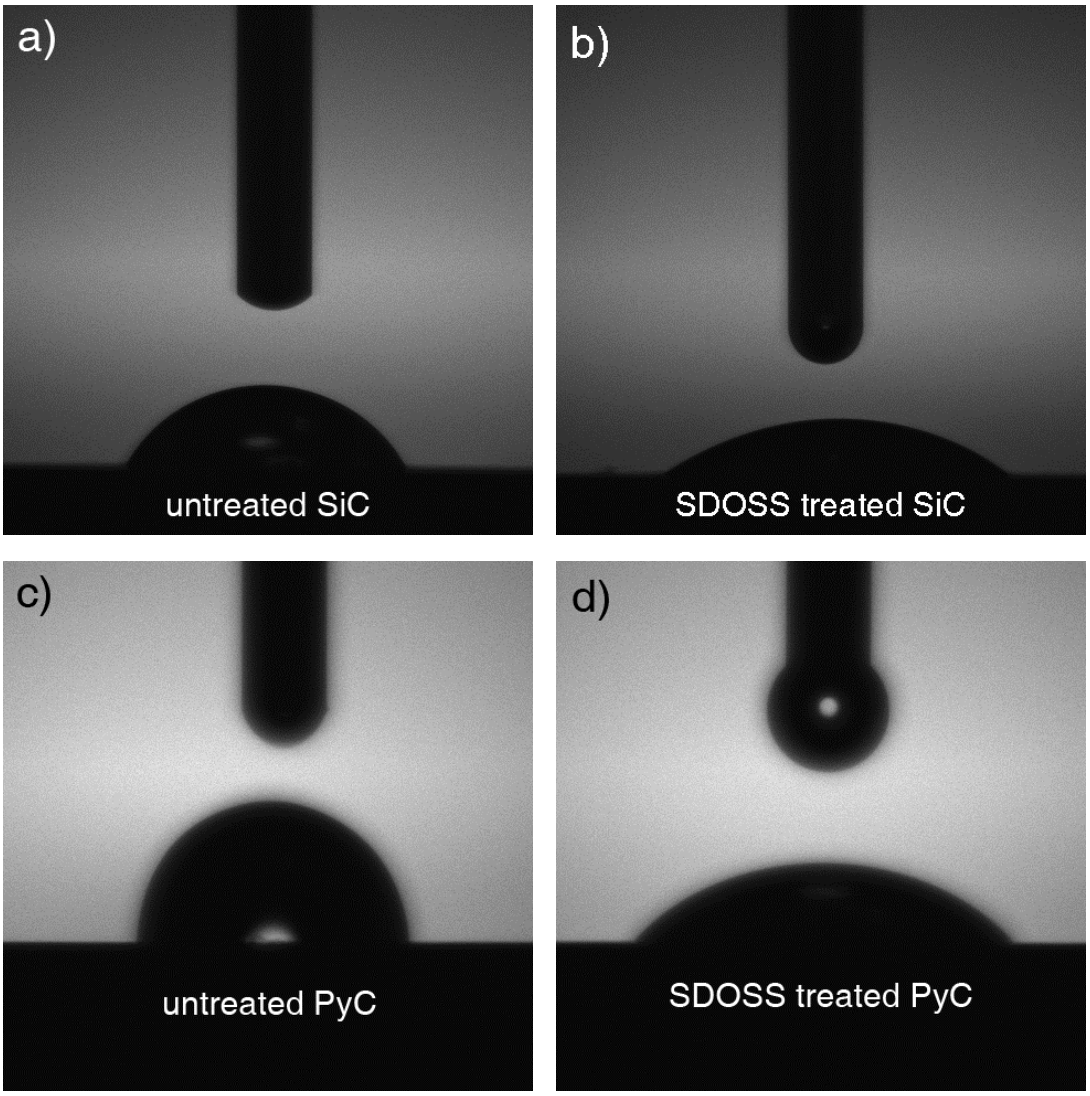

Figure 48: Wetting angle of untreated and SDOSS treated SiC a) and b) and PyC substrate c) and d).

The addition of SDOSS also increased the absolute value of ζ of the fibres (Figure 49). At pH 10, where the maximum is observed (and at which infiltration takes place) for both as-received and SDOSS treated fibres, ζ_f increased from -40 mV to -50 mV. C fibres also exhibited a high negative ζ_f at high pH, achieving a maximum of -58 mV at pH 11.

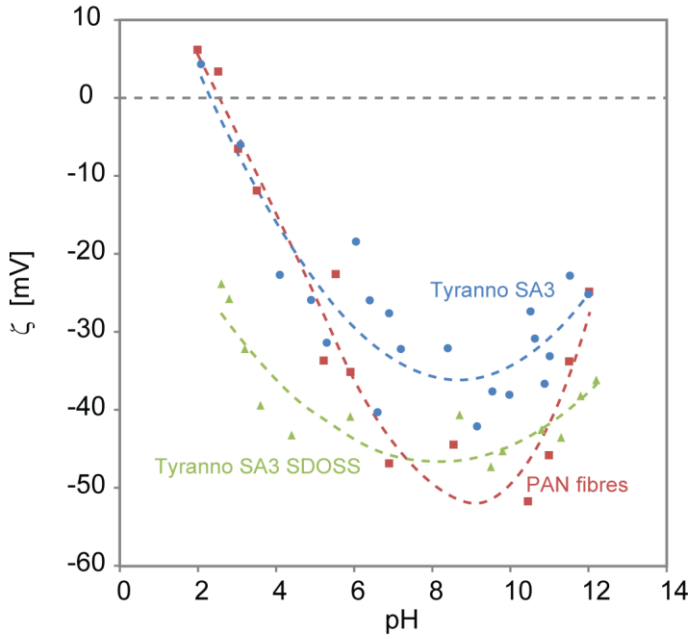

Figure 49: ζ of as-received and SDOSS treated SiC fibres (Tyranno SA3) and carbon (PAN) fibres as a function of pH.

Due to very high price and limited availability of SiC fabric preform, initial infiltration experiments were performed with a 3D woven carbon fabric preform. In the case when fibres were not separated from the anode, there was very little penetration of SiC particles into the preform (Figure 50a), whereas in the case when the preform was placed in front of the anode and separated from it by a cellulose membrane, the particles migrated through the preform and gradually filled the entire thickness of the preform (Figure 50b).

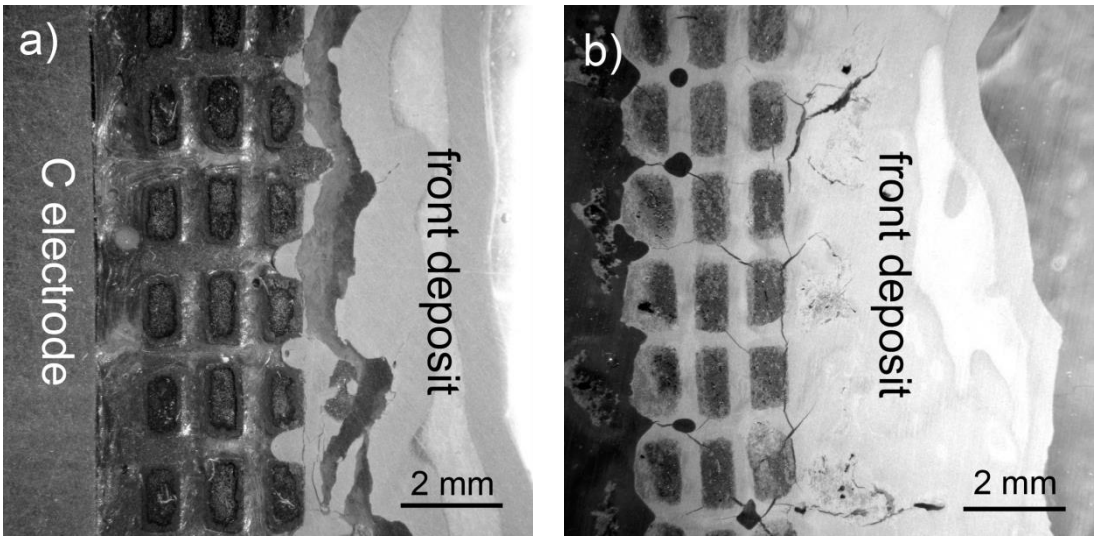

Figure 50: Penetration of particles into 3D carbon fabric preform where a) fibre preform was placed in contact with electrode and b) fibre preform separated from the electrode by cellulose membrane.

Initially, composites exhibited poor infiltration in interbundle areas (formation of large voids), with almost no infiltration of intrabundle areas. Voids (Figure 51a) in inerbundle

areas was ascribed to the entrapped air. In order to enhance the infiltration, fibre preform was evacuated and gradually filled with SiC suspension prior to EP(I)D. In comparison to non-evacuated preform, the infiltration was significantly improved and a more uniform infiltration was achieved (Figure 51b).

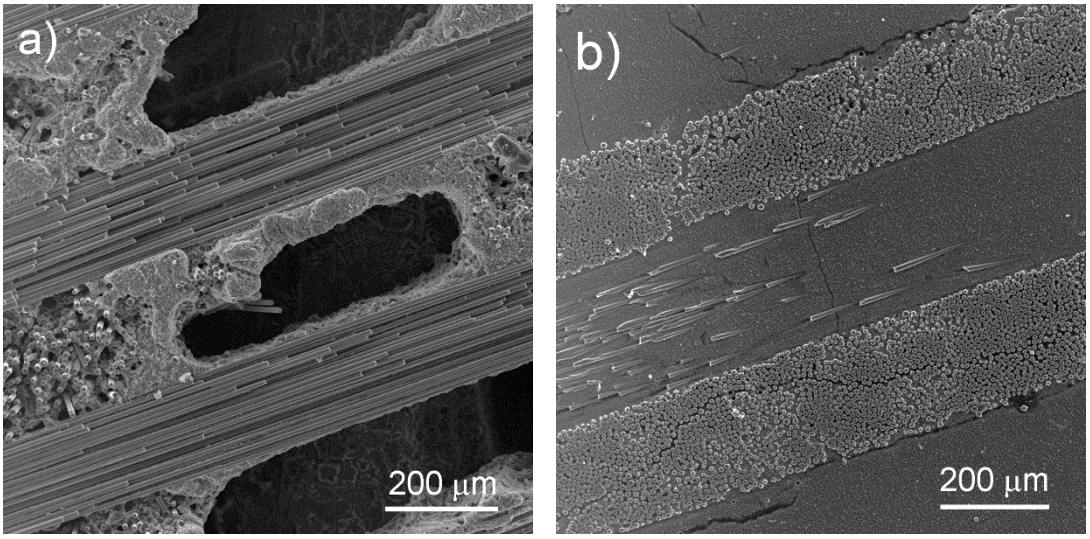

Figure 51: Formation of large voids in the non-evacuated fabric preform a) and homogeneous infiltration in the case of evacuated fibre preform prior to EP(I)D b).

The deposition conditions were determined experimentally. Constant current depositions with current density of 1–10 $mAcm^{-2}$ were performed and optimal process parameters were determined by microstructural investigation of the infiltrated fabrics. The highest degree of infiltration of inter- and intrabundle areas was determined at current density of 2.5 $mAcm^{-2}$ (Figure 51). Composites fabricated at high current density exhibited almost no infiltration of intrabundle areas. On the other hand, composites fabricated at lower current densities exhibited a more homogeneous infiltration with fewer defects and also infiltration of intrabundle areas.

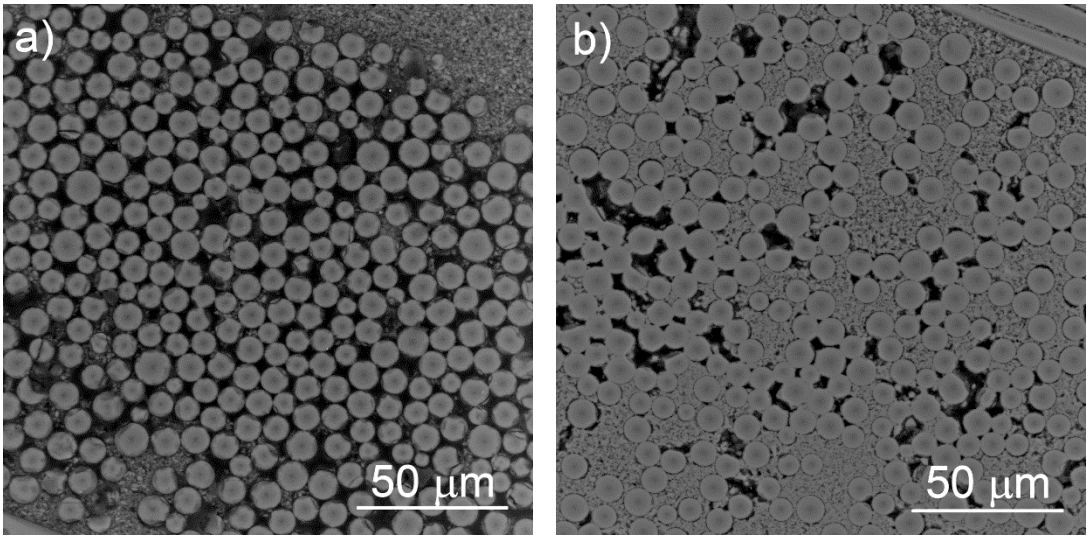

Figure 52: Comparison of degree of infiltration at current density of a) 10 $mAcm^{-2}$ and b) 2.5 $mAcm^{-2}$.

Time needed for complete infiltration of the 5.4 mm thick fibre preform was estimated

on the basis of EP(I)D experiments and finally determined by visual investigation of the deposits and optical micrographs of composites cross sections. Using suitable powder suspension and optimal conditions for electrophoretic deposition, 10 min depositions yielded a fully infiltrated fabric preform with thickness of 5.4 mm (Figure 53) placed at approximately 1 mm distance from the deposition electrode (anode).

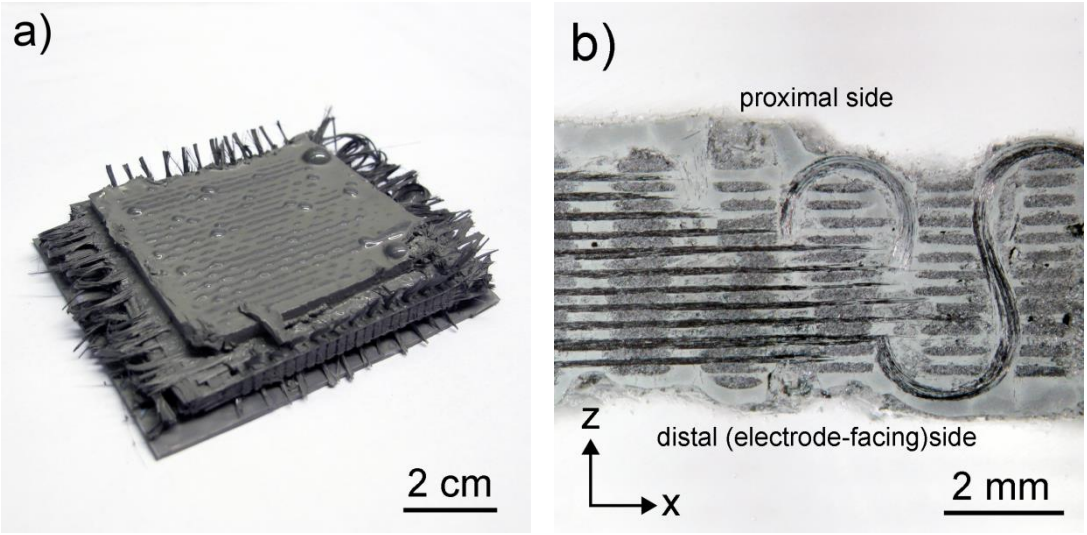

Figure 53: Optical micrographs of infiltrated 3D SiC fibre preform a) after EP(I)D and b) cross-section of infiltrated fabric preform in the x-z direction indicating through thickness infiltration of SiC preform with SiC particles.

4.3.2 Polymer infiltration and pyrolysis (PIP)

Densification by six cycles of polymer infiltration and pyrolysis (EP6) resulted in a relatively homogeneous SiC matrix with good infiltration of interbundle (Figure 54a) as well as intrabundle areas (Figure 54b–c). Initial pores, resulting from incomplete infiltration during EP(I)D in some samples were partially filled with polymer derived SiC (PD-SiC) (Figure 54d)

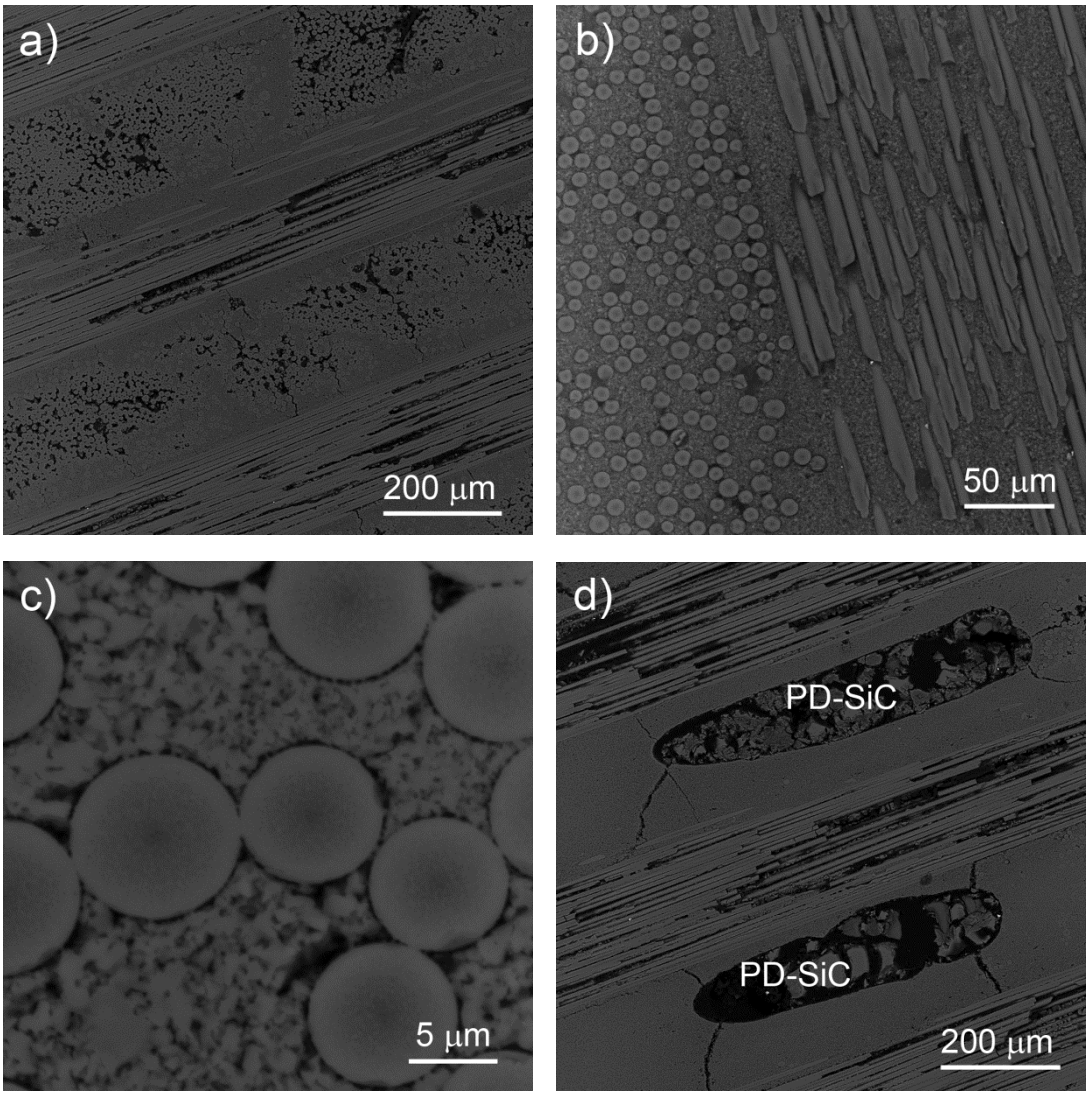

Figure 54: Scanning electron micrographs of a SITE-SiC_f/SiC densified with six PIP cycles (EP6).

It is important to note that after densification the PyC coating on SiC fibres (fibre-matrix interphase layer) (Figure 55a) was not observed in the composites' microstructure. In some parts the SiC fibres even sintered together (Figure 55). Carbon-rich SiC areas determined by EDXS were observed in the matrix near the fibres. From Figure 56 it can be seen that the as-received PyC coating was not uniformly applied to the surface of the fibres.

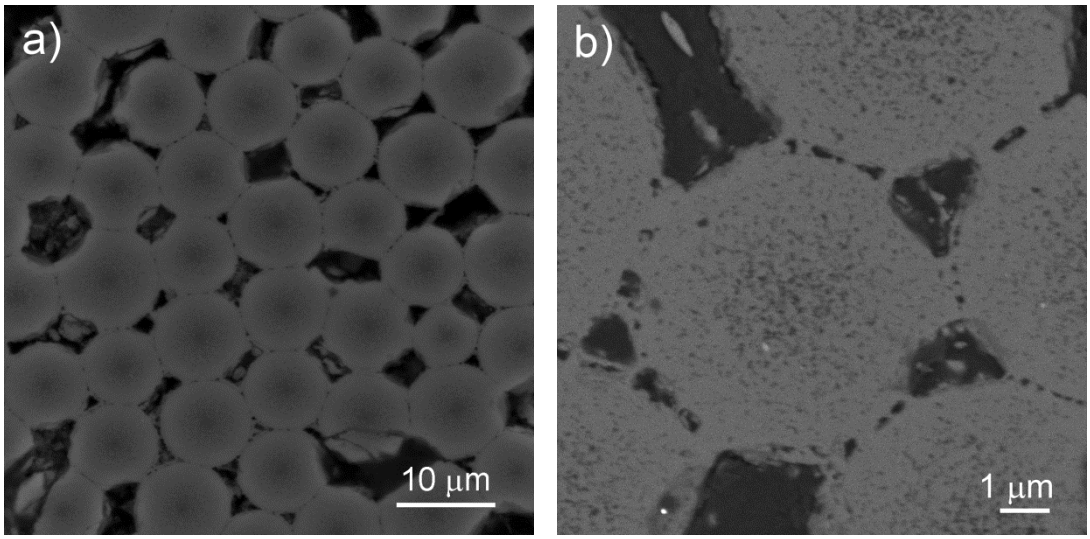

Figure 55: SiC fibres sintered together after crystallisation.

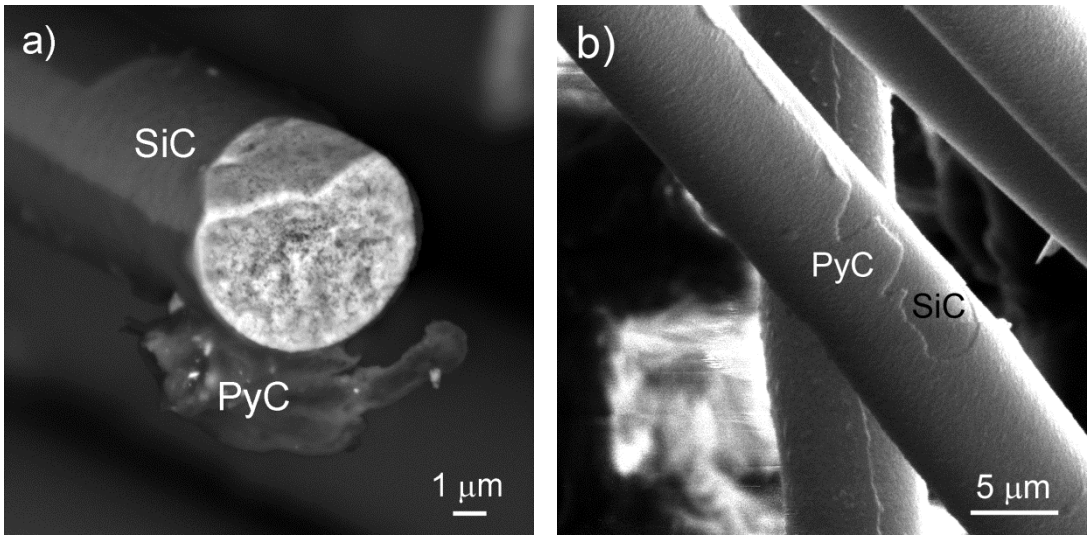

Figure 56: As received PyC coating on Tyranno SA 3 fibres.

4.3.3 Composition of SiC_f/SiC composite

Composition of SiC matrix in SiC_f/SiC composite was evaluated by EDXS and compared to composition of Tyranno SA3 SiC fibres. The composition of near-stoichiometric Tyranno SA3 fibres is well studied and the composition was used as a reference comparison. The resulting EDXS spectra (Figure 57) revealed that the composition of SiC matrix is similar to analysed and reported [27] composition of SiC fibres. In contrast to matrix material SiC fibres also contained a minor amount of Al. Furthermore, the matrix exhibits nearly stoichiometric composition of SiC with minor amount of oxygen (< 1 wt. %), which can be (at least partially) ascribed to the surface oxidation of the samples.

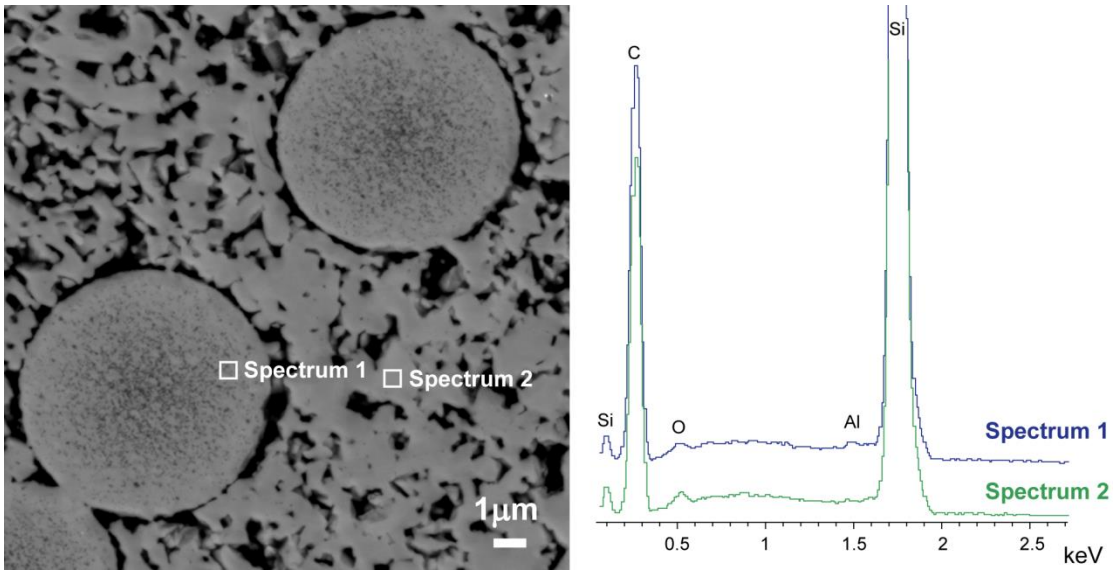

Figure 57: Microstructure and EDXS spectra of SITE-SiC$_f$/SiC

Composition of the material was also verified by XRD (Figure 58). Sharp peaks at 2θ of 35.7°, 42° and 60.2° correspond to the 111, 200 and 202 planes of β-SiC (3C Moissanite, cubic). Minor peaks at 33.65°, 34.18° and 38.23° correspond to 100, 101 and 103 planes of α-SiC (6H Moissanite, hexagonal). Comparable composition was determined also for individual constituents of the composite. The α-SiC phase was determined also in the SiC fibres (100 plane) and initial SiC powder (planes 101 and 103). Same peaks as in SiC powder were also determined for SiC matrix.

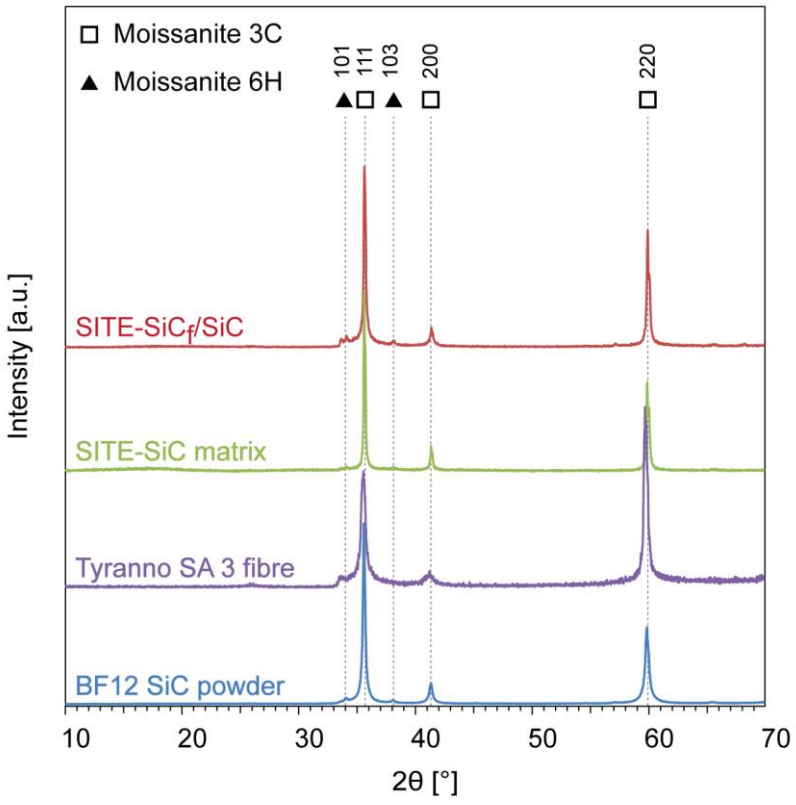

Figure 58: XRD and of SiC$_f$/SiC and its individual constituents.

4.3.4 Density & porosity of SiC_f/SiC

Pore size and porosity distribution was evaluated by Hg-intrusion porosimetry and CT scanning of the samples. Hg- intrusion porosimetry revealed the material contained a broad range of pore size, with the majority of pores below 1 μm and median pore size of 260 nm (Figure 59). By comparison of these results with microstructural observations, the peak at ~ 10 μm can be ascribed to the intrabundle porosity, due to incomplete infiltration during EP(I)D (Figure 54b), whereas porosity < 1 μm can be ascribed to matrix porosity (Figure 54c).

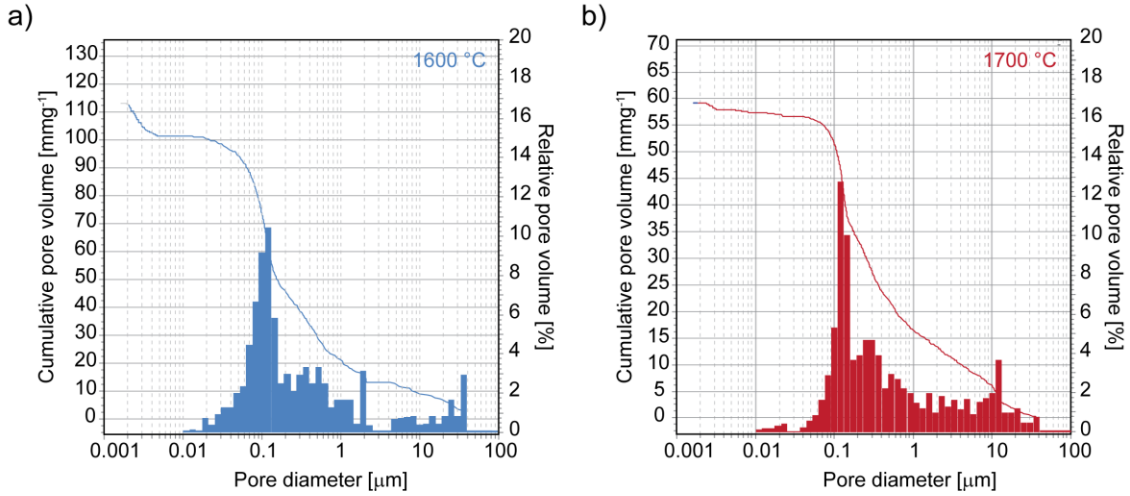

Figure 59: Porosity distribution in SITE-SiC_f/SiC composite.

CT micrographs revealed that the 5.4 mm thick fibre preform is uniformly infiltrated through the thickness of the preform, with no large voids typical for the CVI or PIP process. The micrographs revealed a homogeneous distribution of porosity with the presence of minor amount of larger (”bubble-like”) defects (Figure 60b–f). “Bubble-like” pores in interbundle areas (Figure 60c–d), observed also in the polished cross-sections (Figure 54d) were ascribed to entrapped air bubbles during EPD, majority of which was eliminated by pre-evacuating the preform and gradual infiltration of suspension prior to EPD. In addition, cracks were observed in the in-plane as well as through thickness direction, typical for the drying process of 3D reinforced composites.

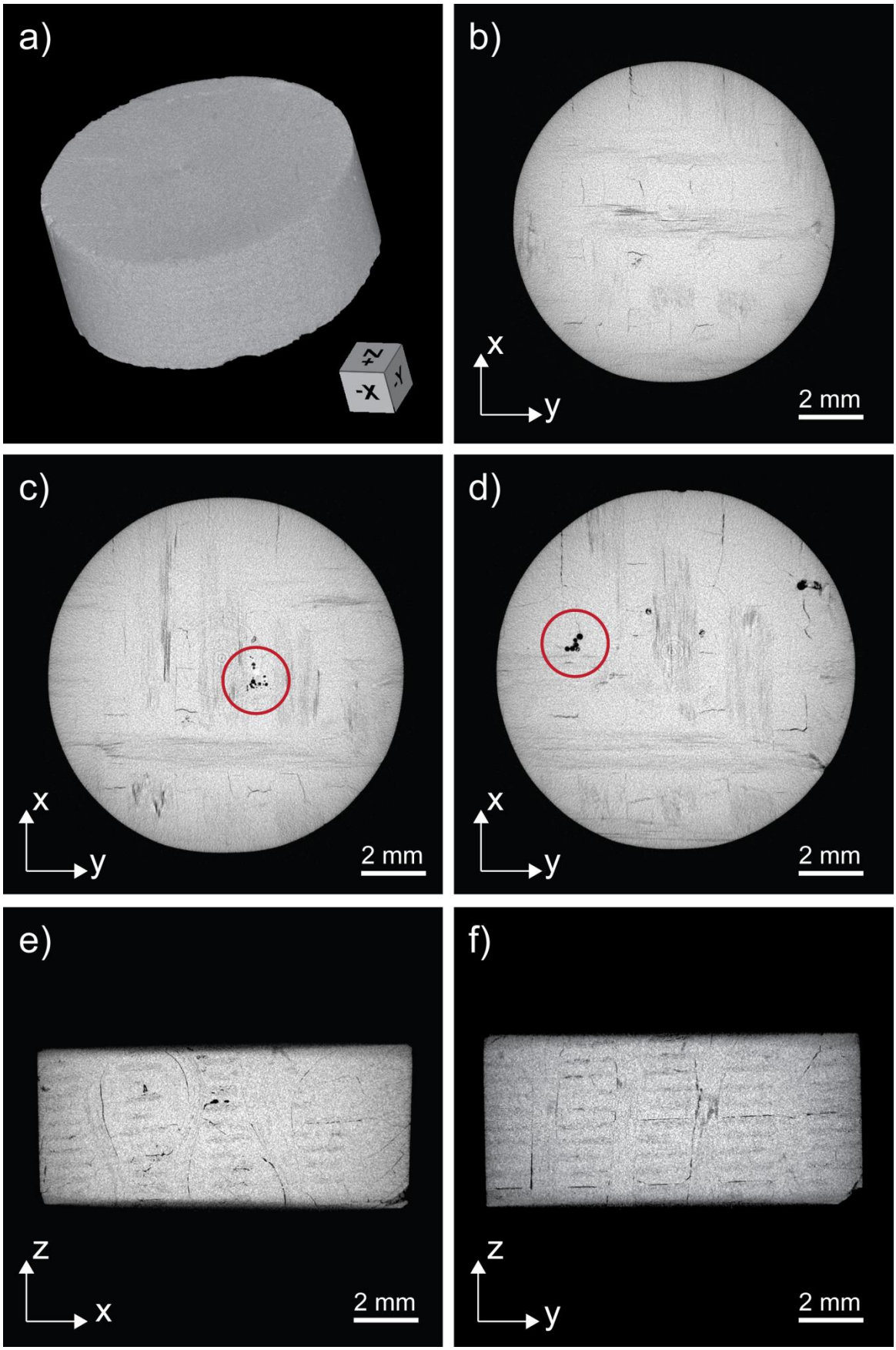

Figure 60: CT 3D rendering and single slices of SITE-SiC_f/SiC composite. Sample diameter was 10 mm.

4.3.5 Mechanical properties

Due to low availability of SiC fibres, only one set of samples (15 samples) was prepared for evaluation of mechanical strength of the material. Since the results for pure SiC matrix indicated an increased strength after densification at 1700 °C in contrast to samples densified at 1600 °C, the composite material was also fabricated at maximal heating temperature of 1700 °C. Measured flexural strength of SITE-SiC_f/SiC was very low, varying from 60 to 90 MPa. The measured strength was retained in the range from room temperature to 1400 °C (higher temperatures were not investigated) regardless of the testing atmosphere (vacuum or air).

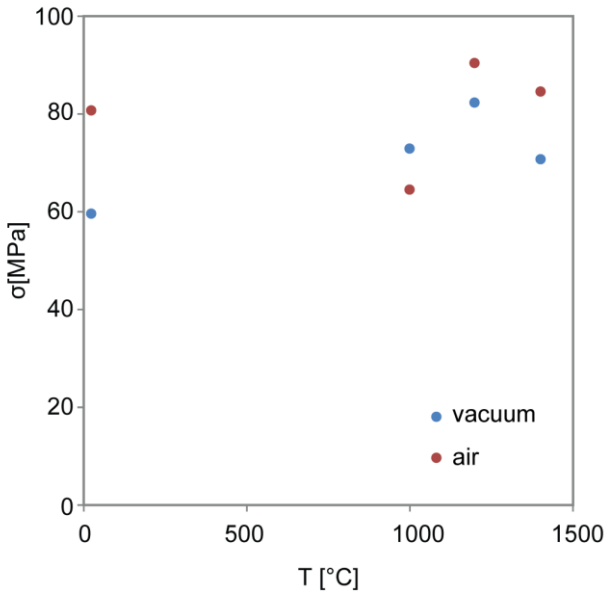

Figure 61: Flexural strength of SITE-SiC_f/SiC composite densified at 1700 °C as a function of temperature in vacuum and in air.

Microstructural examination of fractured samples revealed that the SITE-SiC_f/SiC composite exhibited an unfavourable brittle fracture with no fibre pull-out (Figure 62). Fracture surfaces indicate a partial displacement along the fibres. Brittle fracture is the consequence of the lack of effective interphase layer after processing. The lack of interphase layer combined with polymer derived SiC resulted in sintered fibres as observed in the Figure 62b.

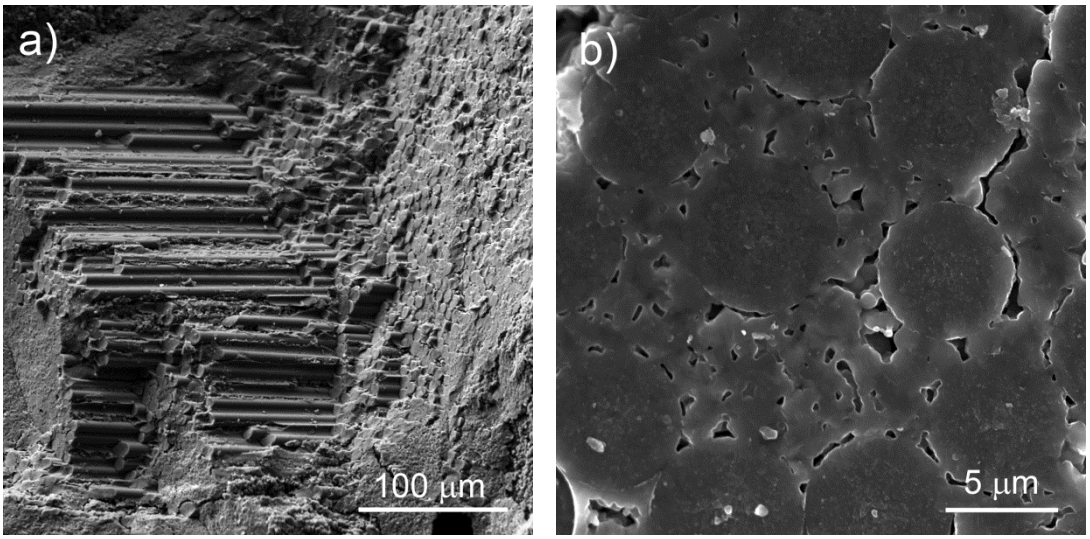

Figure 62: Fracture surface of SITE-SiC_f/SiC at different magnification.

4.3.6 Thermal properties

Measured thermal diffusivity (α) and calculated values of thermal conductivity (λ) of SITE-SiC_f/SiC densified at maximal temperature of 1600 °C or 1700 °C are represented in Figure 63a and Figure 63b respectively. Heat capacity of samples densified at 1700 °C was measured simultaneously with thermal diffusivity, whereas in the case of samples densified at 1600 °C, a mathematical approximation presented in Equations 10–12 was used. Thermal conductivity was calculated according to Equation 9. Thermal diffusivity values decreased from 40 mm^2s^{-1} at room temperature, to 8 mm^2s^{-1} at 1000 °C for samples densified at 1600 °C, whereas for samples densified at 1700 °C thermal diffusivity decreases from 30 mm^2s^{-1} at room temperature, to 7 mm^2s^{-1} at 1000 °C. Also thermal conductivity shows a temperature dependent decrease from 60 $Wm^{-1}K^{-1}$ at room temperature to 30 $Wm^{-1}K^{-1}$ at 1000 °C for samples densified at 1600 °C. Thermal conductivity of samples densified at 1700 °C decreases from nearly 80 $Wm^{-1}K^{-1}$ at room temperature to 25 $Wm^{-1}K^{-1}$ at 1000 °C.

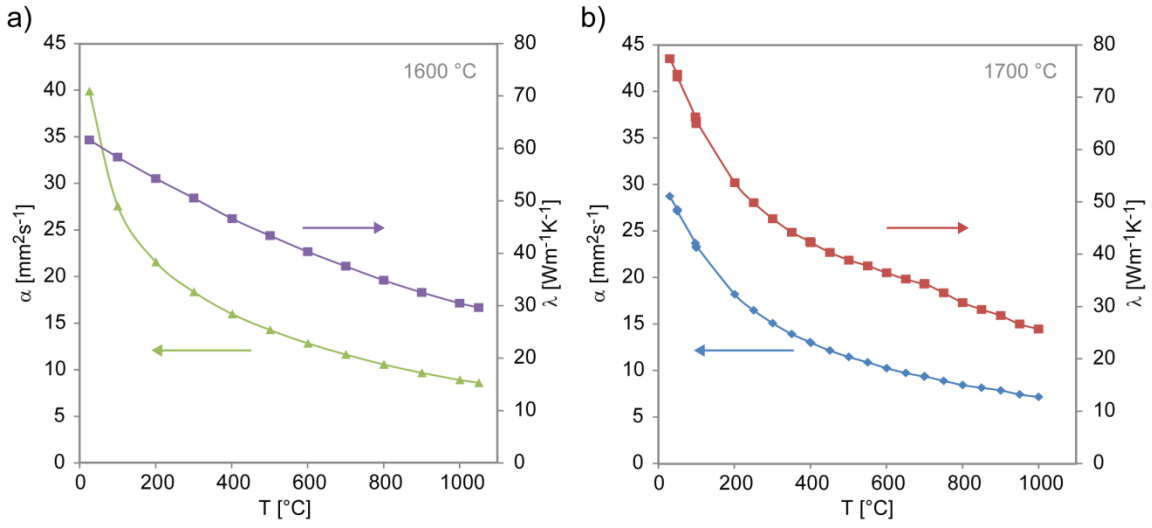

Figure 63: Measured values of thermal diffusivity (α) and corresponding calculated values of thermal conductivity (λ) of SITE-SiC_f/SiC densified by six PIP cycles.

5 Discussion

5.1 Preparation of green parts

Various approaches have been employed in densification of the SiCf/SiC composites but none of them resulted in a composite fulfilling the demanding set of requirements for the application in future fusion reactors. Rather the properties of the materials produced by CVI, PIP, NITE or any combined processes, are a compromise, where one property is achieved on account of another. For many of them, high residual porosity represents the main issue, which is connected not only to the undesired gas permeability but also to the insufficient mechanical properties and thermal conductivity. For this reason in this work the main focus was put into minimising the porosity by introducing a new approach in processing. The proposed approach includes filling of voids in the fibre preform with large amount of filler powder in the first step followed by a pressure-less, moderate temperature process of polymer infiltration and pyrolysis (PIP).

Filling of the large voids in the fibre preform prior further densification has been performed previously by aid of vacuum infiltration [73], which, however, resulted in only limited impregnation of the fabric with the SiC powder. Alternatively, slurry filtration was used [69, 71, 72], however, due to the limited solids content in the used slurry (to keep viscosity low) the voids were only partially filled with the SiC particles. Suspensions with higher volume fraction of powder are not suitable for (pressure) infiltration due to increased viscosity. The use of pressure might also lead to the deformation of the preform leading to incomplete infiltration and density gradients.

In this work, the voids in the SiC-fabric were filled by aid of electrophoretic (infiltration) deposition (EP(I)D), which was assumed to have a potential to better fill the voids than other techniques. The EPD process itself has been long known and has been employed in various systems including infiltration of porous/fibrous preforms, but in this particular case, due to the conductivity of the SiC fibres, instead of frequently used trial-and-error approach, a comprehensive study was needed in order to fully employ the potential of the process. For the effective use of EPD, the control of properties of the suspension is essential in order to obtain high density deposits and successfully infiltrate the preform. As the EP(I)D is the key step in the proposed process for forming SiC/SiC composite, large attention was paid to optimise this process.

5.1.1 Characteristics of suspension for electrophoretic deposition

It is well known that the key characteristics of a suspension to produce dense deposit are their favourable electrokinetic properties, i.e. high surface charge, appropriate conductivity and stability. These characteristics are strongly related to the properties of liquid media, content of powder, its particle size and the chemistry of the particles' surface and critically affect the properties of deposit.

Based on previous investigations [109, 113], in this study water was used as preferred liquid media for the suspension. Electrokinetic investigation of SiC powder suspension in water revealed that the most stable suspensions with the highest zeta potential (ζ) value (-

70 mV) can be achieved by increasing the pH value from initial ~3.5 to 10-11 (Figure 14). Formation of charge on silicon carbide surface in aqueous media is attributed to the dissociation of silanol groups formed at the surface. Since silanols are relatively strongly acidic they easily react with OH^- groups [78] and therefore higher absolute values of ζ are achieved at alkaline pH than at acidic pH (Figure 14). The addition a strong organic base (TMAH), promotes the dissociation of surface silanol groups inducing a negative charge on the surface of SiC particles. The isoelectric point was determined at pH 3.8±0.3 for submicron powder and 3.6±0.2 for nanosized powder (after removal of surface carbon from nanosized particles), which is within the broad range (pH_{iep} =2.5-4.8) reported in the literature [114-116]. The surface oxide layer shifts the isoelectric point of SiC to that of silica (pH_{iep} = 2-3.5). By TEM examination it was confirmed that both SiC powders used in this research were covered with approximately 2 nm thick oxide layer and therefore their pH_{iep} were nearly identical. At higher pH the value of ζ is decreased due to the increased ionic strength of the electrolyte and resulting compressive effect on the particles double layer and simultaneous decrease in the interparticle electrostatic force. Since a more effective charging of SiC particles is obtained in alkaline region where ζ has highly negative values, anodic deposition is more effective and was therefore employed in this investigation.

With the aim to fully employ the potential of the electrophoretic deposition process in infiltration of SiC-fibre preform, deposition of bulk SiC powder was studied first. For a successful electrophoretic (infiltration) deposition in aqueous systems, not only the ζ but also the conductivity (σ) of suspension plays an important role. It is evident from Figure 17 that the optimal depositing conditions (e.g. highest obtained deposit densities) were at pH 10, even though high values of ζ were obtained up to pH 11 (Figure 15). Namely, at pH above 10, the higher suspension conductivity resulted in deposits with lower packing density. Similar was also noted by Sarkar et al. [117], who suggested that too high suspension conductivity results in slower motion of particles. On the other hand, if the conductivity of the suspension is too low, the suspension will be resistive, leading to loss in stability[117].

Therefore, in order to achieve optimal green densities, the suspension conductivity should be within a certain range, which is characteristic for a certain powder-liquid system. As was determined for the case of submicron SiC the value should be between 0.4 $mScm^{-1}$ and 0.6 $mScm^{-1}$, which correspond to 0.1-0.2 wt. % of TMAH addition.

The amount of solids loading indicated a minor effect on the ζ, whereas the effect on σ was more pronounced (Figure 15). For suspensions without additives, there was a minor increase in conductivity, most likely due to dissolution of surface layer. In the case of suspensions where the pH was adjusted to 10, the increase in conductivity was larger that was attributed to the larger amount of dispersant added to the suspension in order to achieve the appropriate pH (and high ζ).

As mentioned above the optimal suspension characteristics for electrophoretic deposition/infiltration experiments were obtained at pH 10, where suspension electrokinetic properties (ζ, σ) were optimal for obtaining deposit with high packing density. The resulting highest packing density (~60 % TD) was obtained with 50 wt. % of solids loading (ζ= -70 mV, σ= ~0.4 $mScm^{-1}$). With the aim of further increasing the packing density of the deposit, the effect of bimodal particle distribution was evaluated. In accordance to suggested optimal composition of bimodal particle packing [118], nanosized particles with 10-times smaller mean size (d_{50}=50 nm) were introduced into the suspension of submicron powder (d_{50}=600 nm). In contrast to expectations, this resulted even in decrease in deposit densities (Figure 22). Up to 15 % of nSiC addition the decrease was minor, while higher fraction of nanosized powder resulted in much lower packing densities of the deposits reaching the lowest value of 43 % TD for the nSiC

powder alone. As it will be presented later, in spite of that, 50 wt. % suspensions without or with 10 % of nanosized SiC were used for the infiltration experiments, since the addition of nanosized powder was expected to improve the infiltration in the intrabundle areas.

In a set of experiments, tungsten or $CrSi_2$ powders (serving as active fillers) were added into the SiC suspension that made the EPD process more complex. As was observed in Figure 40 and Figure 43 $CrSi_2$ and W particles were homogeneously distributed in the deposit. Due to similar elektrokinetic mobility of $CrSi_2$ and SiC in aqueous suspension (at pH10, -1.9×10^{-8} $m^2V^{-1}s^{-1}$ and -2.2×10^{-8} $m^2V^{-1}s^{-1}$ respectively), providing a good dispersion of $CrSi_2$ particles in the suspension, uniform distribution in the deposit was expected. On the other hand, homogeneous distribution of W particles in SiC is more surprising due to much higher density of W (19.25 gcm^{-3}) in comparison with that of SiC (3.21 gcm^{-3}), and much lower electrophoretic mobility in comparison to SiC (in ethanol suspension 0.022×10^{-8} $m^2V^{-1}s^{-1}$ and 0.202×10^{-8} $m^2V^{-1}s^{-1}$ respectively). According to literature data [119], in a multi-component suspension the particles (providing the same charge polarity) deposit at different rates depending on their electrophoretic mobility. However, in the case when the volume fraction of solids is relatively high, as it was in this study, the particles deposit at an equal rate. High concentration particle-particle interactions prevent segregation of different species.

5.1.2 Electrophoretic (Infiltration) Deposition

In electrophoresis the parameters effecting particle mobility (Equation 2-5) are dielectric constant of solute, viscosity of solute, particle zeta potential (ζ_p) and applied electric field. Selection of aqueous suspension for the electrophoretic (infiltration) deposition was based on the fact that water has the highest ratio between dielectric constant and viscosity which affects the mobility and penetration of ceramic particles into porous substrate [88]. High ζ_p affects not only the mobility of the particles but as was already noted in Section 5.1.1. it is also one of the prerequisite conditions to achieve a stable suspension and consequently a high density deposit.

Furthermore, in electrophoretic (infiltration) deposition, the behaviour of the substrate also plays a role. Non-conductive substrates, such as alumina, were successfully infiltrated by placing the preform in front of the depositing electrode and the particles migrating towards the deposition electrode, gradually filled the porous preform [94, 95]. In the case of conducting substrates (C fibre, stainless steel etc.), the porous substrate was used as depositing electrode [96, 97], however such approach, enables only limited infiltration and can be effectively used only with 2D reinforcements.

In contrast to common practice when using conductive fibre reinforcement, in this work the fibres were not used as electrodes. Instead the approach used for infiltration of non-conductive substrates, which are placed in front of the electrode was used. It is important to note that the fibres had to be phisically seperated from the depositing electrode to prevent the contact between the electrode and the fibres. Bao and Nicholson [95] noted that conductive-fibres cannot aid the formation of dense fibre-reinforced ceramics by EPD or EP(I)D due to electric shielding effect. This is true when the fibres are used as a depositing electrode, which was also observed in this investigation (Figure 50). If fibres act as an electrode, there is virtually no electric field penetration through the thickness of the preform due to electric shielding effect. Penetration depth is only double the fibre filament opening distance [95] and therefore only the outer parts of the preform can be infiltrated.

It can be clearly seen from a model representation of a fibre array placed in an external

electric field (Comsol Multiphysics 4.2a, COMSOL, USA) (Figure 64b) that by separating the conductive fibres from the electrode the electric field is not screened and penetrates through the thickness of the preform. Potential gradient between the electrodes can thus be used to stream the particles through the preform towards the depositing electrode.

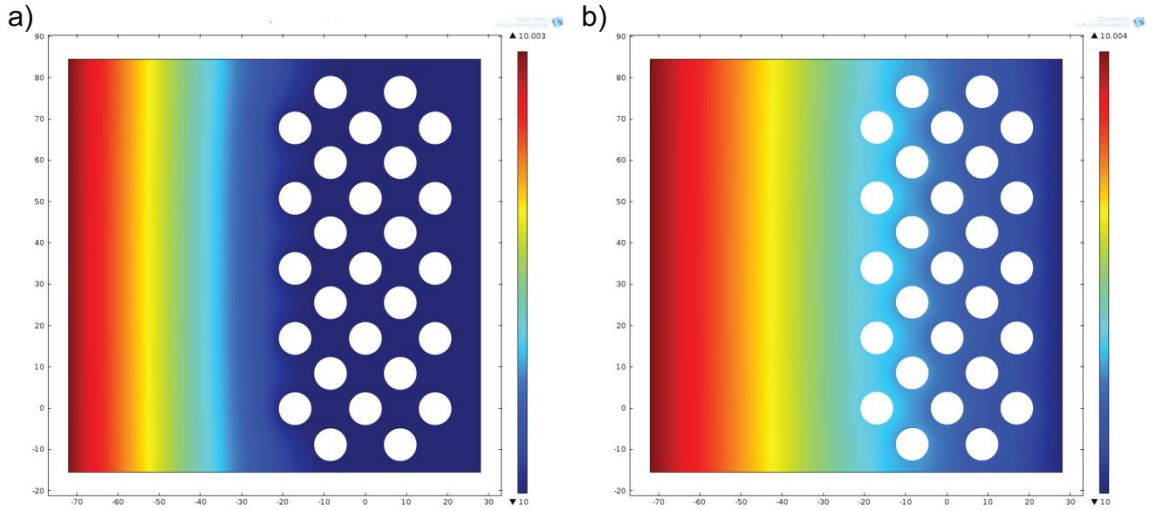

Figure 64: Potential distribution in conductive fibre array a) acting as an electrode or b) placed in front of a charged electrode.

However, we have to take into consideration that, when an electrical conductor is placed into external electric field there is an induced charge formed at its surface [120], which causes the electrolysis of water (if the applied field is large enough) and evolution of hydrogen and oxygen gases. The incorporation of these gas bubbles into the deposit leads to low quality of the deposit. Assuming that the fibre preform architecture is interconnected we can treat the preform as a single porous conductor and thus the induced charge is present only at the cathode-facing and anode-facing side of the preform, therefore bubble incorporation would only occur in front or back of the preform. Maximum potential difference (ΔV_{max}) between the two opposite sides of the conductor with thickness (d), generated by external electric field (E) is given by [121]

$$\Delta V_{max} = E \cdot d \qquad (16)$$

Assuming the required voltage for electrolysis of water is 1.23 V [121], the required electric field strength to cause water electrolysis on a 5.4 mm thick conducting preform is 2.28 Vcm^{-1}. Since SiC is a dielectric with dielectric constant of 9.72, the required external field strength is increased to 22.14 Vcm^{-1} according to equation

$$E_0 = E \cdot \varepsilon \qquad (17)$$

However, since the fibres are coated with a layer of pyrolytic carbon, we must treat the preform as a perfect conductor. Considering the conductivity of the used SiC suspension is 0.5 $mScm^{-1}$, the applied current density in the case of carbon coated fibres should not exceed 1.14 mAcm-2 to avoid electrolysis on the preform (11.07 $mAcm^{-2}$ for uncoated SiC fibres). By macroscopic observation of PyC coated SiC fabric preform immersed into electrolyte solution (σ=0.5 $mScm^{-1}$), it was found that the electrolysis on the fibres occurred only when current densities of > 3 $mAcm^{-2}$ were used.

Furthermore, according to the induced-charge electrokinetic phenomena proposed by Bazant and Squires [122], the induced charge drives the counter-ions from the suspension electrolyte towards the induced potential causing the inhomogeneously distributed induced zeta potential (ζ_i) on the fibres. Considering the negative ζ_f of fibres in absence of external electric field (E_0 = 0 Vcm^{-1}), the ζ_i decreases the absolute value of ζ_f on the cathode facing side of the preform thus reducing the energy barrier between the incoming particles and the fibres.

As was already noted, the zeta potential of fibres (ζ_f) also plays a crucial role in successful penetration (infiltration) of the powder into the fabric preform. As was demonstrated by Stoll et al. [94] (for oxide based composites), if the fibres and the particles have the surface charge of opposite polarity, the particles can be attracted not only to the depositing electrode behind the preform but also to the fibres themselves. The particles attracted to the fibres may cause blockage between the fibres and prevent further infiltration similar as in the case of conducting fabric connected to the electrode. Conversely, the particles and fibres with same surface charge polarity repel each other due to the energy barrier between the particles and the fibres which opposes particles deposition as they pass towards the depositing electrode. The streaming particles deposit on the counter-electrode (in our case anode) and gradually backfill the porous preform (Figure 65). As it is evident from Figure 50b, the same postulate can be applied to conductive fibres (electrically) separated from the electrode. Same sign ζ_f of the fibres induces electroosmotic flow in opposite direction to electrophoretic motion of particles. Due to large κr (~ 105; κ^{-1}=2.86 nm, r=0.3 μm) Helmholtz-Smoluchowski expression can be applied to describe the movement of concentrated suspension of submicron SiC particles in aqueous suspension. Likewise for SiC fibres the value of κr is equal or larger as for the particles considering pores radius is at least the same size as particle radius. The pores sizes estimated from microstructures are in the range of 0.1–10 μm in the intrabundle areas and 100–1000 μm in interbundle areas, so this is a valid approximation. Basic Helmholtz-Smoluchowski expression can also be applied to describe electroosmosis within the preform.

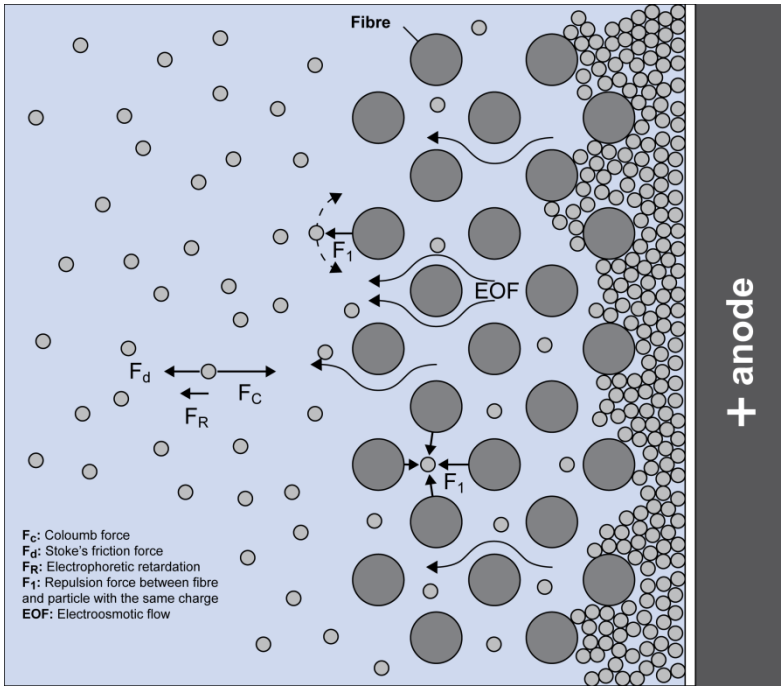

Figure 65: Schematic view of SiC particle penetration (infiltration) through fabric preform.

In view of Equations 5–7 the most successful penetration of colloidal particles into porous substrate can be achieved with particles with high electrophoretic velocity (high Peclet number) and particle-substrate repelling force preventing deposition (low Damköhler number). Both conditions can be satisfied with high same polarity surface charge of particles and pore wall (fibre) influencing particle mobility on one hand and providing electrostatic repulsion between the particles and the wall on the other. For suspension at pH ~10 the combined (electrophoretic and electroosmotic) mobility of migrating colloidal particles is -1.26×10^{-5} $m^2V^{-1}s^{-1}$ (negative, due to migration towards the anode) with *Pe*=126 (assuming median pore size of 100 nm) indicating high particle penetration. Due to large energy barrier between particles and fibres (Figure 66) we can assume that the deposition rate is small ($\delta\rightarrow0$), consequently also the Damköhler number is low thus satisfying both conditions for deep particle penetration.

It has to be mentioned that the PyC-coated SiC fibres are hydrophobic by nature and were, in order to be effectively wet by aqueous SiC suspensions, treated with an anionic surfactant sodium dyoctyl sulfosuccinate (SDOSS) prior infiltration (Figure 49). Due to electrosteric effect of SDOSS the ζ_f was increased from -30 mV to -50 mV at pH10. The SiC and PyC substrates treated with SDOSS solution exhibited lower wetting angles (Figure 48). For an ionically-stabilized suspension, the interaction energy between charged surfaces consists of van der Waals attraction and electrical double-layer repulsion 95. Hamaker2 software [123] was used to evaluate interaction energy between particles and fibres. As the fibre filament (7.5 μm) is far larger than the particle size (0.6 μm), the fibre filament is assumed to be an infinitely large flat surface. As it is evident from Figure 66 the energy barrier is greatly increased by increasing the ζ_f (by treating the fibres with SDOSS). Higher energy barrier between the particles and the fibres results in an enhanced particle penetration and packing, whereas small energy barrier results in poorer infiltration which was also seen in comparison of EP(I)D of SDOSS treated and untreated fibres.

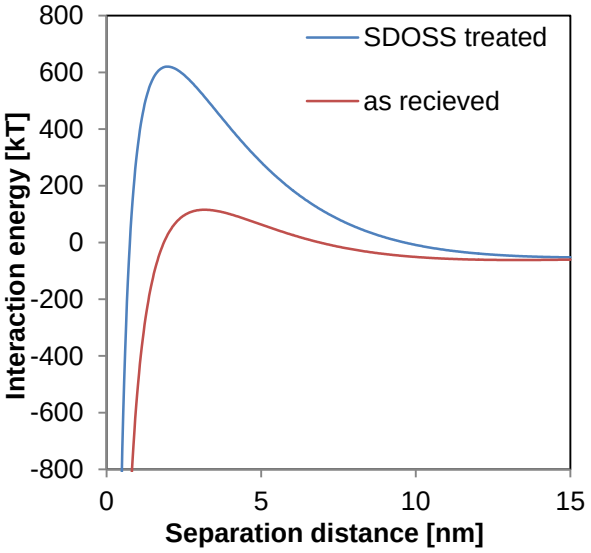

Figure 66: Interaction energy between particle and fibre as a function of separation distance.

Constant current deposition was used since it was reported [79] and experimentally confirmed in this study to produce more uniform deposits with higher yield in comparison to depositions conducted at constant voltage. During deposition, the electric field is kept constant by increasing the potential drop between the electrodes, thus maintaining a

constant velocity of the suspended particles. The deposition conditions (current density, time) needed in order to fill the fibre preform were established experimentally. Based on visual examination of polished cross sections current density of 2.5 $mAcm^{-2}$ was selected for the infiltration experiments, since it produced samples with the highest degree of infiltration. 10 min depositions yielded in full through thickness infiltration of 5.4 mm thick preform and formation of a deposit on the proximal side (Figure 53).

Since a porous membrane was used in order to prevent bubble incorporation due to water electrolysis at the electrode, deposit formation can be primarily described by mechanism proposed by Hamaker and Verwey [84], who stated that the basic function of applied electric field is to move the particles toward the electrode, where accumulated particles deposit because of the pressure exerted on them by those in the outer layers. Electric field strength is generally too low to overcome mutual repulsion between particles, however, high particle concentration near the depositing electrode (or porous membrane) increases the resistance of the suspension and as a result the voltage drop and electric field in the layer are also very high [124]. Approaching particles also undergo a double layer distortion due to fluid dynamics and applied electric field, thinning the double layer ahead of particle so that they can approach the already deposited particles close enough so that Van der Waals attractive forces can dominate and cause deposition [82]. Particle accumulation may be also caused by a shift of zeta potential towards the isoelectric point due to increase of solids loading [83].

In contrast to vacuum or pressure infiltration, electrophoretic (infiltration) deposition enables formation of matrix with higher packing density. From starting suspensions with ~ 30 vol. % of powder, deposits with > 60 vol. % are formed, whereas in the case of (over or under) pressure assisted infiltration the typical density of infiltrated matrix is the same as of the infiltrated suspension (typically 30 vol. % [72]).

5.1.3 Drying

The drying process is very important in the fabrication of defect-free ceramics especially 3D fibre reinforced architectures. Shrinkage of matrix combined with the constraints imposed by the fibres invariably lead to the formation of matrix cracks with large opening displacements (~ 10 μm) [73]. The majority of observed cracks was oriented in the through thickness direction, with minor amount of in-plane cracks caused by the constraint imposed by the through thickness yarns. The formation of cracks was mitigated by slow drying in a humid atmosphere.

5.2 Densification by polymer infiltration and pyrolysis

5.2.1 Infiltration of green compact with liquid preceramic polymer

The next step in production of SiC_f/SiC composite by the combined SITE process is impregnation of the green part prepared by aid of EPD with preceramic polymer and thermal treatment (PIP process).

Infiltration of a porous substrate containing gas (e.g. air) by a liquid (e.g. polymer precursor) occurs by two different mechanisms. First, capillary pressure, *Pc* (and any applied pressure, *Pa*) will cause a wetting liquid to flow into the porous substrate until the opposing internal pressure of the compressed gas, *Pi*, becomes equal to the capillary pressure. Second, entrapped gas can diffuse through the liquid from the interior where the pressure is higher to the surface [125]. Therefore, to reduce the internal pressure of the air

which hinders the infiltration and to minimize entrapment of air in the pores, the SiC green parts prepared by EPD were evacuated prior infiltration with pre-ceramic polymer (Figure 8).

The flow of liquid into porous substrate by capillary pressure is described by Darcy's law

$$h = \left[\frac{2KP_c}{\eta}\right]^{1/2} \cdot t^{1/2} \tag{13}$$

where h is the distance of liquid intruded during time t, K is the permeability of the porous body and η is the viscosity of the liquid. For identical infiltration conditions, the parabolic rate for different porous substrates will depend on the product of their permeability and capillary pressure of intruding liquid. According to the general form of a Laplace's equation, the capillary pressure is given by

$$P_c = \gamma \frac{\partial S}{\partial V} \tag{14}$$

where γ is the surface energy per unit area of the liquid and $\partial S/\partial V$ is the change in wetted solid surface area of the porous substrate per change in volume of intruded liquid. When the porosity is modelled with equivalent capillaries of radius r_e, capillary pressure can be expressed by

$$P_c = \frac{2\gamma \cos\theta}{r_e} \tag{15}$$

where θ is the wetting angle [125].

Assuming that the particles are identical spheres with diameter d, we can estimate the permeability of a porous substrate with Kozeny-Charman equation, which models the substrate as a bundle of tortuous capillary tubes with hydraulic diameters resembling slits [126].

$$K = \frac{d^2(1-\rho)^3}{36c\rho^2} \tag{16}$$

where c is a Kozeny constant that defines the shape and tortuosity of the pore channels (c=5 for many systems) [126].

According to Darcy's law (Equation 13), in order to promote infiltration, viscosity of the infiltrating liquid should be reduced. To reduce the viscosity, the SMP-10 polymer was pre-heated up to 100 °C prior to infiltration. Viscosity was reduced from 0.107 Pas at room temperature to 0.015 Pas after heating the polymer to 100 °C (Figure 16). Higher temperatures might lead to onset of cross-linking indicated by a sharp increase in viscosity at 110 °C and also confirmed by DSC (Figure 28).

Combining Equations 11-14 and assuming the pore size of 224 nm (median pore size of samples pre-sintered at 1700 °C, with relative density of 0.6 and grain size ~ 1μm), wetting angle of 20°, surface tension of SMP-10 polymer of 0.03 Nm^{-1}, the depth of infiltration is doubled after heating the SMP-10 to 100 °C in comparison to room temperature infiltration. Similar relation was determined from experimental observations (Figure 27). The samples infiltrated at room temperature show a good agreement between calculated and experimental values (Figure 67), whereas samples infiltrated with heated polymer (with or without prior evacuation) exhibited lower experimental values than calculated ones. Lower values for the vacuum infiltrated samples can be ascribed to

decrease in temperature of the polymer and therefore related increase in viscosity once the polymer is transferred to the vacuum chamber. Nevertheless, since both vacuum and non-vacuum infiltration procedures with heated polymer were able to fully impregnate the 10 mm thick sample, vacuum infiltration was still used for the infiltration of SITE samples (5.4 mm thick) to prevent any possible air entrapment in the samples.

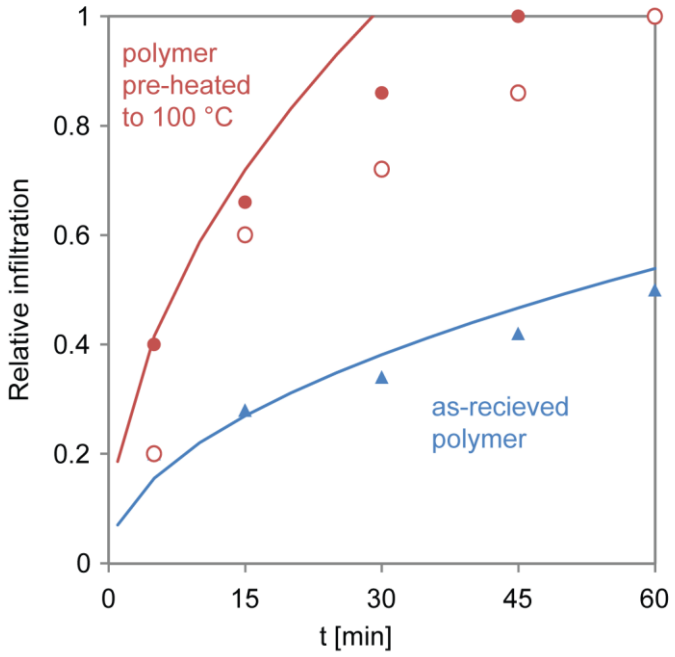

Figure 67: Comparison of calculated and experimental values of infiltration rate as a function of time (t) for as received polymer (▲) or polymer pre-heated to 100 °C, with (○) or without (●) evacuation of samples.

According to Tu and Lange [125], the permeability of the porous substrate has a greater effect on the infiltration period than capillary pressure. Therefore by increasing the density (reducing the pore size) after each PIP cycle, longer times are required in order to fully impregnate the substrate with the liquid polymer. Assuming the density of 87 %TD and pore size of 80 nm (density and median pore size after six PIP cycles), the calculated time needed to infiltrate the substrate is nearly doubled in comparison to the initial infiltration time. The plateau in densification after six PIP cycles is most likely due to inefficient infiltration in the following cycles due to reduced pore size and thus reduced permeability of the material.

5.2.2 Polymer-to-ceramic transformation

At heat treatment polymer starts cross-linking via allyl side groups at 116 °C and a sharp exothermal maximum is observed at 230 °C (Figure 28), which has been attributed to self-cross linking via the loss of hydrogen [103]. Gradual cross-linking with complete removal of hydrogen and transformation to Si-C is achieved with increasing temperature up to 1200 °C (Figure 29). Residual Si-C network is still amorphous and further heat treatment is needed to form a crystalline ceramic (Figure 30). Heat treatment above 1500 °C resulted in a nanocrystalline β-SiC, confirmed by TEM examination and XRD. As was noted by Moraes and Interrante [127] the density of AHPCS derived SiC below 1600 °C is much lower than that of crystalline SiC, indicating an incomplete polymer-to-ceramic transformation.

During heat treatment there is approximately 18 % weight loss after heating up to 1400 °C in N_2 atmosphere (Figure 28). Weight loss occurs in two major stages. At temperatures below 280 °C there is approximately 10 % weight loss attributed to loss of low weight oligomers. At higher temperatures pyrophoric silanes, hydrogen and CH_4 are removed from the structure [103].

SiC powder infiltrated into fibrous preform by EP(I)D prior to polymer infiltration acted as a passive filler during pyrolysis. In the presence of these initial SiC grains, the nanocrystalline polymer-derived SiC is at temperatures above 1500 °C sintered according to the Ostwlad ripening, onto the initial grains, resulting in epitaxial growth of initial grains on the account of the polymer-derived SiC (Figure 32).

In order to densify the material, several PIP cycles were needed, due to large weight loss and low polymer-to-ceramic volume yield (26 vol. % [52]). The density of the samples increased progressively with the number of PIP cycles, achieving ~87 % TD after six PIP cycles. This is significant improvement in comparison to the work of Lee et al.[128], which reported the need of twelve PIP cycles using high-pressure impregnation to achieve the same level of density for pressed samples. Furthermore, in that study authors did not offer any explanation how to introduce high volume fraction of powder needed for successful densification into SiC fibre preform. Usually, in fabrication of SiC_f/SiC by PIP, powder filler is introduced into the polymer, to reduce the amount of PIP cycles and enhance densification. However, only small amount of powder (~10 vol. %) can be added, since higher fractions result in higher viscosity of polymer-powder suspension which is unsuitable for infiltration of fabric preform. High volume fraction of powder is crucial in order to enhance densificaton (fewer PIP cycles) and to obtain a more homogeneous microstructure. Microstructure of SiC_f/SiC composite fabricated by standard PIP processing (PIP-SiC_f/SiC) is characterised by large voids and highly cracked matrix which are the result of dimensional changes during polymer-to-ceramic transformation. In the case of SITE-SiC_f/SiC a more homogeneous microstructure is obtained (Figure 53), due to high particle packing after EP(I)D and pre-sintering of the matrix prior to infiltration with polymer precursor.

As it is evident from Figure 62 the PyC fibre-matrix interphase is no longer observed after densification and the individual fibres were sintered together. The interphase most likely reacted with the polymer precursor during heat treatment resulting in a carbon-rich SiC near the fibres surface. Similar observations were also reported by Kolaya et al. [129] in Hi-Nicalon reinforced composites densified with allyl-hydridopolycarbosilane, after heat treatment above 1600 °C. The reaction of the PyC interphase with SiC matrix appears to be related to polymer decomposition, since such reaction was not observed in other fabrication techniques (e.g. CVI composites heat treated at temperatures up to 2000 °C [130]). In order to prevent this reaction a more stable interphase (preferably SiC-PyC multilayer) should be applied.

The incorporation of active fillers, W and $CrSi_2$ did not result in an expected increase in density, although both reacted with the preceramic polymer as reported in literature [70]. In the case of tungsten addition, dense material was obtained only in the case of high tungsten fraction, resulting in a material consisting of W_2C, W_5Si_3 and W. Preliminary examination of the material revealed interesting properties (high mechanical properties, increasing thermal conductivity with temperature) that make the material potentially interesting for high heat flux application.

5.3 Characteristics of the produced composites

5.3.1 Composition

Composition of a polymer derived ceramic is dependent mostly on the initial composition of the polymer and atmosphere conditions during pyrolysis [131]. Next to relatively high ceramic yield in comparison to other polycarbosilanes, SMP-10 polymer was selected primarily due to the fact that it yields a near-stoichiometric β-SiC. By combining this precursor with β-SiC powders as passive filler and near-stoichiometric SiC fibres, the expectation was to produce pure SiC matrix material.

Composition of the material evaluated by several techniques (XRD, EDXS, TEM) revealed that the matrix material, as expected, consists of only SiC. XRD spectra reveals that the predominant phase in the material is cubic β-SiC, with minor amount of α-SiC also present. The presence of α-SiC was also detected in the used powder (8.6 % of α-SiC present [101]) and fibres. The resulting presence of α-SiC in the material can therefore be ascribed to the used materials and not the densification process itself. Minor quantities of Al were also detected in the fibres, which is used as a sintering aid in the fabrication of the fibres. The obtained composition of the composite indicates that pure β-SiC composite can be achieved when initial constituents of the composites, i.e. powder and fibres, are composed of only β-SiC. Thus, the employed processing technique represents an important advantage for the production of fusion-grade SiC-composite, for which, due to the absence of usual sintering additives, low neutron activation may be expected. On the other side, in comparison with CVI and standard PIP that also yield in pure SiC, a more favourable pore size and porosity distribution as well as high crystallinity (especially in comparison to PIP) should result in enhanced mechanical and thermal properties of the composite.

5.3.2 Mechanical properties

Mechanical properties of the matrix material (without fibres) were increasing with consecutive PIP cycles that gradually increased relative density. Hardness of EP-SiC matrix achieved maximal values of 2300HV and 1740HV for samples heat treated at 1600 °C and 1700 °C, respectively. Increase with densification was also observed for elastic modulus (E) reaching 260 GPa (EP6) for samples densified at either 1600 °C or 1700 °C. In comparison with elastic modulus of dense SiC ceramics (>400 GPa for dense polycrystalline SiC [16, 17]), much lower values of the EP-SiC matrix can be ascribed to the residual pore volume fraction (V_p) porosity, which exponentially decreases the value of (room temperature) E- modulus according to

$$E = E_0 e^{(-CV_p)} \tag{18}$$

where E_0 is the elastic modulus of a dense material and C is a constant[16].

The flexural strength reached 230±160 MPa for the SiC-matrix sintered at 1600 °C and 337±75 MPa when sintered at 1700 °C. The reported values of room temperature strength of polycrystalline SiC vary from 200 to over 500 MPa, depending on the fabrication technique and composition (sintering additives, free silicon) [16]. Matrix samples densified with maximal heating temperature of 1600 °C exhibited a large scatter of measured values, mainly due to microcracks that were formed during densification, especially at and near the surface of the samples. Pre-sintering and final densification at 1700 °C led to a material with a more uniform structure and failure behaviour.

Although mechanical properties, in particular flexural strength and fracture toughness, are highly important for the proposed application, due to the limited amount of the SiC-fabric, only a preliminary examination of mechanical properties of the SITE-SiC_f/SiC composites could be performed, i.e. the number of samples was insufficient for the reliable analysis. The measured flexural strength was between 60 and 90 MPa, which is much lower in comparison to the SiC-matrix without fibres. SITE-SiC_f/SiC composite material exhibited brittle fracture behaviour with minimal fibre pull-out as is evident form Figure 62. Very low measured strength of the material is most likely the result of non-existing interphase layer and consequential sintering of individual fibres. By sintering of the fibres the role of fibre reinforcement was lost and the material behaved as a porous monolithic ceramic. In comparison to literature values of flexural strength of composites fabricated without the interphase layer (but with unaffected fibres) the measured values are approximately three times lower [132]. The application of a more stable interphase layer is essential and is expected to significantly increase the strength of the material, by providing a weak fibre-matrix bonding and even more importantly, providing chemical protection, preventing the sintering of the fibres.

The composite without a functional interphase layer and fibres to provide pseudoplastic behaviour of the material, should behave as a SiC matrix alone, which was not true. This is due to larger pore size (especially in intrabundle areas) in comparison to bulk SiC matrix, which resulted in much lower flexural strength.

5.3.3 Thermal transport properties

Thermal conductivity of the matrix material was gradually increased with the number of PIP cycles as a result of densification. Crystalline material is required in order to obtain high thermal conductivity of the material. Composites fabricated by standard PIP process normally exhibited low thermal conductivity due to only partially crystalline matrix, the result of low processing temperatures (< 1500 °C).

Measured thermal conductivity of SITE-SiC_f/SiC was compared to literature data for state-of-art SiC_f/SiC composites (Figure 48). Most relevant properties of compared composite materials (fibre volume fraction, density etc.) are summarised in Table 5.

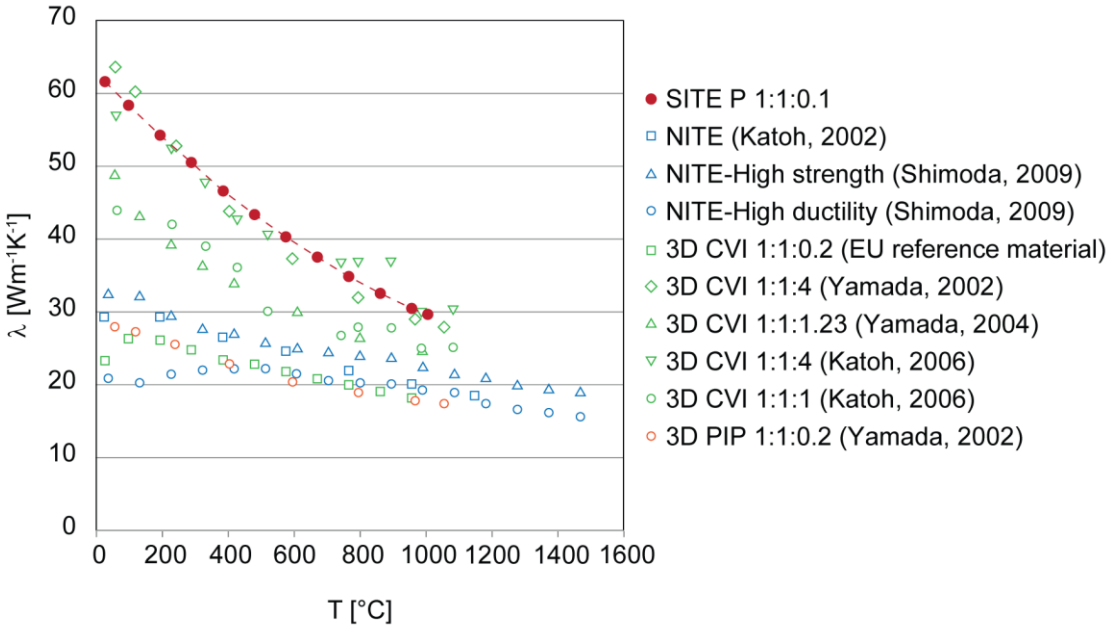

Figure 68: Comparison of thermal conductivity of SITE-SiC_f/SiC with literature data.

Table 5: State of art SiC/SiC [47, 66, 133-136]

Author	Fabrication tehnique	Fiber	Reinforcement architecture	V_f	Fibre orientation	Interphase	Density
				[%]	x:y:z		gcm^{-3}
	SITE-P	Tyranno™ SA3	3D Orthogonal	35	1:1:0.1	PyC (100 nm)	2.77
Blagoeva, 2011	isothermal CVI (EU ref. material)	Tyranno™ SA3	3D	31[a]	1:1:0.2[a]	PyC (80 nm)	2.65[a]
Katoh, 2006	isothermal/isobaric CVI	Tyranno™ SA3	3D Orthogonal	45	1:1:4	PyC (150 nm)	2.8
	CVI	Tyranno™ SA3	3D Orthogonal	45	1:1:1	PyC (150 nm)	2.8
Yamada, 2002	CVI	Tyranno SA	3D	23	1:1:4	-	2.89
	PIP	Tyranno SA	3D	34	1:1:0.2	SiC	2.57
Yamada, 2004	isothermal CVI	Tyranno SA	3D		1:1:1.23		2.88
Katoh, 2002	NITE	Tyranno™ SA3	2D-UD	30		PyC (800 nm)	2.85[b,*]
Shimoda, 2009	NITE-high strength	Tyranno™ SA3	2D-UD	53		PyC (500 nm)	3.11*
	NITE-high ductility	Tyranno™ SA3	2D-UD	52		PyC (500 nm)	2.98*

[b] Densitiy for sample sintered at 1780 °C, thermal conductivity for sample sintered at 1800 °C

[*] Density including YAG phase (ρ_{YAG}=4.55 gcm^{-3})

As is evident from Figure 68 the thermal conductivity of SITE-P samples is among the highest measured values for SiC_f/SiC composite materials. In contrast to CVI EU reference material (fabricated by MT Aerospace) with comparable volume fraction of fibres and x:y:z ratio it exhibits much higher values. Higher values can be on the one hand attributed to a more uniform porosity with smaller pore size (Figure 59) and on the other hand to larger grains, which are beneficial to thermal transport properties. Francl and Kingery [137] showed that the pore size, shape and orientation of pores in the direction of heat flow has a significant effect on the thermal conductivity of ceramic materials. The pore size and emissivity becomes especially important at higher temperatures [137]. The effect of large flat voids on the thermal conductivity of SiC_f/SiC composites was already discussed by Yamada et al. [138]. They concluded that the presence of large flat voids reduces the through thickness thermal conductivity of CVI composites.

Other SiC_f/SiC composites prepared by CVI (Katoh, 2006; Yamada 2002) which exhibit higher values of thermal conductivity, comparable to SITE-P SiC_f/SiC, have in contrast to SITE much higher fraction of fibres oriented in z-direction (through

thickness). As was already noted by Katoh et al. [68], in orthogonal 3D CVI composites, higher fraction of fibres oriented in z-direction contribute to higher through-thickness thermal conductivity, because the fibres and the matrix shells around the tows carry a major fraction of heat.

Although the densities of NITE samples were higher than for other fabrication techniques (~3.0 gcm^{-3}), reported values of thermal conductivity were lower (~30 $Wm^{-1}K^{-1}$ at RT and below 20 $Wm^{-1}K^{-1}$ at 1000 °C). Main reason for lower thermal conductivity is most likely the presence of oxide phase (~ 10 %) in the NITE matrix due to sintering additives used in the process. As was reported by Sigl [139] in the study of LPS-SiC materials, the presence of oxide secondary phases and in particular amorphous grain boundaries films can significantly reduce the overall thermal conductivity of the material even at low amount of sintering additives. In the case of NITE composites there is also no fibres oriented in the z-direction due to 2D reinforcement architecture and therefore there is no contribution of the fibres to the through-thickness thermal conductivity.
Measured values of through thickness thermal conductivity exceed in most cases the design assumed value of 20 $Wm^{-1}K^{-1}$ at operational temperatures (1000 °C), however due to inevitable reduction of thermal conductivity due to neutron irradiation induced swelling, the need for even higher values remains.

6 Conclusions

The aim of this research was to develop a novel technique for fabrication of SiC_f/SiC composites, one of the candidate materials for structural application in future fusion power plants. The combined process of electrophoretic (infiltration) deposition and polymer infiltration and pyrolysis was investigated as a possible route for densification of 3D reinforced SiC fabric preform at moderate temperatures (<1800 °C) and pressures. The main emphasis in the work was on infiltration of fabric preform with high fraction of SiC powder with electrophoretic (infiltration) deposition prior to densification by aid of polymer infiltration and pyrolysis, as the presence of large voids in the SiC matrix was recognised as the main reason for insufficient density and thermal conductivity. The main idea was to fill the pore space of the preform with a passive filler (high packing density) and/or active filler to achieve a more uniform matrix with reduced porosity.

In the first part of the investigation, the parameters for deposition of SiC matrix with highest possible density were determined based on deposition of bulk SiC matrix (without fibres). High packing densities of ~60 %TD were obtained. The attempts to further increase the green density of SiC matrix by use of bimodal particle suspensions (submicron and nano-sized powder) or by active filler controlled pyrolysis (W, $CrSi_2$), did not result in an increased density, due to the fact that the initial green densities of deposits were lower than in the case of submicron SiC matrix. Low pressure, moderate temperature densification by six cycles of polymer infiltration and pyrolysis process followed by additional heat treatment at 1600 °C or 1700 °C (EP6) resulted in pure, crystalline SiC matrix material with ~87 % TD. Six PIP cycles were selected for densification, since further cycles did not increase the density of the material, most likely due to inability to further infiltrate the material with preceramic polymer. Further densification might be achieved by application of pressure in the next polymer infiltration steps; however, this approach was not adopted within this work. Densified material was characterised by flexural strength of 337±75 MPa, hardness of 1740HV, elastic modulus of 260 GPa and room temperature thermal conductivity of 60 $Wm^{-1}K^{-1}$.

Electrophoretic deposition has proven in this work to be an effective way of infiltration of thick conductive substrates such as 3D woven fibre preforms. Several important finding were identified in order to successfully infiltrate thick conductive preforms by EP(I)D. It is essential that the fibres are separated from the electrode to prevent electric field shielding and deposition only on the proximal side of the preform. By separating the fibres from the electrode, the particles stream through the thickness of the preform due to the potential gradient between the electrodes. To prevent particle deposition on the fibres and to achieve full penetration of powder through the preform an electrostatic repulsion force must exist between the particles and the fibres. Both constituents (particles, fibres) had a similar electrokinetic behaviour in aqueous suspensions and depositions were performed at pH10 where both possessed a high (negative) zeta potential. To promote infiltration wetting of the fibres with aqueous suspension was enhanced by treating the surface of fibres with anionic surfactant. To prevent any air entrapment within the preform, fabric was also evacuated and gradually filled with the suspension prior to electrophoretic (infiltration) deposition. The process resulted in a preform infiltrated through the entire thickness (5.4 mm) with excellent infiltration in the interbundle areas

and partial infiltration of intrabundle areas. Further improvement of infiltration might be achieved by infiltration by nanosized particles. As-deposited composites were carefully dried to mitigate the formation of drying cracks.

Prior to polymer infiltration and pyrolysis, dried EP(I)D compacts were strengthened to prevent cracking associated with dimensional changes of polymer precursor during polymer-to-ceramic conversion. Strengthening without shrinkage was accomplished by pre-sintering the deposits at temperatures < 1700 °C, which resulted in neck formation and facetation of particles and increase in pore size, beneficial for further infiltration with polymer precursor. For a successful infiltration, polymer precursor was heated up to 100 °C to reduce its viscosity. Densification by polymer infiltration and pyrolysis resulted in a gradual filling of the voids within the infiltrated material. After six PIP cycles the composite SiC_f/SiC material density was ~ 2.8 gcm^{-3} (~87 %TD). Full densification was not achieved, however, a more homogeneous microstructure with majority of pores < 1μm without the presence of large voids in interbundle areas, typical for standard PIP (and CVI) processing shows a significant improvement in comparison to these processes. The resulting composite material was composed of β-SiC with minor amounts of α-SiC, which was attributed to the α-SiC present in the starting materials (powder, fibres).

SITE-SiC_f/SiC samples exhibited brittle fracture behaviour and low mechanical strength, much lower than that for the SiC matrix alone. Such result is the consequence of the unfavourable microstructure in which the fibre-matrix interphase layer, essential for pseudoplastic behaviour in ceramic matrix composites, was not present after final processing. Obviously, during heat treatment above 1600 °C the PyC fibre-matrix interphase layer reacted with the polymer derived SiC. In order to ensure non-brittle behaviour of the material and to justify the role of fibres within the material, PyC interphase should be replaced by a more stable interphase such as (PyC-SiC)n multilayer.

Through thickness thermal conductivity of SITE SiC_f/SiC is among the highest measured values in comparison to other state-of-art materials. Comparable values were obtained by CVI-SiC_f/SiC, however only in the case where the amount of fibres oriented in the z-direction was much higher; therefore we can conclude that the contribution of matrix phase in case of SITE samples was much higher than in the case of CVI. A more uniform matrix with larger grain size and the absence of large interbundle voids, play a crucial role in high thermal conductivity of the material.

The composed work offers a new insight into the use of electrophoretic (infiltration) deposition (EP(I)D) for infiltration of thick porous bodies such as fabric reinforcements in composite materials. It contributes to a better understanding of electrophoretic infiltration of porous conductive structures. It also shows for the first time that the process of polymer infiltration and pyrolysis can be, by using appropriate processing conditions, effectively utilised to form a highly crystalline material with high thermal conductivity. The SITE, a novel process combining EP(I)D and PIP was presented as a promising technique for fabrication of SiC-based ceramic matrix composites. For full implementation of such material optimisation of the interphase layer would be needed.

7 Acknowledgements

This work was financially supported by the Slovenian Research Agency (PN: 1000-08-310084) and was carried out within the framework of the European Fusion programme financially supported under the Contract of Association between EURATOM and the Ministry of Education, Science, Culture and Sport of the Republic of Slovenia. The content of this work is the sole responsibility of its authors and it does not necessarily represent the views of the European Commission or its services.

Firstly I would like to thank my PhD supervisor, Asst. prof. Saša Novak Krmpotič for the encouragement, support and guidance during my work and study at the Jožef Stefan Institute, as well as for all the advice, ideas and valuable discussions.

I would also like to thank Dr. Peter Greil and Dr. Nahum Travitzky for their help with active-filler controlled pyrolysis and giving me the opportunity to work in their research group at Tächnische Fakultät Erlangen-Nürnberg. The secondment was financed by the European Commission (EURATOM – Fusion programme) in the frame of the Staff mobility scheme.

My thanks also go to Darina Blagoeva from NRG, Petten and Andrei Galatanu from the National Institute of Materials Physics, Bucharest for preforming high temperature thermal conductivity measurements; to Llion Marc Evans from Manchester University for preforming computer tomography; to Dr. Srečo Škapin for XRD measurements; to Prof.dr. Goran Dražić for TEM analysis and interpretation of results; to Medeja Gec for TEM sample preparation; to Dr. Zoran Samardžija for EDXS analysis of the composite; to Dare Eterovič for assistance in measuring room temperature mechanical properties.

I would also like to thank Jaro Bele, Marko Lukek, Janko Štajner and Matej Kocen for their technical assistance.

8 References

1. Chen, F. F. *An Indispensable Truth How Fusion Power Can Save the Planet* (Springer, New York, 2011).
2. EFDA | European Fusion Development Agreement. http://www.efda.org/ (accessed December 2012).
3. Llewellyn Smith, C.; Ward, D. Fusion. *Energy Policy* **36**, 4331–4334 (2008).
4. Garin, P.; Sugimoto, M. Status of IFMIF Design and R&D. *Fusion Engineering and Design* **83**, 971–975 (2008).
5. Baker, C. C. Advances in fusion technology. *Journal of Nuclear Materials* **283–287, Part 1**, 1–9 (2000).
6. Zinkle, S. J. Advanced materials for fusion technology. *Fusion Engineering and Design* **74**, 31–40 (2005).
7. McCracken, G.; Stott, P. *Chapter 11 - Fusion Power Plants* (Academic Press, Burlington, 2005).
8. Maisonnier, D.; Cook, I.; Sardain, P.; Andreani, P. R.; Pace, L. D.; Forrest, R.; Giancarli, L.; Hermsmeyer, S.; Norajitra, P.; Taylor, N.; Ward, D. *A Conceptual Study of Commercial Fusion Power Plants: Final Report of the European Power Plant Conceptual Study* (European Fusion Development Agreement, Garching, 2005).
9. Giancarli, L.; Bonal, J. P.; Caso, A.; Le Marois, G.; Morley, N. B.; Salavy, J. F. Design requirements for SiC/SiC composites structural material in fusion power reactor blankets. *Fusion Engineering and Design* **41**, 165–171 (1998).
10. Raffray, A. R.; El-Guebaly, L.; Gordeev, S.; Malang, S.; Mogahed, E.; Najmabadi, F.; Sviatoslavsky, I.; Sze, D. K.; Tillack, M. S.; Wang, X. High performance blanket for ARIES-AT power plant. *Fusion Engineering and Design* **58–59**, 549–553 (2001).
11. Nishio, S.; Ueda, S.; Aoki, I.; Kurihara, R.; Kuroda, T.; Miura, H.; Kunugi, T.; Seki, Y.; Nagashima, T.; Ohta, M.; Adachi, J.; Yamazak, S.; Kawaguchi, I.; Hashimoto, T.; Shinya, K.; Murakami, Y.; Takase, H.; Nakamura, T. Improved tokamak concept focusing on easy maintenance. *Fusion Engineering and Design* **41**, 357–364 (1998).
12. Norajitra, P.; Bühler, L.; Fischer, U.; Kleefeldt, K.; Malang, S.; Reimann, G.; Schnauder, H.; Giancarli, L.; Golfier, H.; Poitevin, Y.; Salavy, J. F. The EU advanced lead lithium blanket concept using SiCf/SiC flow channel inserts as electrical and thermal insulators. *Fusion Engineering and Design* **58–59**, 629–634 (2001).
13. Hopkins, G. R. Silicon carbide and graphite materials for fusion reactors. in *5. conference on plasma physics and controlled nuclear fusion research*. (International Atomic Energy Agency, Tokyo, 1975).
14. Snead, L. L.; Nozawa, T.; Ferraris, M.; Katoh, Y.; Shinavski, R.; Sawan, M. Silicon carbide composites as fusion power reactor structural materials. *Journal of Nuclear Materials* **417**, 330–339 (2011).

15. Izhevskyi, V. A.; Genova, L. A.; Bressiani, J. C.; Bressiani, A. H. A. Review article: silicon carbide. Structure, properties and processing. *Cerâmica* **46**, 4–13 (2000).
16. Snead, L. L.; Nozawa, T.; Katoh, Y.; Byun, T.-S.; Kondo, S.; Petti, D. A. Handbook of SiC properties for fuel performance modeling. *Journal of Nuclear Materials* **371**, 329–377 (2007).
17. Schwetz, K. A. Riedel, R. (ed.) *Silicon Carbide Based Hard Materials* (Wiley-VCH Verlag GmbH, Weinheim, 2008).
18. Sawan, M. E.; Ghoniem, N. M.; Snead, L.; Katoh, Y. Damage production and accumulation in SiC structures in inertial and magnetic fusion systems. *Journal of Nuclear Materials* **417**, 445–450 (2011).
19. Taguchi, T.; Nozawa, T.; Igawa, N.; Katoh, Y.; Jitsukawa, S.; Kohyama, A.; Hinoki, T.; Snead, L. L. Fabrication of advanced SiC fiber/F-CVI SiC matrix composites with SiC/C multi-layer interphase. *Journal of Nuclear Materials* **329–333, Part A**, 572–576 (2004).
20. Shimoda, K.; Park, J. S.; Hinoki, T.; Kohyama, A. Microstructural optimization of high-temperature SiC/SiC composites by NITE process. *Journal of Nuclear Materials* **386–388**, 634–638 (2009).
21. IEST Co. Ltd. http://www.iest.jp/english/top.html (accessed December 2012).
22. Wiederhorn, S. M. Brittle-Fracture and Toughening Mechanisms in Ceramics. *Annual Review of Materials Science* **14**, 373–403 (1984).
23. Chawla, K. K. (ed.) *Composite materials* (Springer-Verlag, New York, 1998).
24. Yajima, S.; Okamura, K.; Hayashi, J.; Omori, M. Synthesis of Continuous SiC Fibers with High Tensile Strength. *Journal of the American Ceramic Society* **59**, 324–327 (1976).
25. Clauß, B. *Fibers for Ceramic Matrix Composites* (Wiley-VCH Verlag GmbH & Co. KGaA, Weinheim, 2008).
26. Bunsell, A.; Piant, A. A review of the development of three generations of small diameter silicon carbide fibres. *Journal of Materials Science* **41**, 823–839 (2006).
27. Buet, E.; Sauder, C.; Poissonnet, S.; Brender, P.; Gadiou, R.; Vix-Guterl, C. Influence of chemical and physical properties of the last generation of silicon carbide fibres on the mechanical behaviour of SiC/SiC composite. *Journal of the European Ceramic Society* **32**, 547–557 (2012).
28. Specialty Materials Inc. http://specmaterials.com/ (accessed December 2012).
29. Tisics Ltd. http://www.tisics.co.uk/ (accessed December 2012).
30. Drazic, G.; Toplisek, T.; Gec, M.; Ivekovic, A.; Novak, S. Electron Microscopy of SiC Fibers Used in SiC Based Ceramic Composite Material for Fusion Application. *Microscopy and Microanalysis* **18**, 1884–1885 (2012).
31. Behera, B. K.; Mishra, R. 3-Dimensional weaving. *Indian Journal of Fibre and Textile Research* **33**, 274–287 (2008).
32. Gries, T.; Stüve, J.; Grundmann, T. *Textile Reinforcement Structures* (Wiley-VCH Verlag GmbH & Co. KGaA, Weinheim, 2008).
33. Long, A. C.; L.P., B. Boisse, P. (ed.) *Modelling the geometry of textile reinforcements for composites: TexGen* (Woodhead Publishing Ltd, Cambridge, 2011).
34. Naslain, R. R. The design of the fibre-matrix interfacial zone in ceramic matrix composites. *Composites Part A: Applied Science and Manufacturing* **29**, 1145–1155 (1998).

35. He, X.-B.; Yang, H. Preparation of SiC fiber-reinforced SiC composites. *Journal of Materials Processing Technology* **159**, 135–138 (2005).
36. Droillard, C.; Lamon, J. Fracture Toughness of 2-D Woven SiC/SiC CVI-Composites with Multilayered Interphases. *Journal of the American Ceramic Society* **79**, 849–858 (1996).
37. Hasegawa, A.; Kohyama, A.; Jones, R. H.; Snead, L. L.; Riccardi, B.; Fenici, P. Critical issues and current status of SiC/SiC composites for fusion. *Journal of Nuclear Materials* **283–287, Part 1**, 128–137 (2000).
38. Katoh, Y.; Nozawa, T.; Snead, L. L. Mechanical Properties of Thin Pyrolitic Carbon Interphase SiC–Matrix Composites Reinforced with Near-Stoichiometric SiC Fibers. *Journal of the American Ceramic Society* **88**, 3088–3095 (2005).
39. Miller, J. H.; Liaw, P. K.; Landes, J. D. Influence of fiber coating thickness on fracture behavior of continuous woven Nicalon® fabric-reinforced silicon-carbide matrix ceramic composites. *Materials Science and Engineering: A* **317**, 49–58 (2001).
40. Liu, H.; Cheng, H.; Wang, J.; Che, R.; Tang, G.; Ma, Q. Microstructural investigations of the pyrocarbon interphase in SiC fiber-reinforced SiC matrix composites. *Materials Letters* **63**, 2029–2031 (2009).
41. Rebillat, F.; Lamon, J.; Guette, A. The concept of a strong interface applied to SiC/SiC composites with a BN interphase. *Acta Materialia* **48**, 4609–4618 (2000).
42. Udayakumar, A.; Sri Ganesh, A.; Raja, S.; Balasubramanian, M. Effect of intermediate heat treatment on mechanical properties of SiCf/SiC composites with BN interphase prepared by ICVI. *Journal of the European Ceramic Society* **31**, 1145–1153 (2011).
43. Krenkel, W. (ed.) *Ceramic Matrix Composites* (Wiley-VCH, Weinheim, 2008).
44. Kelly, B. T.; Burchell, T. D. Structure-related property changes in polycrystalline graphite under neutron irradiation. *Carbon* **32**, 499–505 (1994).
45. Snead, L. L.; Osborne, M. C.; Lowden, R. A.; Strizak, J.; Shinavski, R. J.; More, K. L.; Eatherly, W. S.; Bailey, J.; Williams, A. M. Low dose irradiation performance of SiC interphase SiC/SiC composites. *Journal of Nuclear Materials* **253**, 20–30 (1998).
46. Xu, Y.; Cheng, L.; Zhang, L.; Yin, X.; Yin, H. High performance 3D textile Hi-Nicalon SiC/SiC composites by chemical vapor infiltration. *Ceramics International* **27**, 565–570 (2001).
47. Katoh, Y.; Nozawa, T.; Snead, L. L.; Hinoki, T.; Kohyama, A. Property tailorability for advanced CVI silicon carbide composites for fusion. *Fusion Engineering and Design* **81**, 937–944 (2006).
48. Leuchs, M. *Chemical Vapour Infiltration Processes for Ceramic Matrix Composites: Manufacturing, Properties, Applications* (Wiley-VCH Verlag GmbH & Co. KGaA, Weinheim, 2008).
49. Motz, G.; Schmidt, S.; Beyer, S. *The PIP-Process: Precursor Properties and Applications* (Wiley-VCH Verlag GmbH & Co. KGaA, 2008).
50. Katoh, Y.; Kotani, M.; Kishimoto, H.; Yang, W.; Kohyama, A. Properties and radiation effects in high-temperature pyrolyzed PIP-SiC/SiC. *Journal of Nuclear Materials* **289**, 42–47 (2001).
51. Starfire Systems Inc. http://www.starfiresystems.com/ (accessed December 2012).
52. Kotani, M.; Katoh, Y.; Kohyama, A.; Narisawa, M. Fabrication and Oxidation-Resistance Property of Allylhydridopolycarbosilane-Derived SiC/SiC Composites. *Journal of the Ceramic Society of Japan* **111**, 7 (2003).

53. Heidenreich, B. *Melt Infiltration Process* (Wiley-VCH Verlag GmbH & Co. KGaA, Weinheim, 2008).

54. Lee, S. P.; Katoh, Y.; Park, J. S.; Dong, S.; Kohyama, A.; Suyama, S.; Yoon, H. K. Microstructural and mechanical characteristics of SiC/SiC composites with modified-RS process. *Journal of Nuclear Materials* **289**, 30–36 (2001).

55. Honglei, W.; Xingui, Z.; Jinshan, Y.; Yingbin, C.; Rongjun, L. Microstructure, mechanical properties and reaction mechanism of KD-1 SiCf/SiC composites fabricated by chemical vapor infiltration and vapor silicon infiltration. *Materials Science and Engineering: A* **528**, 2441–2445 (2011).

56. Noviyanto, A.; Yoon, D.-H. One component metal oxide sintering additive for β-SiC based on thermodynamic calculation and experimental observations. *Metals and Materials International* **18**, 63–68 (2012).

57. Prochazka, S.; Scanlan, R. M. Effect of Boron and Carbon on Sintering of SIC. *Journal of the American Ceramic Society* **58**, 72–72 (1975).

58. Gomez, E.; Echeberria, J.; Iturriza, I.; Castro, F. Liquid phase sintering of SiC with additions of Y2O3, Al2O3 and SiO2. *Journal of the European Ceramic Society* **24**, 2895–2903 (2004).

59. Ihle, J.; Herrmann, M.; Adler, J. Phase formation in porous liquid phase sintered silicon carbide: Part I:: Interaction between Al2O3 and SiC. *Journal of the European Ceramic Society* **25**, 987–995 (2005).

60. Baud, S.; Thévenot, F.; Pisch, A.; Chatillon, C. High temperature sintering of SiC with oxide additives: I. Analysis in the SiC–Al2O3 and SiC–Al2O3–Y2O3 systems. *Journal of the European Ceramic Society* **23**, 1–8 (2003).

61. Wu, L.; Chen, Y.; Jiang, Y.; Huang, Z. Liquid phase sintering of sic with AlN-Re 2O 3 additives. *Kuei Suan Jen Hsueh Pao/ Journal of the Chinese Ceramic Society* **36**, 593–596 (2008).

62. Negita, K. Effective Sintering Aids for Silicon Carbide Ceramics: Reactivities of Silicon Carbide with Various Additives. *Journal of the American Ceramic Society* **69**, 308–310 (1986).

63. Rieth, M.; Dafferner, B.; Röhrig, H. D. Embrittlement behaviour of different international low activation alloys after neutron irradiation. *Journal of Nuclear Materials* **258–263, Part 2**, 1147–1152 (1998).

64. Koyanagi, T.; Kondo, S.; Hinoki, T. The influence of sintering additives on the irradiation resistance of NITE SiC. *Journal of Nuclear Materials* **417**, 435–439 (2011).

65. Sudre, O.; Lange, F. F. Effect of Inclusions on Densification: I, Microstructural Development in an Al2O3 Matrix Containing a High Volume Fraction of ZrO2 Inclusions. *Journal of the American Ceramic Society* **75**, 519–524 (1992).

66. Katoh, Y.; Dong, S. M.; Kohyama, A. Thermo-mechanical properties and microstructure of silicon carbide composites fabricated by nano-infiltrated transient eutectoid process. *Fusion Engineering and Design* **61–62**, 723–731 (2002).

67. Dong, S.; Katoh, Y.; Kohyama, A. Preparation of SiC/SiC Composites by Hot Pressing, Using Tyranno-SA Fiber as Reinforcement. *Journal of the American Ceramic Society* **86**, 26–32 (2003).

68. Katoh, Y.; Snead, L. L.; Henager Jr, C. H.; Hasegawa, A.; Kohyama, A.; Riccardi, B.; Hegeman, H. Current status and critical issues for development of SiC composites for fusion applications. *Journal of Nuclear Materials* **367–370, Part A**, 659–671 (2007).

69. Nannetti, C. A.; Ortona, A.; de Pinto, D. A.; Riccardi, B. Manufacturing SiC-Fiber-Reinforced SiC Matrix Composites by Improved CVI/Slurry Infiltration/Polymer Impregnation and Pyrolysis. *Journal of the American Ceramic Society* **87**, 1205–1209 (2004).
70. Greil, P. Active-Filler-Controlled Pyrolysis of Preceramic Polymers. *Journal of the American Ceramic Society* **78**, 835–848 (1995).
71. Suzuki, K.; Nakano, K.; Kume, S.; Chou, T. W. *Fabrication and Characterization of 3D Carbon Fiber Reinforced SiC Matrix Composites via Slurry and Pulse-CVI Joint Process* (John Wiley & Sons, Inc., 2008).
72. Lee, S.-H.; Weinmann, M.; Aldinger, F. Fabrication of Fiber-Reinforced Ceramic Composites by the Modified Slurry Infiltration Technique. *Journal of the American Ceramic Society* **90**, 2657–2660 (2007).
73. Yang, J. Y.; Weaver, J. H.; Zok, F. W.; Mack, J. J. Processing of Oxide Composites with Three-Dimensional Fiber Architectures. *Journal of the American Ceramic Society* **92**, 1087–1092 (2009).
74. Shaw, D. J. *Introduction to colloid and surface chemistry* (Butterworth-Heinemann, 1992).
75. Delgado, A. V.; González-Caballero, F.; Hunter, R. J.; Koopal, L. K.; Lyklema, J. Measurement and interpretation of electrokinetic phenomena. *Journal of Colloid and Interface Science* **309**, 194–224 (2007).
76. Brett, C. M. A.; Brett, A. M. O. *Electrochemistry: Principles, Methods, and Applications* (Oxford Science Publications, 1993).
77. Singh, B.; Jena, J.; Besra, L.; Bhattacharjee, S. Dispersion of nano-silicon carbide (SiC) powder in aqueous suspensions. *Journal of Nanoparticle Research* **9**, 797–806 (2007).
78. Zhou, L.; Huang, Y.; Xie, Z. Gelcasting of concentrated aqueous silicon carbide suspension. *Journal of the European Ceramic Society* **20**, 85–90 (2000).
79. Besra, L.; Liu, M. A review on fundamentals and applications of electrophoretic deposition (EPD). *Progress in Materials Science* **52**, 1–61 (2007).
80. Dickerson, J. H.; Boccaccini, A. R. *Electrophoretic Deposition of Nanomaterials* (Springer, New York, 2011).
81. Masliyah, J. H.; Bhattacharjee, S. *Electrokinetic and Colloid Transport Phenomena* (John Wiley & Sons, Inc., Hoboken, 2005).
82. Sarkar, P.; Nicholson, P. S. Electrophoretic Deposition (EPD): Mechanisms, Kinetics, and Application to Ceramics. *Journal of the American Ceramic Society* **79**, 1987–2002 (1996).
83. Fukada, Y.; Nagarajan, N.; Mekky, W.; Bao, Y.; Kim, H.-S.; Nicholson, P. S. Electrophoretic deposition—mechanisms, myths and materials. *Journal of Materials Science* **39**, 787–801 (2004).
84. Hamaker, H. C.; Verwey, E. J. W. Part II.-(C) Colloid stability. The role of the forces between the particles in electrodeposition and other phenomena. *Transactions of the Faraday Society* **35**, 180–185 (1940).
85. Grillon, F.; Fayeulle, D.; Jeandin, M. Quantitative image analysis of electrophoretic coatings. *Journal of Materials Science Letters* **11**, 272–275 (1992).
86. De, D.; Nicholson, P. S. Role of Ionic Depletion in Deposition during Electrophoretic Deposition. *Journal of the American Ceramic Society* **82**, 3031–3036 (1999).
87. Haber, S.; Gal-Or, L. Deep Electrophoretic Penetration and Deposition of Ceramic Particles inside Porous Substrates : I . Analytical Model. *J. Electrochem. Soc.* **139**,

8 (1992).

88. Gal-Or, L.; Liubovich, S.; Haber, S. Deep electrophoretic penetration and deposition of ceramic particles inside porous substrates. II: Experimental model. *Journal of the Electrochemical Society* **139**, 1078–1081 (1992).
89. Keh, H. J.; Wei, Y. K. Diffusioosmosis and Electroosmosis of Electrolyte Solutions in Fibrous Porous Media. *Journal of Colloid and Interface Science* **252**, 354–364 (2002).
90. Ohshima, H. Electroosmotic Velocity in Fibrous Porous Media. *Journal of Colloid and Interface Science* **210**, 397–399 (1999).
91. Kozak, M. W.; Davis, E. J. Electrokinetic phenomena in fibrous porous media. *Journal of Colloid and Interface Science* **112**, 403–411 (1986).
92. Keh, H. J.; Chiou, J. Y. Electrophoresis of a colloidal sphere in a circular cylindrical pore. *AIChE Journal* **42**, 1397–1406 (1996).
93. Boccaccini, A. R.; Kaya, C.; Chawla, K. K. Use of electrophoretic deposition in the processing of fibre reinforced ceramic and glass matrix composites: a review. *Composites Part A: Applied Science and Manufacturing* **32**, 997–1006 (2001).
94. Stoll, E.; Mahr, P.; Krüger, H. G.; Kern, H.; Thomas, B. J. C.; Boccaccini, A. R. Fabrication technologies for oxide–oxide ceramic matrix composites based on electrophoretic deposition. *Journal of the European Ceramic Society* **26**, 1567–1576 (2006).
95. Bao, Y.; Nicholson, P. S. Constant Current Electrophoretic Infiltration Deposition of Fiber-Reinforced Ceramic Composites. *Journal of the American Ceramic Society* **90**, 1063–1070 (2007).
96. Boccaccini, A. R.; MacLaren, I.; Lewis, M. H.; Ponton, C. B. Electrophoretic deposition infiltration of 2-D woven SiC fibre mats with mixed sols of mullite composition. *Journal of the European Ceramic Society* **17**, 1545–1550 (1997).
97. Kaya, C.; Kaya, F.; Boccaccini, A. R. Electrophoretic deposition infiltration of 2-D metal fibre-reinforced cordierite matrix composites of tubular shape. *Journal of Materials Science* **37**, 4145–4153 (2002).
98. Streckert, H.; Norton, K.; Katz, J.; Freim, J. Microwave densification of electrophoretically infiltrated silicon carbide composite. *Journal of Materials Science* **32**, 6429–6433 (1997).
99. Müller, E.; Dittrich, R.; Moritz, K. Studies on a Novel Route to C/SiC. *Advanced Engineering Materials* **6**, 568–572 (2004).
100. Lee, J.-H.; Gil, G.-Y.; Yoon, D.-H. Fabrication of SiCf/SiC Composites using an Electrophoretic Deposition. *Journal of the Korean Ceramic Society* **46**, 447–451 (2009).
101. Gil, G.-Y.; Yoon, D.-H. Densification of SiCf/SiC composites by electrophoretic infiltration combined with ultrasonication. *Journal of Ceramic Processing Research* **12**, 371–375 (2011).
102. Yoshida, K. Development of silicon carbide fiber-reinforced silicon carbide matrix composites with high performance based on interfacial and microstructure control. *Journal of the Ceramic Society of Japan* **118**, 82–90 (2010).
103. Sreeja, R.; Swaminathan, B.; Painuly, A.; Sebastian, T. V.; Packirisamy, S. Allylhydridopolycarbosilane (AHPCS) as matrix resin for C/SiC ceramic matrix composites. *Materials Science and Engineering: B* **168**, 204–207 (2010).
104. Interrante, L. V.; Moraes, K.; Liu, Q.; Lu, N.; Puerta, A.; L. G. Sneddon, L. G. Silicon-based ceramics from polymer precursors. *Pure and Applied Chemistry* **74**, 2111–2117 (2002).

105. Langford, J. I.; Wilson, A. J. C. Scherrer after sixty years: A survey and some new results in the determination of crystallite size. *Journal of Applied Crystallography* **11**, 102–113 (1978).
106. Börger, A.; Supancic, P.; Danzer, R. The ball on three balls test for strength testing of brittle discs: stress distribution in the disc. *Journal of the European Ceramic Society* **22**, 1425–1436 (2002).
107. Maex, K.; Van Rossum, M. (eds.) *Properties of Metal Silicides* (INSPEC, the Institution of Electrical Engineers, London, 1995).
108. Lassner, E., Schubert, Wolf-Dieter *Tungsten: Properties, Chemistry, Technology of the Element, Alloys, and Chemical Compounds* (Springer, 1999).
109. Novak, S.; Dražić, G.; Mejak, K. Electrophoretic Deposition of Green Parts for LPS SiC-Based Ceramics. in *2nd International Conference on Electrophoretic Deposition: Fundamentals and Applications*. (Trans Tech Publications Ltd., Castelvecchio Pascoli, Italy, 2005).
110. Novak, S.; Dražić, G.; König, K.; Iveković, A. Preparation of SiCf/SiC composites by the slip infiltration and transient eutectoid (SITE) process. *Journal of Nuclear Materials* **399**, 167–174 (2010).
111. Novak, S.; Iveković, A. Fabrication of SiCf/SiC composites by SITE-P process. *Journal of Nuclear Materials* **427**, 110–115 (2012).
112. Toplišek, T. *Keramični kompoziti z dolgimi vlakni iz silicijevega karbida* (Univerza v Ljubljani, Ljubljana, 2011).
113. Novak, S.; Rade, K.; König, K.; Boccaccini, A. R. Electrophoretic deposition in the production of SiC/SiC composites for fusion reactor applications. *Journal of the European Ceramic Society* **28**, 2801–2807 (2008).
114. Li, W.; Chen, P.; Gu, M.; Jin, Y. Effect of TMAH on rheological behavior of SiC aqueous suspension. *Journal of the European Ceramic Society* **24**, 3679–3684 (2004).
115. Ramachandra Rao, R.; Roopa, H. N.; Kannan, T. S. Effect of pH on the dispersability of silicon carbide powders in aqueous media. *Ceramics International* **25**, 223–230 (1999).
116. Huang, Q.; Chen, P.; Gu, M.; Jin, Y.; Sun, K. Effect of surface modification on the rheological behavior of concentrated, aqueous SiC suspensions. *Materials Letters* **56**, 546–553 (2002).
117. Sarkar, P.; Haung, X.; Nicholson, P. S. Structural Ceramic Microlaminates by Electrophoretic Deposition. *Journal of the American Ceramic Society* **75**, 2907–2909 (1992).
118. Zok, F.; Lange, F. F.; Porter, J. R. Packing Density of Composite Powder Mixtures. *Journal of the American Ceramic Society* **74**, 1880–1885 (1991).
119. Van der Biest, O. O.; Vandeperre, L. J. Electrophoretic Deposition of Materials. *Annual Review of Material Science* **29**, 327–353 (1999).
120. Wu, Z.; Li, D. Induced-charge electrophoretic motion of ideally polarizable particles. *Electrochimica Acta* **54**, 3960–3967 (2009).
121. Loget, G.; Larcade, G.; Lapeyre, V.; Garrigue, P.; Warakulwit, C.; Limtrakul, J.; Delville, M. H.; Ravaine, V.; Kuhn, A. Single point electrodeposition of nickel for the dissymmetric decoration of carbon tubes. *Electrochimica Acta* **55**, 8116–8120 (2010).
122. Bazant, M. Z.; Squires, T. M. Induced-Charge Electrokinetic Phenomena: Theory and Microfluidic Applications. *Physical Review Letters* **92**, 066101 (2004).
123. Aschauer, U.; Burgos-Montes, O.; Moreno, R.; Bowen, P. Hamaker 2: A Toolkit

for the Calculation of Particle Interactions and Suspension Stability and its Application to Mullite Synthesis by Colloidal Methods. *Journal of Dispersion Science and Technology* **32**, 470–479 (2011).

124. Zhitomirsky, I. I. Cathodic electrodeposition of ceramic and organoceramic materials. Fundamental aspects. *Adv Colloid Interface Sci* **97**, 279–317 (2002).
125. Tu, W.-C.; Lange, F. F. Liquid Precursor Infiltration Processing of Powder Compacts: I, Kinetic Studies and Microstructure Development. *Journal of the American Ceramic Society* **78**, 3277–3282 (1995).
126. Lange, F. F. Powder Processing Science and Technology for Increased Reliability. *Journal of the American Ceramic Society* **72**, 3–15 (1989).
127. Moraes, K. V.; Interrante, L. V. Processing, Fracture Toughness, and Vickers Hardness of Allylhydridopolycarbosilane-Derived Silicon Carbide. *Journal of the American Ceramic Society* **86**, 342–346 (2003).
128. Lee, S. G.; Fourcade, J.; Latta, R.; Solomon, A. A. Polymer impregnation and pyrolysis process development for improving thermal conductivity of SiCp/SiC–PIP matrix fabrication. *Fusion Engineering and Design* **83**, 713–719 (2008).
129. Kolaya, L. E.; Lewis, N. *The Influence of Carbon on the Structure of Preceramic Polymer Derived SiC* (John Wiley & Sons, Inc., 1997).
130. Yang, W.; Araki, H.; Kohyama, A.; Yang, Q.; Noda, T. Effects of heat treatment on the microstructure and flexural properties of CVI–Tyranno-SA/SiC composite. *Ceramics International* **33**, 141–146 (2007).
131. Colombo, P.; Mera, G.; Riedel, R.; Sorarù, G. D. Polymer-Derived Ceramics: 40 Years of Research and Innovation in Advanced Ceramics. *Journal of the American Ceramic Society* **93**, 1805–1837 (2010).
132. Araki, H.; Yang, W.; Suzuki, H.; Hu, Q.; Busabok, C.; Noda, T. Fabrication and flexural properties of Tyranno-SA/SiC composites with carbon interlayer by CVI. *Journal of Nuclear Materials* **329–333, Part A**, 567–571 (2004).
133. Blagoeva, D.; Hegeman, J. B. J.; Heijna, M. C. R. *Current progress of the SiC/SiC activities at NRG* (EFDA, Garching, 2011).
134. Yamada, R.; Igawa, N.; Taguchi, T.; Jitsukawa, S. Highly thermal conductive, sintered SiC fiber-reinforced 3D-SiC/SiC composites: experiments and finite-element analysis of the thermal diffusivity/conductivity. *Journal of Nuclear Materials* **307–311, Part 2**, 1215–1220 (2002).
135. Yamada, R.; Igawa, N.; Taguchi, T. Thermal diffusivity/conductivity of Tyranno SA fiber- and Hi-Nicalon Type S fiber-reinforced 3-D SiC/SiC composites. *Journal of Nuclear Materials* **329–333, Part A**, 497–501 (2004).
136. Shimoda, K.; Hinoki, T.; Katoh, Y.; Kohyama, A. Development of the tailored SiC/SiC composites by the combined fabrication process of ICVI and NITE methods. *Journal of Nuclear Materials* **384**, 103–108 (2009).
137. Francl, J.; Kingery, W. D. Thermal Conductivity: IX, Experimental Investigation of Effect of Porosity on Thermal Conductivity. *Journal of the American Ceramic Society* **37**, 99–107 (1954).
138. Yamada, R.; Taguchi, T.; Nakano, J.; Igawa, N. Thermal Conductiviy of CVI and PIP SiC/SiC Composites. in *23rd Annual Conference on Composites, Advanced Ceramics, Materials, and Structures: A: Ceramic Engineering and Science Proceedings*. (John Wiley & Sons, Inc., Coccoa Beach, 2008).
139. Sigl, L. S. Thermal conductivity of liquid phase sintered silicon carbide. *Journal of the European Ceramic Society* **23**, 1115–1122 (2003).

Index of Figures

Index of Tables

Appendix

ARTICLES AND OTHER COMPONENT PARTS

Original scientific article

Iveković, A.; Novak, S.; Dražić, G.; Blagoeva, D.; Gonzales de Vincente, S. Current status and prospects of SiC_f/SiC for fusion structural applications. *Journal of European Ceramic Society*, In Press.

Novak, S.; Iveković, A. SiC-CNT composite prepared by electrophoretic Co-deposition and polymer infiltration and pyrolysis process. *Journal of Physical Chemistry, B Condens. mater. surf. interfaces biophys.* **117**, 1680–1685 (2013).

Novak, S.; Iveković, A. Fabrication of SiCf/SiC composites by SITE-P process. *Journal of Nuclear Materials* **427**, 110–115 (2012).

Iveković, A.; Dražić, G.; Novak, S. Densification of a SiC-matrix by electrophoretic deposition and polymer infiltration and pyrolysis process. *Journal of European Ceramic Society* **31**, 833–840 (2011).

Novak, S.; Dražić, G.; Koenig, K.; Iveković, A. Preparation of SiCf/SiC composites by the slip infiltration and transient eutectoid (SITE) process. *Journal of Nuclear Materials* **399**, 167–174 (2010).

Koenig, K.; Novak, S.; Iveković, A.; Rade, K.; Meng, D.; Boccaccini, A. R.; Kobe S. Fabrication of CNT-SiC/SiC composites by electrophoretic deposition. *Journal of European Ceramic Society* **30**, 1131–1137 (2010).

Novak S.; Koenig K.; Iveković A.; Boccaccini A. R. Infiltration of a 3-D fabric for the production of SiC/SiC composites by means of electrophoretic deposition. *Key Engineering Materials* **412**, 237–242 (2009).

Independent scientific component part or a chapter in a monograph

Novak, S.; Koenig, K.; Iveković, A. Electrophoretic deposition in production of ceramic matrix composites. In: Dickerson, J. H. (ed.), Boccaccini, A. R. (ed.) *Electrophoretic deposition of nanomaterials* (Nanostructure science and technology). (Springer, New York, 2011).

Published scientific conference contribution

Toplišek, T.; Iveković, A.; Novak, S.; Dražić, G. Analytical electron microscopy of W-core β-SiC fibers for use in SiC in based composite material for fusion application. In: *Proceedings of 5th International Union of Microbeam Analysis Societies, 8th International Symposium on Atomic Level Characterizations for New Materials and Devices'11*. 160 (Advanced Analysis Center, Korea Institute of Science and Technology, Seoul, Korea, 2011).

Iveković, A.; Koenig, K.; Novak, S.; Dražić, G. Investigation of thermal conductivity in SiC_f/SiC composites for fusion application. In: *Proceedings of International Conference Nuclear Energy for New Europe 2009*. (Nuclear Society of Slovenia, Bled, Slovenia, 2009).

Published scientific conference contribution abstract (invited lecture)

Novak, S.; Iveković, A.; Dražić, G. Preparation of SiC_f/SiC composites by SITE process. In: *35th International Conference and Exposition on Advanced Ceramics and Composites.* (The American Ceramic Society, Daytona Beach, Florida, 2011).

Published scientific conference contribution abstract

Iveković, A.; Novak, S. Fabrication of SiC based composite for fusion application by SITE-P process. In: *21st International Conference Nuclear Energy for New Europe, Ljubljana 2012 Conference program*. (Nuclear Society of Slovenia, Ljubljana, Slovenia, 2012).

Iveković A.; Novak. S. Fabrication of SiC[sub]f/SIC composite by SITE-P process. In: *Program and abstract book of 6th Young Researchers' Day 2012*. (Jožef Stefan Institute, Ljubljana, Slovenia, 2012).

Iveković, A.; Novak, S. Fabrication of SiC_f/SIC composite by SITE-P process. In: *Program and abstract book of 20. Jubilee Conference on Materials and Technology*. (Inštitut za kovinske materiale in tehnologije, Portorož, Slovenija. 2012).

Novak, S.; Iveković, A.; Rizzo, S.; Casalegno, V. W/SiC based joining of SiC/SiC composites. In: *Program and abstract book of 27th Symposium on Fusion Technology, - SOFT*. (Belgian Nuclear Research Centre, Liège, Belgium, 2012).

Iveković, A.; Dražić, G.; Novak, S. Densification of SiC-matrix by hybrid process of EPD-PIP. In: *Program and abstract book of 35th International Conference and Exposition on Advanced Ceramics and Composites.* (The American Ceramic Society, Daytona Beach, Florida, 2011).

Iveković, A.; Novak, S.; Dražić, G. Densification of SiC-matrix in SiC_f/SiC composites by SITE-P process. In: *Program and abstract book of 20th International Conference Nuclear Energy for New Europe 2011*. (Nuclear Society of Slovenia, Bovec, Slovenia, 2011).

Iveković, A.; Novak, S.; Dražić, G. Densification of SiC-matrix in SiC based composites by SITE-P. In: *Program and abstract book of 19th Conference on Materials and Technology*. (Inštitut za kovinske materiale in tehnologije, Portorož, Slovenia, 2011).

Iveković, A.; Jagodič, M.; Novak, S. ; Dražić G. Zgoščevanje SiC matrice v SiC_f/SiC kompozitu za fuzijsko aplikacijo. In: *Program and abstract book of 5th Young Researchers' Day 2011.* (Jožef Stefan Institute, Ljubljana, Slovenia, 2011).

Iveković A.; Novak. S. Infiltration of 3D fabric preform for the fabrication of SiC_f/SiC composite. In: *Program and abstract book of 4th International Conference on Electrophoretic Deposition: Fundamentals and Applications.* (Trans Tech Publications, Puerto Vallarta, Mexico, 2011).

Iveković, A.; Jagodič, M.; Novak, S. ; Dražić, G. Densification of SiC matrix in SiC_f/SiC composites for fusion application. In: *Program and abstract book of 26th Symposium on Fusion Technology - SOFT.* (Instituto de Plasmas e Fusão Nuclear, Porto, Portugal, 2010).

Iveković, A.; Koenig, K.; Novak, S.; Dražić, G. Consolidation of SiC deposition by polymer infiltration and pyrolysis method. In: *Abstracts of 12th International Ceramics Congress, International Conferences on Modern Materials & Technologies - CIMTEC 2010* (Techna Group, Montecatini Terme, Italy, 2010).

Iveković, A.; Jagodič, M.; Novak, S.; Dražić, G. Densification of SiC matrix in SiC-based composites. In: *Book of abstracts: SLONANO 2010* (Jožef Stefan Institute, Ljubljana, Slovenia, 2010).

Ivekovič, A.; Novak, S.; Dražić, G. A novel route for preparation of SiCf/SIC composites. In: *Book of abstracts: International Conference Nuclear Energy for New Europe 2010.* (Nuclear Society of Slovenia, Ljubljana, Slovenia, 2010).

Dražić, G.; Toplišek, T.; Iveković, A.; Novak, S. Compatibility of W-core [beta]-SIC fibers with SiC based composite material for fusion application. In: *Book of abstracts*: *International Conference Nuclear Energy for New Europe 2010.* (Nuclear Society of Slovenia, Ljubljana, Slovenia, 2010)

Rožič, B.; Iveković, A.; Šmuc, A.; Pavšič, J.; Kastivnik J. Jurske in spodnjekredne plasti Slovenskega bazena v dolini reke Mirne. In: *3. Slovenski geološki kongres, Povzetki in ekskurzije* (Znanstvenoraziskovalni center Slovenske akademije znanosti in umetnosti, Bovec, Slovenia, 2010).

Ivekovič, A.; Koenig, K.; Novak, S.; Dražić, G. Zgoščevanje matrice iz silicijevega karbida z metodo infiltracije in pirolize polimera. In: *Program and abstract book of 4th Young Researcher's Day 2010*. (Jožef Stefan Institute, Ljubljana, Slovenija, 2010).

Iveković, A.; Jagodič, M.; Novak, S.; Dražić G. Polymer infiltration and pyrolysis of silicon carbide matrix. In: *Slovenski kemijski dnevi 2010, Zbornik povzetkov referatov s posvetovanja* (Fakulteta za kemijo in kemijsko tehnologijo, Maribor, Slovenia, 2010).

Dražić, G.; Novak, S.; Toplišek, T.; Koenig, K.; Iveković, A. Preparation of SiC_f/SiC composites for fusion applications using ceramic routes. In: *Book of abstracts: MRS fall meeting 2008* (Cambridge University Press, Boston, Massachusetts, 2008).

Iveković, A.; Novak, S. Izdelava SiC[spodaj]f/SiC kompozitov z infiltracijo 3D SiC tkanine. In: *Program and abstract book of 3rd Young Researcher's Day 2009.* (Jožef Stefan Institute, Ljubljana, Slovenia, 2009)

Iveković, A.; Koenig, K.; Jagodič, M.; Novak, S.; Dražić, G. Investigation of thermal conductivity in SiC_f/SiC composites for fusion application. In: *Program and abstract book of 17th Conference on Materials and Technology*. (Inštitut za kovinske materiale in tehnologije, Portorož, Slovenija, 2009).

Novak, S.; Koenig, K.; Iveković, A.; Uršnik, P. Infiltration of a 3-D fabric for the production of SiC_f/SiC composites by means of electrophoretic deposition. In: *Program and abstract book of 3rd International Conference on Electrophoretic Deposition: Fundamentals and Applications*, (Trans Tech Publications, Hyogo, Japan, 2008).

Iveković, A.; Novak, S. Production of SiC_f/SiC composite by infiltration of 3D SiC fabric. In: *Program and abstract book of 1st International Conference on Materials and Technology sponsored by FEMS and IUVSTA* (Inštitut za kovinske materiale in tehnologije, Portorož, Slovenia, 2008).

Treatise, preliminary study, study

Novak, S.; Iveković, A. *Fabrication and characterization of W-SiC composites.* Annual report on EFDA task activities in 2012, 11282 (2013).

Novak, S.; Iveković, A. *3-D SiC_f/SiC composites prepared by SITE-P process.* Annual report on EFDA task activities in 2012, 11283 (2013).

Novak, S.; Iveković, A.; Dražić, G. *Production of a dense SiC based composite with closed porosity using elements with low neutron activation and potential irradiation effects*:Aannual report on EFDA task activities in 2011, 11279 (2012).

Dražić, G.; Novak, S.; Toplišek, T.; Iveković, A. *Optimisation of thermal conductivity of SiC-based composite*. Annual report on EFDA task activities in 2011, 11280 (2012).

Iveković, A.; Novak, S.; Dražić, G. *Definition of a fabrication route for an optimised SiC-based composite*. Annual report on EFDA task activities in 2011, 11281 (2012).

Novak, S.; Iveković, A.; Dražić, G. *Development of a dense β-SiC matrix in 3D perform.* Annual report on EFDA task activities in 2010, 11277 (2011).

Dražić, G.; Novak, S.; Toplišek, T.; Iveković, A. *Optimisation of β-SiC-coated W fibres.* Annual report on EFDA task activities in 2010, 11278 (2011).

Dražić, G.; Novak, S.; Iveković, A. *Assessment of the current status and outline for the future research and development in the field of silicon carbide based materials for fusion application*. IJS work report, 10519 (2010).

Novak, S.; Dražić, G.; Iveković, A.; Toplišek, T.; Koenig, K.; Bele, J.; Ford, A. *SiC_f composites for structural application in fusion reactor*. IJS work report, 10521 (2010).

Novak, S.; Dražić, G.; Koenig, K.; Iveković, A.; Snoj, L.; Lengar, I.; Ravnik, M. *SiC_f/SiC composite development*. IJS work report, 10176 (2009).